MODELLING OF IRON LOSSES OF PERMANENT MAGNET SYNCHRONOUS MOTORS

By

Chunting Mi

A thesis submitted in conformity with the requirements

for the Degree of Doctor of Philosophy in the

Department of Electrical and Computer Engineering

University of Toronto

MODELLING OF IRON LOSSES OF PERMANENT MAGNET SYNCHRONOUS MOTORS

Chunting Mi

A thesis submitted in conformity with the requirements

for the Degree of Doctor of Philosophy in the

Department of Electrical and Computer Engineering

University of Toronto

ABSTRACT

This thesis proposes a refined approach to evaluate iron losses of surface-mounted permanent magnet (PM) synchronous motors.

PM synchronous motors have higher efficiency than induction machines with the same frame and same power ratings. However, in PM synchronous motors, iron losses form a larger portion of the total losses than in induction machines. Therefore, accurate calculation and minimization of iron losses is of particular importance in the design of PM synchronous motors.

Although time-stepped FEM can provide good estimations of iron losses, it requires high effort and is very time-consuming for most designs and particularly for optimizations. Besides, FEM analysis can only be performed after the machine geometrical dimensions have

been determined. In contrast, approximate analytical loss model yields quick insight while requiring much less computation time and are readily available during the preliminary stage when the motor design is being iterated. Therefore, it is desirable to develop iron loss models that produce an acceptable prediction of the overall iron losses in a relatively simple way and provide machine designers a more reliable method to estimate iron losses in the initial design of PM machines.

In this thesis, simplified models for the estimation of tooth and yoke eddy current losses are developed based on the observations of FEM results and analytical analyses of the magnetic fields taking into account detailed geometrical effects. The effectiveness and limitations of the models are investigated. Correction factors are derived for geometrical influences.

The nature of the flux density waveform has great impact on iron losses. Therefore, reduction of iron losses can be achieved by properly shaping the magnets, designing the slots and choosing appropriate number of poles. Some guidelines are provided to minimize iron losses of PM synchronous motors.

In order to test the proposed simplified loss models, measurements were performed on two surface-mounted PM synchronous motors. Particular attention was focused on the measurement of PWM waveforms and decomposition of no-load losses. Experimental results of the two motors confirmed the validity of the proposed iron loss models.

ACKNOWLEGEMENTS

I am eternally grateful to my supervisors, Professor G. R. Slemon and Professor R. Bonert, for their invaluable guidance, encouragement and financial support throughout the period of my course study and thesis research. Their attitude, enthusiasm and dedication towards scientific research deeply influenced me and will benefit for all my life.

I sincerely thank Professor Lavers and Professor Dawson for their precious suggestions and technical discussions.

I am also thankful to Dr. K.V. Namjoshi for spending much of his spare time reading the draft of my thesis and giving me a lot of advice. Special thanks are due to the leaders and fellows at Xi'an Petroleum Institute for granting me the opportunity to study abroad. The author also wishes to extend his gratitude to his Master's thesis supervisor Professor Jiang Zongrong, one of the pioneers in the field of rare-earth PM machines, for his excellent quality of teaching.

Special appreciation goes to my wife Yuhong for her understanding and support during my Ph.D studies. This thesis is also a gift to my lovely daughter Shishi for the many sacrifices she suffered during the years of my research work. This thesis is also dedicated to my parents and my parents-in-law for their understanding, encouragement and mental support.

The financial supports from the Ontario Graduate Scholarship for Science and Technology (OGSST), the University of Toronto S.G.S International Student Award, the University of Toronto Doctorial Fellowships and Ontario Student Assistant Program (OSAP), are gratefully acknowledged.

CONTENTS

LIST OF FIGURES

LIST OF TABLES

LIST OF SYMBOLS

α	Fractional magnet coverage (pole enclosure)
β	Empirically determined constants for hysteresis loss
	Angle of magnet beveling
δ	Airgap length
	Power angle (angle between back emf E_o and terminal voltage U)
θ	Angle between phase-a current and d-axis
γ	Relative slot closure
σ	Conductivity of the medium of electromagnetic field
ε	Permittivity of the medium of electromagnetic field
μ	Permeability of the medium of electromagnetic field
ν	Reluctivity of the medium of electromagnetic field
τ	Pole pitch
φ	Power factor angle (angle between phase-a current I_a and terminal voltage U)
λ	Slot pitch
λ_2	Projected slot pitch at the middle of yoke
ψ_m	Total flux linkage per phase
ψ_d	d-axis flux linkage
ψ_q	q-axis flux linkage
ω	Angular speed
ω_s	Angular frequency of the magnetic field
ρ_v	Volume electrical charge density
$\mathbf{A}$	Vector magnetic potential
$\mathbf{A}_k$	Magnetic potential of node k

A_e	Area of element e in FEM
$\mathbf{B}$	Vector flux density
$\hat{B}$	Maximum flux density in the iron
B_{lg}	rms values of the airgap flux density
$\hat{B}_c$	Plateau value of the circumferential component of yoke flux density
$\hat{B}_r$	Plateau value of the radial/normal component of yoke flux density
$\hat{B}_{rs}$	Plateau value of the radial component of yoke flux density above slots
$\hat{B}_{rt}$	Plateau value of the radial component of yoke flux density above teeth
B_{th}	Plateau value of tooth flux density
B_y	Plateau value of yoke flux density
C_1	Constants represent unary boundary constraint values
C_2	Constants represent binary boundary constraint values
C_e	Machine constant
C_m	Machine constant
$\mathbf{D}$	Electrical flux density
d_t	Slot height
d_y	Yoke depth
d_{y2}	Yoke depth of 2-pole motor configuration
e	Subscript for element e
$\mathbf{E}$	Electrical field density
E	Total number of elements of the stator core in FEM
E_o	Induced back emf
f	Frequency
$\mathbf{H}$	Magnetic field intensity
i, j, m	Subscripts for nodes i, j, m of element e
I_a	Phase-a current
I_d	d-axis current
I_q	q-axis current

$\mathbf{J}$	Electrical density
J	Inertia
K_{ls}	rms values of the linear current density on the stator inner periphery.
k_c	Correction factor for effect of circumferential component of tooth flux density
k_e	Empirically determined eddy current loss constant
k_h	Empirically determined hysteresis loss constant
k_I	Gain of current PI
k_m	Magnetic usage
k_p	Gain of speed PI
k_q	Correction factor for effect of magnet thickness and airgap length
k_r	Correction factor for effect of circumferential component of yoke flux density
k_T	Torque constant
k_y	Ratio of yoke eddy current loss of radial component to circumferential component
l_1	Unary boundary enclosed by S
l_2	Binary boundary enclosed by S
l_{fe}	Stator stack length
L_d	d-axis inductance
L_q	q-axis inductance
l_m	Magnet length
m	Number of phases
m_a	Modulation ratio
n	Speed
	Subscripts used for time step n in time stepped FEM
n_{max}	Maximum operation speed
N	Total number of slots used in time stepped FEM for half period
p	Number of poles
P_{cu}	Copper loss
p_e	Eddy current loss density
P_{et}	Tooth Eddy current loss

P_{etc} Eddy current loss induced by circumferential component of tooth flux density

P_{etr} Eddy current loss induced by radial/normal component of tooth flux density

$P_{etr,APP}$ Eddy current loss induced by radial/normal component of tooth flux density calculated by Approximation model

$P_{etr,FEM}$ Eddy current loss induced by radial/normal component of tooth flux density calculated by FEM

P_{ey} Yoke eddy current loss

P_{eyc} Eddy current loss induced by circumferential component of yoke flux density

$P_{eyc,FEM}$ Eddy current loss induced by circumferential component of yoke flux density calculated by FEM

P_{eyr} Eddy current loss induced by normal component of yoke flux density

P_{fw} Friction and windage loss

p_h Hysteresis loss density

P_{ht} Hysteresis loss of the teeth

P_{hy} Hysteresis loss of the yoke

p_{iron} Total iron loss density

P_{out} Output power of the motor

q Number of slots per pole per phase

r Inner radius of stator

r_a Stator phase resistance

r_j Out radius of stator

S Magnetic field region

S Number of stator slots

t Time

Δt Time interval used in time stepped FEM

Rise time of tooth or yoke flux density

T Period

T_e Electrical time constant

T_i Sampling period

T_I	Time constant of current PI
T_m	Mechanical time constant
T_p	Time constant of speed PI
T_q	Torque
U	Phase voltage
U_d	DC-link voltage
U_{LL}	Line-line voltage
V_t	Total volume of stator teeth
V_y	Total volume of stator yoke
W	Total number of turns of stator winding
w_m	Magnet width
w_o	Slot openings
w_t	Tooth width
x, y	Subscripts for x and y component respectively
Δx	Distance needed for flux density to rise from zero to plateau
X_d	d-axis reactance
X_q	q-axis reactance
Z_{base}	Base reluctance

Chapter 1

Introduction

1.1 Thesis Objectives

The main objective of this thesis is to develop a simplified model to evaluate iron losses in surface-mounted permanent magnet (PM) synchronous motors.

PM synchronous motors have higher efficiency than standard induction machines with the same power rating and the same frame. However, iron losses in PM synchronous machines form a larger proportion of the total losses than is usual in induction machines. This is partly due to the elimination of significant rotor losses and partly due to their operation at near unity power factor. Therefore, accurate evaluation and minimization of iron losses is of particular importance in PM synchronous motor design [1]. This thesis addresses this issue with particular emphasis on the eddy current loss in the stator teeth and stator yoke.

Iron losses in electrical machines are usually predicted by assuming that the magnetic flux in the magnetic core has only one alternating component that is sinusoidal. The iron losses evaluated in this approach may be 20% lower than the measured values and the discrepancy is even larger in PM machines [2].

An alternative approach considers the harmonics of the magnetic flux density and

obtains the sum of losses of each component [3-6]. The finite element method (FEM) is often used to obtain the field distribution in the motor. Since the FEM is considered as a precise tool in the calculation of electromagnetic fields, it is commonly accepted that a good estimation of iron losses can be achieved with this approach [7]. However, this approach needs high effort for general use in most designs and is not practical during the preliminary design iteration stages.

An analytical model, developed by *Slemon* and *Liu,* uses a simple approach to estimate the iron losses in PM synchronous motors [8]. It assumed that: (1) the tooth and yoke flux waveforms are trapezoidal with regard to time; (2) the eddy current loss is proportional to the square of time change rate of the magnitude of flux density. While the overall application of these approximations produced an acceptable prediction of the total measured iron losses in an experimental machine, the validity of each approximation remained in doubt.

Deng [9] and *Tseng* [10] evaluated the iron losses of PM synchronous machines in a similar procedure to [8]. The geometrical effects were also ignored and only the magnitude of magnetic flux density was used to perform the calculation.

Therefore, there is need of a verified simple approach to evaluate iron losses in PM synchronous motors for use in the motor design studies including detailed geometrical effects of the design. This simplified iron loss model should be able to reliably predict the iron losses of PM synchronous motors but avoid the high effort of FEM tools. The simplified approximation iron loss model will be developed and validated based on these guidelines.

Based on the proposed model, design guidelines will be provided to design low loss PM synchronous motors including geometrical effects.

To complement the main objective, the thesis will also investigate the measurement of iron losses of PM synchronous motors.

Loss measurement in electrical machines has been a difficult task for the electrical industry [11]. There is no effective approach to measure the iron losses in PM machines reliably to verify differences in designs so far [12-14].

Measurement of iron losses involves the decomposition of no-load losses of a PM synchronous motor, since iron losses and mechanical losses in a PM synchronous motor are always present simultaneously.

Although no-load loss of a synchronous machine can be measured when the machine is driven by a dynamometer, it is more desirable to measure the losses when the machine is operated as a motor. As PM synchronous motors are usually designed without damping, a close-loop controlled inverter is necessary to run the motor. Therefore, the measurement of losses also involves the measurement of pulse-width-modulated (PWM) waveforms.

The theoretical and experimental studies are focused on two PM synchronous motors with surface-mounted magnets.

1.2 Thesis Outline

This thesis contains six chapters. The contents of the thesis are summarized below.

In Chapter 2, the evaluation of iron losses in PM machines is reviewed and the time-stepped FEM is introduced. FEM analysis is performed on three PM synchronous motors including two existing PM motors. Equations are developed to calculate iron losses using time-stepped FEM.

In Chapter 3, simplified iron loss models are developed. In order to achieve the simplified models, the proposed analytical model in [8] is reviewed and tested with the FEM for different cases. A refined simplified tooth eddy current loss model is developed taking into account the detailed geometrical shape of different designs. The effects of magnet width, slot closure, number of slots per pole per phase, airgap length, tooth width and magnet thickness are studied. A correction factor is introduced to reflect the geometrical influences. Another correction factor is introduced to reflect the iron loss induced by the circumferential component of the tooth flux density.

A new simplified yoke eddy current loss model is developed based on the two orthogonal components of yoke flux density. The waveform of the circumferential component of the yoke flux density can be approximated by a trapezoidal waveform. The waveform of the normal component of the yoke flux density is found to have the same shape as that of the normal component of tooth flux density. The two components of yoke flux density are related to each other through the dimensions of the yoke.

Some examples are tabulated for each of the simplified models to demonstrate the use and validate the effectiveness of the model. These models are simple formula for the machine designer to calculate iron losses in PM synchronous motors.

Chapter 4 investigates the measurement of iron losses in PM synchronous motors. Measurements of iron losses are performed when the motor is driven by a dynamometer and when the motor is fed by an inverter. Separation of iron losses and mechanical losses is also investigated. The experimental work of two PM synchronous motors is presented here. The comparison between the measured iron losses and the predicted iron losses confirmed the validity of the proposed iron loss model. Despite the difficulties to measure iron losses, the experiment provides an indication of the usefulness of the proposed model.

Chapter 5 proposes effective ways to minimize iron losses in PM synchronous motors. A series of approaches are provided to minimize iron losses of PM synchronous motors

Finally, the conclusions and contributions of the thesis are presented in Chapter 6. Suggestions for future studies are also included.

Chapter 2

Iron Losses and Time-Stepped FEM of PM Synchronous Motors

2.1 PM Synchronous Motors

A typical PM synchronous motor drive system consists of a PM synchronous motor, an inverter, a shaft encoder and a microcontroller.

A PM synchronous motor has a similar structure to a DC excited synchronous motor except that the magnetic field is supplied by PM material in a PM machine.

With the latest development in rare-earth PM material, it is now possible to develop high efficiency, high power factor, and high power density PM motors for industrial and residential purposes. The modern rare-earth PM material, neodymium-iron-boron (Nd-Fe-B), has 1.4T of residual flux, 11kA/m of coercive force and 13.6kA/m intrinsic coercive force. The dropping cost and lower temperature sensitivity have made Nd-Fe-B an ideal material for developing high performance PM synchronous motors.

The stator structure of a PM synchronous motor is similar to that of an induction machine. Depending on its application, the winding distribution could be near sinusoidal or trapezoidal. It is preferable to build the PM motor winding with a near sinusoidal distribution

if a smoother torque is desired at low speed. In order to avoid cogging torque, skewed stator slots may be used.

The rotor structure of a PM synchronous motor can be built either with surface-mounted magnets, inset magnets or circumferential magnets. Typical rotor structures are shown in Fig.2.1.

Among the major types of rotor structures, rotors with surface-mounted magnets as shown in Fig.2.1(a) are commonly used in PM synchronous motors for their simplicity. The drawback is that the magnets may easily peel off from the surface if they are originally glued on the rotor surface. Rare-earth PM materials are fragile and rust and scratch easily. Therefore, the life span of the magnets is reduced if they are exposed directly to air. The author has experienced several times the magnets flying off the rotor surfaces during the operation of PM motors. One effective but costly way to avoid the mechanical weakness of surface-mounted PM synchronous motors is to bond the magnets with a cylindrical sleeve made of high strength alloy as shown in Fig.2.1(b) [15-17].

Rotors with inset magnets as shown in Fig.2.1(c) can provide a more secure magnet setting. It can also produce more maximum torque due to its unequal d-axis and q-axis reluctance [18]. Both the surface-mounted and the inset rotor structures Fig.2.1(a) and (b) require arc shaped magnets which greatly increases the manufacturing cost. Segmented rectangular strips may be used to reduce the manufacturing cost.

PM motors with magnets buried just below the surface have a mechanical advantage over surface mounted PM motors especially at high speed. Although the possible use of rectangular magnets eases the manufacture of magnets, the manufacture of rotor laminations is more complicated than those for surface mounted magnets.

It is possible to build the motor with circumferentially magnetized buried magnets as shown in Fig.2.1(d). The overall cost can be significantly reduced by using rectangular shaped magnets. The circumferential structure is normally suitable for machines with six or more poles.

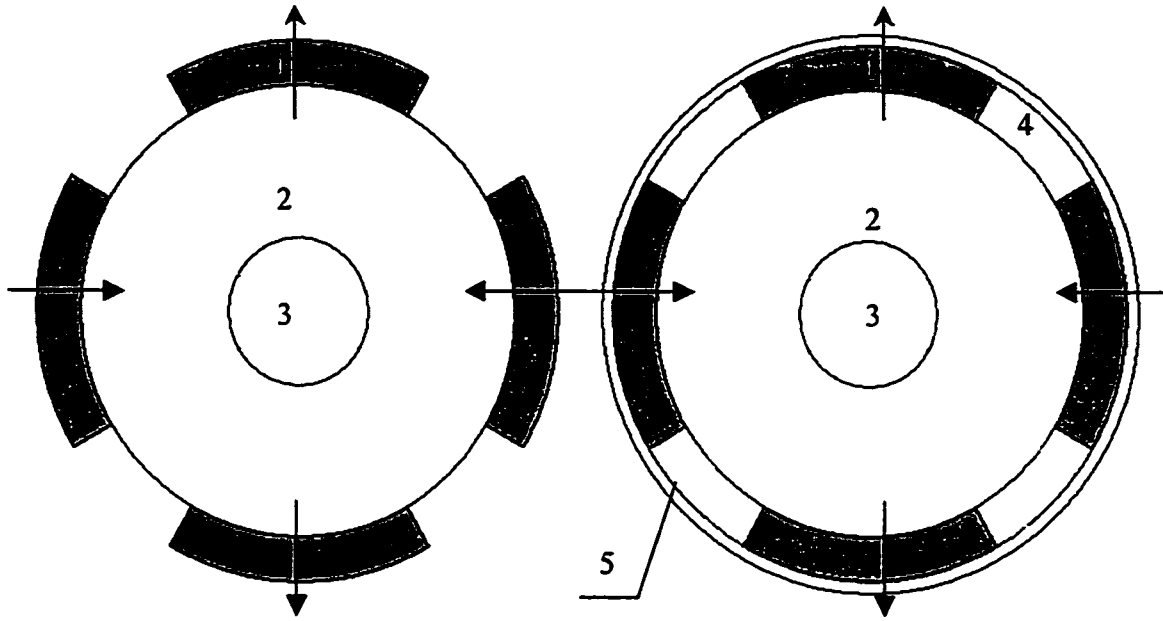

(a). Surface-mounted magnets (b). Surfaced magnets with rotor sleeve

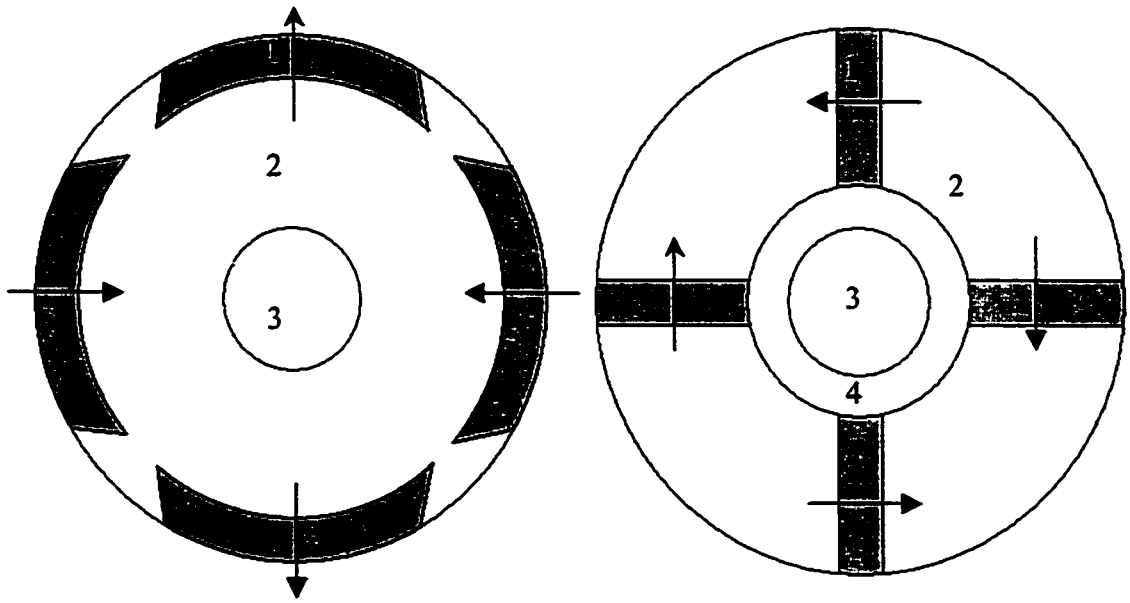

(c). Inset magnets (d). Circumferential magnets

1—magnet 2—core 3—shaft 4—non-magnetic material 5—rotor sleeve

Fig.2.1 Rotor structures of PM synchronous motors

2.2 Iron Losses in PM Machines

According to IEEE Std 115-1995 [35], the losses of a synchronous motor are decomposed into the following individual components: mechanical loss (friction and windage loss); iron loss (open circuit core loss); stray-load loss (short circuit core loss); stator copper loss and field copper loss. In the case of a PM motor, there is no field copper loss.

The mechanical loss is due to the bearing friction, windage on the rotor, ventilation fan and cooling pump. These losses are constant at constant speed and vary in direct proportion to the changes in speed. The iron loss is due to the change of magnetic field in the stator and rotor core. It usually decomposed into hysteresis loss and eddy current loss. Hysteresis loss is due to the existence of a hysteresis loop in the core B/H characteristics. Eddy current loss is due to the currents induced in the core material, which is also a conductor of electricity. The stray-load is due to the armature reaction, flux leakage and mechanical imperfections of the motor. The short-circuit core loss of a PM synchronous motor includes the extra copper loss (eddy current loss in the stator winding), the harmonic iron loss in the teeth and a loss in the end structure of the machine. The copper loss is due to the current flow in the winding. It increases slightly with load due to the skin effect and eddy current in the winding.

The calculation of copper losses is relatively simple and accurate. The prediction of mechanical loss is usually predicted by comparing the losses with that of a similar machine. The calculation of iron losses and stray-load loss of electrical machines is far from complete. The procedure suggested in [19] has been used for decades to calculate the stray-load loss of large motors. For small to medium size electrical machines, the usual practice is to assume a percentage of the total input power as the stray-load loss [20, 49]. In classical motor designs, the iron losses are viewed as being caused mainly by the fundamental frequency variation of the magnetic field [21]. The measured iron losses in electrical machines are usually much larger than that calculated from the sinusoidal assumption. The thesis will be focused on the evaluation of iron losses of PM synchronous motors.

Massive experimental results show that the iron losses consist of two components: one component is proportional the frequency and the other is proportional to the square of the frequency. The former is usually linked hysteresis loss and the latter is usually linked eddy current loss.

For a sinusoidal flux density, over the working range of frequency, the total iron losses can be represented by the sum of the hysteresis loss (proportional to the frequency) and eddy current loss (proportional to the square of frequency):

$$p_{iron} = p_h + p_e = k_h \hat{B}^{\beta} \omega_s + k_e \hat{B}^2 \omega_s^2 \qquad (\mathrm{W/m^3}) \qquad (2.1)$$

where $\hat{B}$ is the maximum flux density in the iron, p_{iron} is the total iron loss density, p_h is the hysteresis loss density and p_e is the eddy current loss density; ω_s is the angular frequency of the magnetic field; k_h, k_e and β are empirically determined constants which can be obtained by curve fitting from manufacturer's data measured with sinusoidal flux density. Typical values for silicon iron material frequently used in induction machines, with the stator frequency given in *rad/s*, are k_h=44-56, β=1.5-2.5, k_e=0.01-0.07.

An expression for the classical eddy current loss can also be developed based on the resistivity of the core material [21]. The result is generally found to be less than that from the second term of (2.1).

In surfaced-mounted PM synchronous machines, the iron losses are mainly in the stator core. The flux density waveform in the stator core is neither uniform nor sinusoidal. This non-sinusoidal waveform of flux density doesn't affect the hysteresis loss provided there are no minor loops, but is critical to the eddy current loss. It is therefore desirable to restate the eddy current loss density formula in the following format for general flux waveforms [8, 21]:

$$p_e = 2k_e \left| \frac{d\mathbf{B}}{dt} \right|^2 \qquad (\mathrm{W/m^3}) \qquad (2.2)$$

In (2.2), the time derivative of vector flux density $\mathbf{B}$ is used to evaluate the instantaneous

eddy current loss density p_e. It also shows that the iron losses are induced by the field variation, whether it is pulsating or rotating [29]. The eddy current loss is related not only to the magnitude of the flux density, but also to the way in which each of the two orthogonal components of the flux density changes [21-22].

For periodic variable fields, the average eddy current loss density can be obtained by integrating (2.2) over one period:

$$P_e = \frac{2k_e}{T}\int_0^T \left|\frac{d\mathbf{B}}{dt}\right|^2 dt \qquad (\mathrm{W/m^3}) \qquad (2.3)$$

2.3 Finite Element Method of Electromagnetic Field Problems

Although it requires high effort for general use in PM motor designs, time-stepped FEM remains the most powerful tool to calculate electromagnetic field distributions and field-related parameters [2-6].

Time stepped FEM is also used as an effective tool to verify loss calculation based on simpler loss models [9-10, 23-24], as it is economically and technically impractical to verify all loss predictions with experiments.

Time stepped FEM will be used as the tool to develop the simplified loss models and to validate the proposed iron loss models in this thesis.

2.3.1 Maxwell's Equations

All electromagnetic phenomena are governed by *Maxwell's* Equations. The differential form of *Maxwell's* Equations can be expressed as:

$$\nabla \times \mathbf{E} = -\frac{\partial \mathbf{B}}{\partial t} \qquad (2.4)$$

$$\nabla \times \mathbf{H} = \mathbf{J} + \frac{\partial \mathbf{D}}{\partial t} \tag{2.5}$$

$$\nabla \cdot \mathbf{B} = 0 \tag{2.6}$$

$$\nabla \cdot \mathbf{D} = \rho_v \tag{2.7}$$

where **E** is the electrical field intensity, **D** is the electrical flux density, **H** is the magnetic field intensity, **J** is the electrical current density, ρ_v is the volume electrical charge density.

For isotropic medial material, the constitutive equations to *Maxwell*'s equations are:

$$\mathbf{B} = \mu \mathbf{H} \tag{2.8}$$

$$\mathbf{J} = \sigma \mathbf{E} \tag{2.9}$$

$$\mathbf{D} = \varepsilon \mathbf{E} \tag{2.10}$$

where μ, σ, and ε are the permeability, conductivity and permittivity of the medium of electromagnetic field respectively.

Maxwell's equations can be further simplified if the dimension of the current carrying system is small when compared with the wavelength in free space. The displacement current is zero and (2.5) can be re-written as:

$$\nabla \times \mathbf{H} = \mathbf{J} \tag{2.11}$$

2.3.2 The Magnetic Vector Potential

A fundamental result of vector analysis is that the divergence of the curl of any twice differentiable vector **A** vanishes identically:

$$\nabla \cdot \nabla \times \mathbf{A} = 0 \tag{2.12}$$

Comparing (2.12) to (2.6), it can be concluded that:

$$\mathbf{B} = \nabla \times \mathbf{A} \tag{2.13}$$

where **A** is referred to as magnetic vector potential. Of course, the vector potential is not fully defined by (2.13) because the *Helmholtz* theorem of vector analysis states that a vector is uniquely defined if and only if both its curl and divergence are known, as well as its value at some space points. A common choice for the divergence of A is know as *Coulomb* convention, which is generally used for static field problems and low frequency electromagnetic problems:

$$\nabla \cdot \mathbf{A} = 0 \tag{2.14}$$

2.3.3 Two Dimensional FEM Formulation of Magnetostatic Problems

The magnetic field of a no-load PM synchronous motor can be considered as a magnetostatic problem. In solving this two-dimensional non-linear magnetic field problem, the laminated material can be assumed to be isotropic in the radial direction. Therefore, substituting (2.13) to (2.11) leads to:

$$\nabla \times (\nu \nabla \times \mathbf{A}) = \mathbf{J} \tag{2.15}$$

where ν is the magnetic reluctivity of the medium:

$$\nu = 1/\mu \tag{2.16}$$

Therefore, the two-dimensional non-linear partial differential equation for a magnetostatic problem can be derived from (2.15). In region S enclosed by unary boundary l_1 and binary l_2, the differential equation is:

$$\begin{aligned} &\frac{\partial}{\partial x}\left(\nu \frac{\partial \mathbf{A}}{\partial x}\right) + \frac{\partial}{\partial y}\left(\nu \frac{\partial \mathbf{A}}{\partial y}\right) = -J \\ &\mathbf{A}\big|_{l1} = C_1 \\ &\nu \frac{\partial \mathbf{A}}{\partial n}\bigg|_{l2} = C_2 \end{aligned} \tag{2.17}$$

where C_1 and C_2 are constants represent unary and binary boundary constraint values

respectively.

The field problem of (2.17) can be expressed in variational terms as an energy functional; the minimizing of which yields the required solution:

$$\Re = \iint\left[\int_0^B \nu\delta d\delta - \mathbf{J}\cdot\mathbf{A}\right]dxdy - \oint_s \mathbf{A}\frac{\partial \mathbf{A}}{\partial n}ds \qquad (2.18)$$
$$\mathbf{A}|_{l1} = C$$

where

$$\delta = \sqrt{(\frac{\partial \mathbf{A}}{\partial x})^2 + (\frac{\partial \mathbf{A}}{\partial y})^2} \qquad (2.19)$$

For the first order triangular finite elements of unrestricted geometry, the potential solution is defined in terms of shape functions of the triangular geometry and its node values of potential.

$$\mathbf{A} = \sum_{k=i,j,m}\zeta_k \mathbf{A}_k \qquad (2.20)$$

The minimization of the functional (2.18) is performed with respect to each of the nodal potentials:

$$\left.\frac{\partial \Re}{\partial \mathbf{A}_k}\right|_{k=i,j,m} = \sum_{k=i,j,m}\left[\sum_{l=i,j,m}(b_k b_l + c_k c_l)\mathbf{A}_k - \mathbf{J}(\frac{\partial \mathbf{A}}{\partial \mathbf{A}_k})\right] = 0 \qquad (2.21)$$

When the minimization described by (2.21) is carried out for all the triangles of the field region, the following matrix equation can be obtained. By solving the following equation, the unknown vector potential can be determined.

$$[\mathbf{K}][\mathbf{A}] = [\mathbf{P}] \qquad (2.22)$$

where [**K**] is a nonlinear symmetric matrix, [**P**] is the excitation matrix. *Newton-Raphson* iteration can then be used to solve the above nonlinear equation.

2.3.4 Magnetization Models of Magnets

There are two models commonly used to represent permanent magnets: a magnetization vector and an equivalent current sheet. These two methods have different starting points but lead to the same set of equations [25]. In the FEM package (MagNet5.1 from Infolytica Co.) used in this thesis, the equivalent current sheet is used to represent the magnets [26].

With an equivalent current model, the magnet is represented by a thin layer of elements with current along the surface of the magnets. For a rotary PM synchronous motor with arc-shaped surface-mounted magnets, there are two possibilities of magnetization for the magnets: radial magnetization and parallel magnetization. The representations are shown in Fig.2.2.

(a). Radial magnetization (b). Parallel magnetization

Fig.2.2 Magnetization models of permanent magnets

It has been shown that the usage of PM material in parallel-magnetized surface mounted machines is less than that with radial magnetization [27]. The magnetic usage can be written as

$$k_m = \sin(\alpha\pi / p)/(\alpha\pi / p) \tag{2. 23}$$

where α is magnet coverage ($0<\alpha<1$) and p is the total number of poles.

Sometimes, rectangular shaped magnet strips are used to replace arc shaped magnets to reduce the manufacturing cost. In this case, individual magnet strip is parallel magnetized while each of the strips has a different orientation of magnetic field.

In this thesis, one of the experimental PM motors (8-pole) is parallel magnetized while the other one (4-pole) is radially magnetized.

2.4 Time-Stepped FEM of PM Synchronous Motors

The iron losses and the flux density waveforms in the core of a PM synchronous motor can be obtained by time-stepped FEM [5].

In the analysis of time-stepped FEM, it must accommodate the motion of the rotor or the stator. This can be accomplished by developing compatible mesh structures on stator and rotor respectively and shifting them to simulate the actual motion. At each time step, FEM itself is performed on static electromagnetic fields. The shifting of meshes simulates the actual motion of the machine.

2.4.1 Construction of Meshes

The PM motor contains a standstill stator and a moving rotor. In establishing the meshes for the analysis, the rotor should be moved and positioned at each time step such that it does not disturb the integrity of the mesh structure as it moves. The initial meshes of the stator and the rotor are generated such that half of the air gap belongs to the stator and the other half to the rotor. The stator mesh and the rotor mesh share the same boundary at the middle of the air gap. The inner stator circumference at the air gap and the outer rotor circumference are divided into equal steps so that their nodes coincide. To provide movement of the rotor, the time step is chosen so that the angle or length of each step is equal to the interval between two neighboring nodes along the middle of the air gap. Because of periodicity of the magnetic field, only one pair of poles need be modeled. Similarly, because of the half wave symmetry of flux density, only a half period need be calculated.

2.4.2 Boundary Conditions

There are three types of boundary constraints in electromagnetic problems. The first type of boundary is described as ***no constraints***. In which case, the boundary condition is

assumed as satisfying $\frac{\partial \mathbf{A}}{\partial n} = 0$. This is the natural boundary condition which will be satisfied automatically by FEM if the potential of a boundary node is not specified.

The second type of boundary is called ***unary*** boundary on which the potential of each node is specified as a constant.

The third kind of boundary is called ***binary*** boundary. In this case, it implies that the potentials on one side of the region are equal or opposite to the potentials on the other side of the region. This is the case when only one pole or a pair of poles of the motor is modeled. An important practical point is that the model must have an equal number of nodes for binary constraints.

If one pair of poles is chosen as a FEM model, the boundaries can be summarized as shown in Fig.2.3 for a linear PM synchronous motor (LSM) with longitudinal laminations.

In Fig.2.3, the outer boundaries of the stator Z_1 and the rotor Z_2 are unary boundaries. Boundaries (Y_1 , Y_1') and (Y_3 , Y_3') on the cross sections of the LSM are binary boundaries. Along the middle of the air gap when the rotor is moved out of stator, (Y_2 , Y_2') are also binary boundaries, where the dots simulate the moving of meshes.

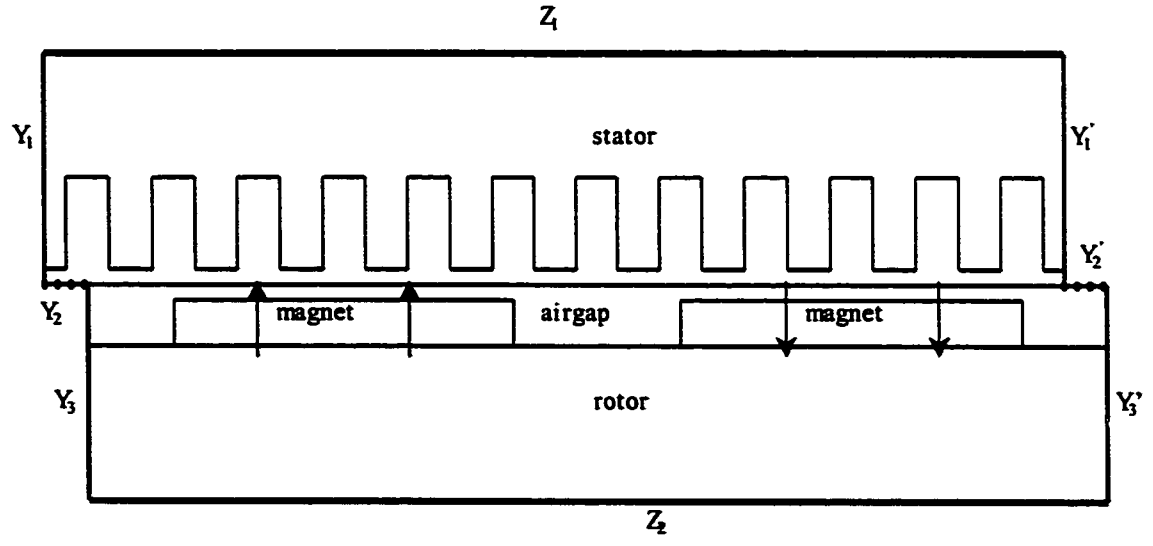

Fig.2.3 A linear PM machine for time-stepped FEM analysis

2.4.3 Examples Used in the Thesis

Three PM synchronous motors were used to evaluate iron losses and validate the simplified models. The linear motor is a pure design example and the 4-pole and 8-pole PM motors are existing motors.

Case I: A Linear PM Synchronous Motor

FEM analyses were performed on a simple idealized linearly arranged 3-phase PM synchronous motor with longitudinal laminations (**the linear motor**) with dimensions given in Table II-1.

Since a LSM with longitudinal laminations is also called a longitudinal flux LSM (the flux lines lie in the plane which is parallel to the direction of the travelling magnetic field), "longitudinal flux" is referred to the flux which is parallel to the travelling magnetic field. Similarly, "Normal flux" is referred to the flux which is perpendicular to the travelling magnetic field or the movement of the rotor.

In rotary machines, the circumferential component (equivalent to the longitudinal component in linear machines) and radial (or normal) component will be used to represent the two orthogonal components of flux density.

The flux distribution of the linear PM motor of Fig.2.3 is shown in Fig.2.4. The dimensions of this motor will be varied in Chapter 3 to test the geometric effect on iron losses.

Table II-1 Parameters and dimensions of the linear motor

Pole pitch τ	100.8×10^{-3}m	Yoke depth d_y	20×10^{-3}m
Magnet width w_m	67.28×10^{-3}m	Tooth/slot width w_t	8.4×10^{-3}m
Magnet coverage α	0.667	Tooth/slot height d_t	15×10^{-3}m
Magnet thickness l_m	3×10^{-3}m	Airgap length δ	0.5×10^{-3}m
Slots per pole per phase q	2	Frequency f	120 Hz

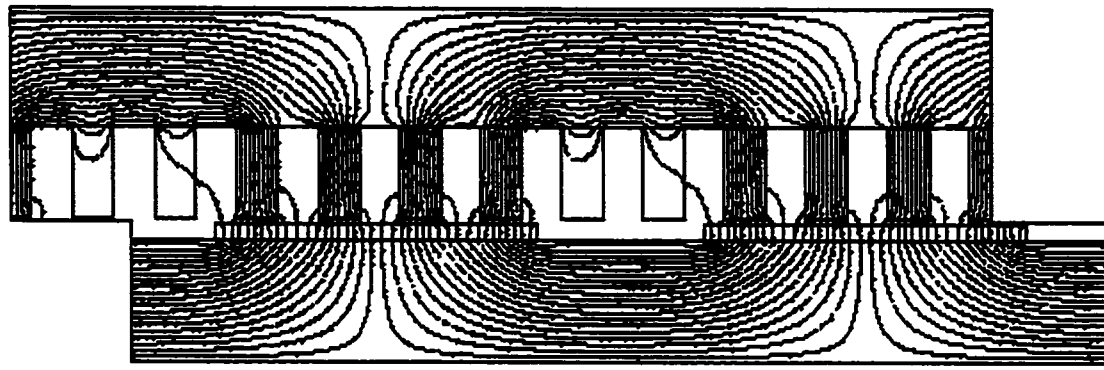

Fig.2.4 Flux distribution of the linear PM synchronous motor

Fig.2.4 shows that the magnetic field in the stator teeth over the magnets is essentially uniform and in the normal direction. The flux density in a tooth is essentially zero when it is above the middle of the space between the two magnets. The flux density is constant when it is fully covered by the magnet.

In the bottom region of the teeth where the magnetic flux passes along the teeth and emerges into the yoke, the flux turns from the normal direction into the longitudinal direction. As the magnetic flux penetrates further into the yoke, the longitudinal component begins to dominate and can be regarded as being essentially uniform in the longitudinal direction. In other words, in the yoke where it is above the space between the magnets, the flux density is mainly in the longitudinal direction. In the yoke where it is above the magnets, the flux density is mainly in the normal direction. The longitudinal flux is seen to be uniformly distributed over the thickness of the yoke while the normal flux is not.

Case II: A 4-Pole 5hp PM Synchronous Motor

As a second example, an existing 4-pole, 5hp, 1800rpm, surface mounted PM motor **(the 4-pole motor)** with dimensions shown in Table II-2 was simulated through time-stepped FEM. A cross-section of the motor along with its meshes is shown in Fig.2.5. A detailed mesh around the airgap area is shown in Fig.2.6. The field distribution of the motor during one step of the time-stepped FEM is shown in Fig.2.7.

Table II-2 Parameters and dimensions of the 4-pole motor

Airgap radius r	58.5×10^{-3}m	Tooth width w_t	5.3×10^{-3}m
Slots per pole per phase q	3	Tooth/slot height d_t	17.2×10^{-3}m
Outer radius of stator r_j	95×10^{-3}m	Airgap length δ	2×10^{-3}m
Stator length l_{fe}	76×10^{-3}m	Frequency f	60 Hz
Pole pitch τ	91.9×10^{-3}m	Number of slots S	36
Magnet coverage α	0.667	Slot opening w_o	3×10^{-3}m
Magnet thickness l_m	6.3×10^{-3}m	Teeth volume V_t	0.3802×10^{-3}m^3
Yoke depth d_y	17.4×10^{-3}m	Yoke volume V_y	0.8382×10^{-3}m^3

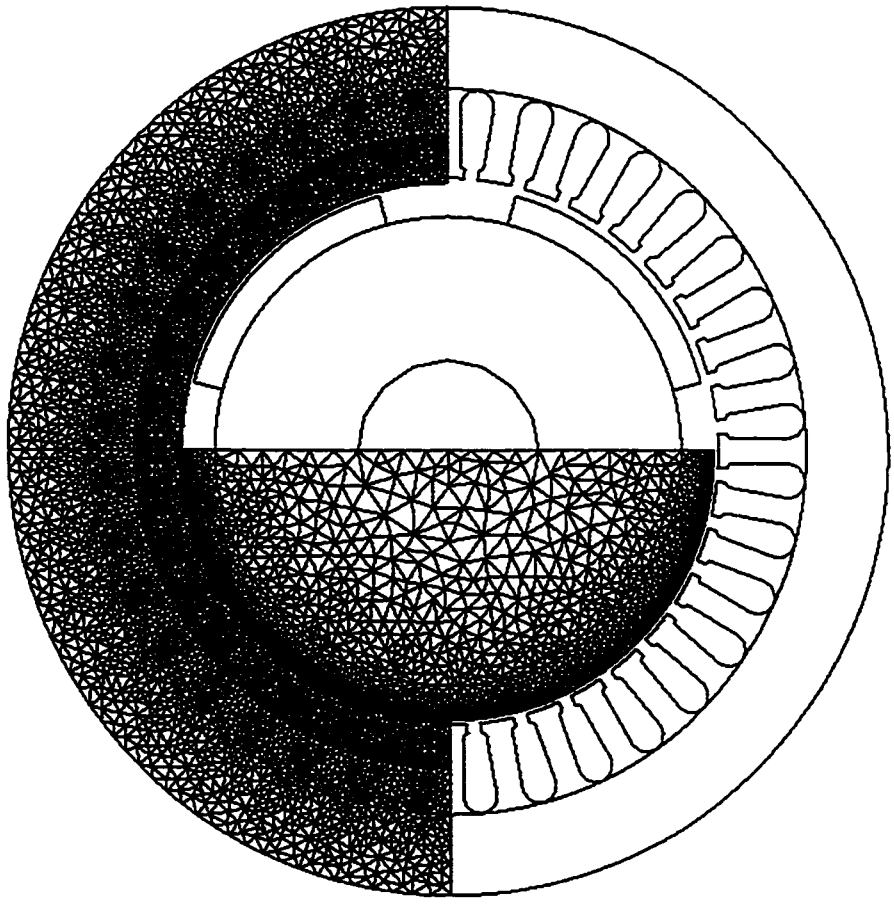

Fig.2.5 Cross-section with meshes of the 4-pole PM motor

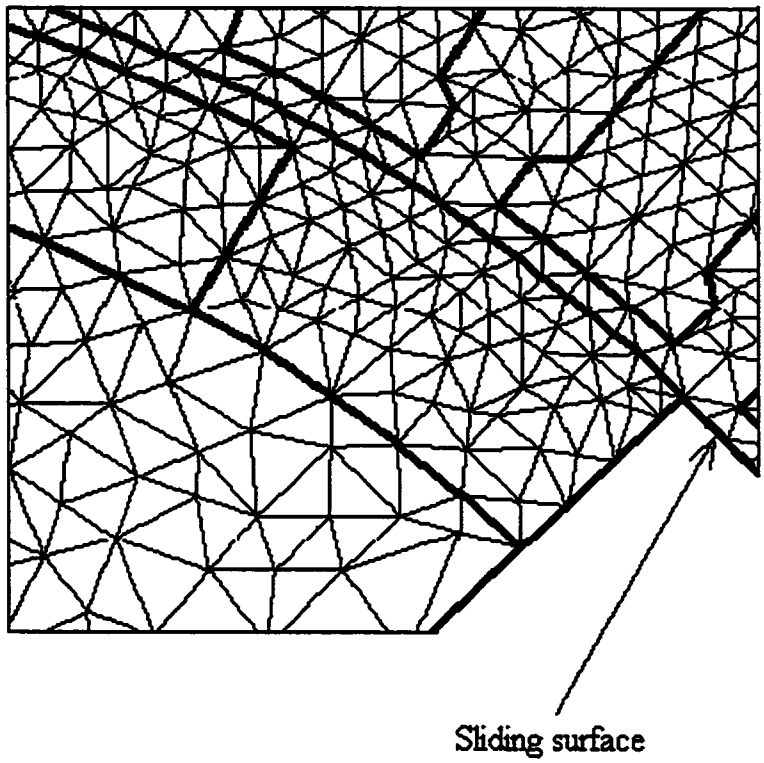

Fig.2.6 Detailed meshes around the airgap of the 4-pole motor

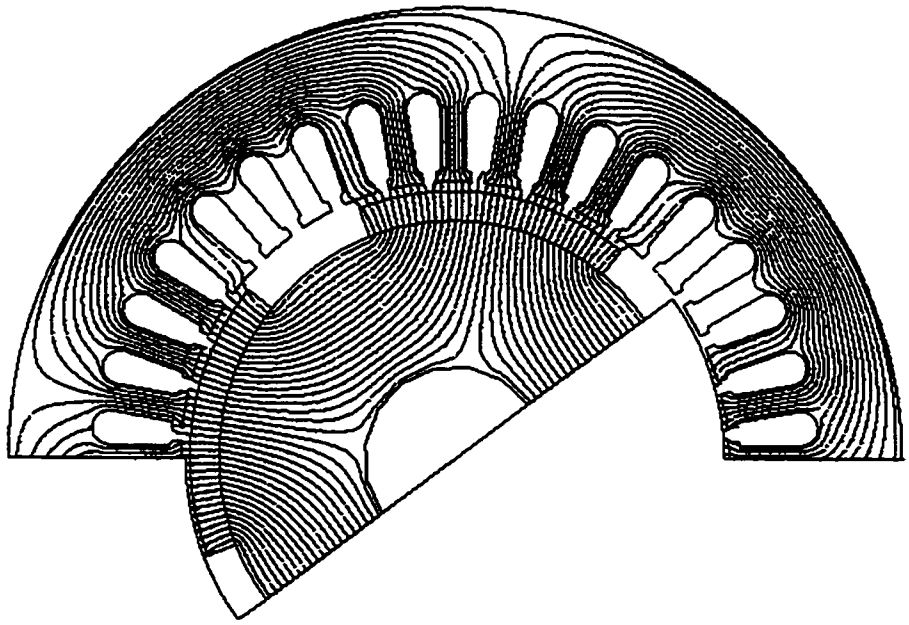

Fig.2.7 Flux distribution of the 4-pole motor

The flux patterns in Fig.2.7 shows that the magnetic field in the stator teeth of a surface-mounted PM motor is roughly uniform and is mainly in the normal direction. The flux density in a tooth remains near zero when it is not above the magnet. The flux density in a tooth reaches maximum when it is above the magnet.

The magnetic flux is partially in the circumferential direction in the shoe area of the teeth. In the region near the bottom of the teeth where the magnetic flux passes along the teeth and emerges into the yoke, the flux turns from the radial direction to the circumferential direction. As the magnetic flux penetrates further into the yoke, the circumferential component begins to dominate and can be regarded as being essentially uniform in the circumferential direction. The circumferential flux seems to be uniformly distributed over the thickness of the yoke.

Case III: An 8-pole 2.5hp PM Synchronous Motor

A third example is another available PM motor (**the 8-pole motor**) with dimensions given in Table II-3. It is an 8-pole, 2.5hp, 1800rpm, surface mounted PM motor. A cross section of the motor along with meshes and flux lines is shown in Fig.2.8.

Table II-3 Parameters and dimensions of the 8-pole motor

Airgap radius r	53×10^{-3}m	Tooth/slot height d_t	17×10^{-3}m
Outer radius of stator R	80×10^{-3}m	Airgap length δ	0.55×10^{-3}m
Stator length l_{fe}	57×10^{-3}m	Frequency f	120 Hz
Slots per pole per phase q	1	Number of slots S	24
Magnet coverage α	0.722	Pole pitch τ	41.6×10^{-3}m
Magnet thickness l_m	2.35×10^{-3}m	Slot opening w_o	2×10^{-3}m
Yoke depth d_y	10×10^{-3}m	Teeth volume V_t	0.1746×10^{-3}m^3
Tooth/slot width w_t	6.94×10^{-3}m	Yoke volume V_y	0.2686×10^{-3}m^3

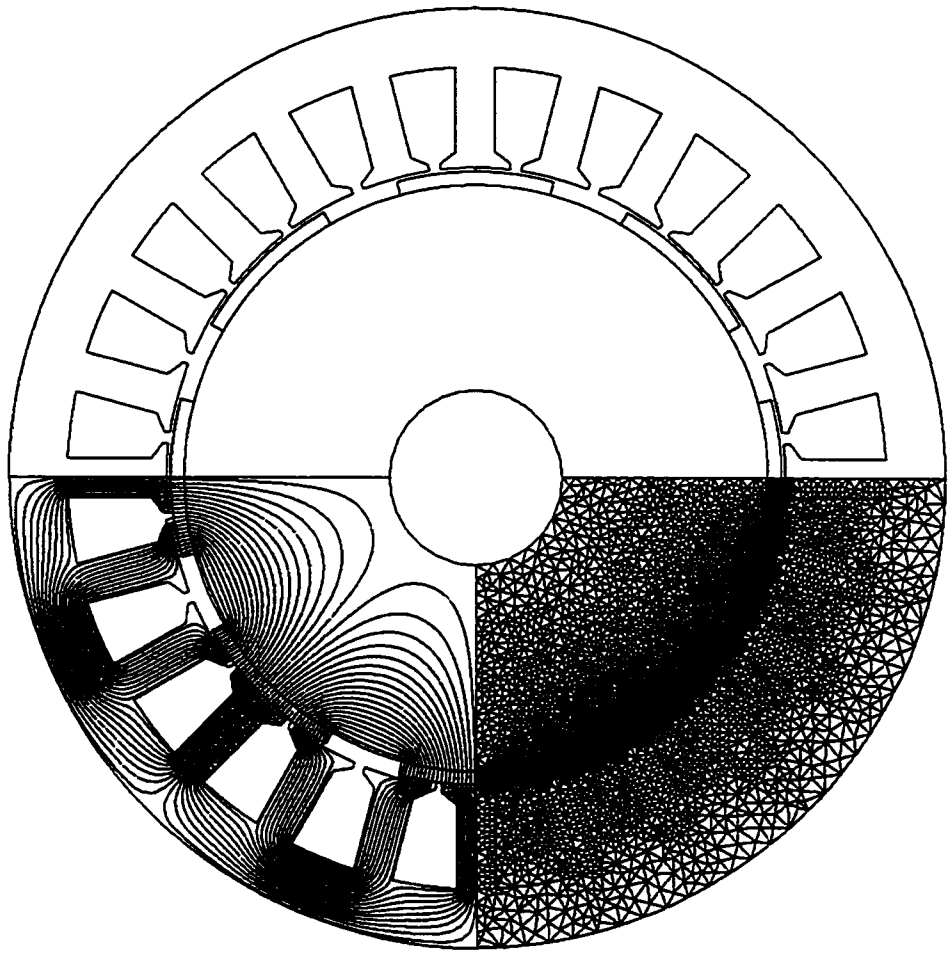

Fig.2.8 Geometry, meshes and flux distribution of the 8-pole PM motor

By observing the flux patterns in Fig.2.8, it can be concluded that the magnetic field in the teeth is mainly in the normal direction. Since this motor has only one slot per pole per phase, no tooth has zero flux during the rotation of the rotor. The flux in the tooth reaches maximum when the tooth is above the middle of the magnet.

The magnetic flux is also mainly in the circumferential direction in the shoe area of the teeth. In the yoke where it is above the magnet, the flux density is mainly in the radial direction. In the yoke where it is above the space between the magnets, the flux density is mainly in the circumferential direction.

2.5 Evaluation of Iron Losses with FEM

2.5.1 Eddy Current Loss

The eddy current loss is induced by the variation of magnetic flux, whether it is pulsating or rotating. The flux density in the core is usually decomposed into two orthogonal components and the eddy current loss can be obtained by considering the eddy current loss contributed by each component [2, 28, 29, 32]. If the magnetic field is periodic in the time domain, the eddy current loss density can be derived from (2.2):

$$p_e = \frac{2k_e}{T}\int_0^T \left|\frac{d\mathbf{B}}{dt}\right|^2 dt = \frac{2k_e}{T}\int_0^T \left(\frac{dB_x}{dt}\right)^2 dt + \frac{2k_e}{T}\int_0^T \left(\frac{dB_y}{dt}\right)^2 dt \quad (\mathrm{W/m^3}) \tag{2.24}$$

Eddy current loss can be obtained by discretizing (2.24) in the time domain when performing FEM. If the two orthogonal components of the flux density of element e in the stator iron at time instant t_n are represented by $B_{ex,n}$, $B_{ey,n}$, the square of the derivative of vector flux density **B** can be written as:

$$\left|\frac{d\mathbf{B}}{dt}\right|^2 = \left(\frac{B_{ex,n} - B_{ex,n-1}}{t_n - t_{n-1}}\right)^2 + \left(\frac{B_{ey,n} - B_{ey,n-1}}{t_n - t_{n-1}}\right)^2, \qquad n = 1, 2, \cdots, N \tag{2.25}$$

where N is the total number of steps used for time-stepped FEM analysis in a half period.

When performing time stepped FEM, the whole stator is divided into a number of elements. The flux density of each element at each time instant can be determined. If only a half period is analyzed, the time interval between two consecutive FEM steps is

$$\Delta t = t_n - t_{n-1} = \frac{T}{2N} = \frac{1}{2Nf}, \qquad n = 1,2,\cdots N \tag{2.26}$$

where f is the frequency of the magnetic field.

Substituting (2.25) and (2.26) into (2.24), the total eddy current loss can be expressed as:

$$P_e = 4pN k_e l_{fe} f^2 \sum_{e=1}^{E} A_e \left[\sum_{n=1}^{N} (B_{ex,n} - B_{ex,n-1})^2 + \sum_{n=1}^{N} (B_{ey,n} - B_{ey,n-1})^2\right] \quad \text{(W)} \quad (2.27)$$

where A_e is the area of element e, E is the total number of elements of the stator core and l_{fe} is the stack length of the stator.

2.5.2 Hysteresis Loss

Assuming no minor loops, hysteresis loss is proportional to the quasi-static hysteresis loop area times the frequency and is therefore not affected by the shape of flux density. For a given material, once the peak flux density of each element has been found, the hysteresis loss can be obtained. Hysteresis loss can be approximated from experiments by [22]:

$$p_h = k_h \omega_s B^{\beta} \quad \text{(W/m}^3\text{)} \quad (2.28)$$

By performing time-stepped FEM analysis, the peak value of flux density $B_{e,max}$ during a period in each element can be found. The hysteresis loss in the stator is:

$$P_h = k_h \sum_{e=1}^{E} [A_e l_{fe} B_{e,\max}^{\beta} \omega_s] = 2\pi k_h l_{fe} f \sum_{e=1}^{E} [A_e B_{e,\max}^{\beta}] \quad \text{(W)} \quad (2.29)$$

2.5.3 Total Iron Losses

The total iron losses in the stator are the sum of hysteresis loss and eddy current loss:

$$P_{iron} = P_e + P_h \quad \text{(W)} \quad (2.30)$$

Actual iron losses can be predicted for different regions of the motor using FEM. The results can then be used to develop and validate simplified iron loss models.

Chapter 3

Simplified Iron Loss Model

Although time-stepped FEM can provide good estimations of iron losses, time-stepped FEM itself remains a cumbersome tool and very time-consuming for most designs and particular for optimizations. FEM analysis can only be performed after the machine geometrical dimensions have been determined. Repeated FEM is not practical for the preliminary design of an electrical motor with its many iterations in geometry.

In contrast, approximate analytical loss models yield quick insight while requiring much less computation time and are readily available during the preliminary stage of a motor design. Therefore, it is desirable to develop iron loss models that will produce an acceptable prediction of overall iron losses in a relatively simple way and provide machine designers with a more reliable method to estimate iron losses in the initial design of PM machines.

In this chapter, the iron losses of a PM synchronous motor will be decomposed into four components to develop simplified models respectively: tooth eddy current loss, yoke eddy current loss, tooth hysteresis loss and yoke hysteresis loss. Simplified models for the estimation of tooth and yoke eddy current losses are developed based on the observations of FEM results and analytical analyses of the magnetic field taking into account detailed geometrical effects. The assumptions made in [8] will be examined. The effectiveness and limitations of the models will be investigated. Correction factors will be derived for geometrical influences and the losses induced by the minor component of the flux density.

3.1 Review of Analytical Iron Loss Model

A simple analytical iron loss model, developed by Slemon and Liu [8], has been used by a few authors to determine the iron losses of PM synchronous motors [9-10, 30-32].

In the preliminary study on iron losses of surface mounted PM motors in [8], a number of tentative conclusions were derived:

- The eddy current loss was assumed to be dependent on the square of time rate of change of the flux density vector in the stator core.

- The tooth eddy current loss was assumed to be concentrated in those teeth which are near the edges of the surface-mounted magnets and thus was independent of the angular width of magnets.

- The flux density in a tooth was assumed to be approximately uniform.

- As the magnet rotates, the flux density in a stator tooth at the leading edge of the magnet was assumed to rise linearly from zero to a maximum and then remain essentially constant while the magnet passes. At the lagging edge, the tooth flux drops from maximum to zero in the same pattern.

- The rise or fall time of the tooth flux density was assumed to be the time interval for the magnet edge to traverse one tooth width.

- For a given torque and speed rating, the tooth eddy current loss was stated as approximately proportional to the number of poles divided by the width of a tooth. Alternatively, the tooth eddy current loss was approximately proportional to the product of poles squared and slots per pole per phase.

- For a given frequency, the tooth eddy current loss was stated to be proportional to the number of slots per pole per phase.

- The eddy current loss in the stator yoke was approximated using only the circumferential component of yoke flux density.

While the overall application of these approximations produced an acceptable prediction of the total measured losses in an experimental machine, the validity of each individual approximation remained in doubt. The uncertainties in these models are (1). The validity and accuracy of the derived flux waveform, both in the teeth and in the yoke. (2). The error caused by only using the magnitude of the flux density. (3). The error caused by neglecting geometry effects on flux waveforms and eddy current loss of the motors.

In this chapter, these assumptions are examined in turn and their results are compared with those obtained by time-stepped FEM.

3.2 Test of Linear Waveforms of Tooth Flux Density

In order to examine and refine the assumptions made in [8], the tooth flux density waveforms were obtained by time stepped FEM on the linear PM motor shown in Fig.3.1. The tooth marked *1* in Fig.3.1(a) is taken as an example to obtain the tooth flux density waveform. The flux density in the tooth is obtained as a function of distance x, where x is defined as the distance from the middle of tooth to the middle of the space between the two poles. It can be seen from Fig.3.1 that:

- The flux density in the tooth remains zero when the tooth is above the middle of the space between the two poles (x=0) as shown in Fig.3.1(a).

- The flux increases when the front edge of the magnet approaches the tooth (x=τ/6) as shown in Fig.3.1(b). The flux keeps increasing when the magnet edge passes the tooth (x=τ/3) as shown in Fig.3.1(b) and Fig.3.1(c)

- The flux approaches a maximum when the front edge of the magnet leaves the tooth

(x=τ/3) as shown Fig.3.1(c).

- The flux in the tooth remains constant when it is above the magnet (x=τ/2) as shown in Fig.3.1(d)

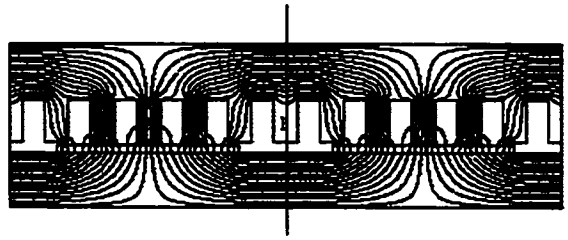

(a). When the tooth is above the middle of the two poles (x=0)

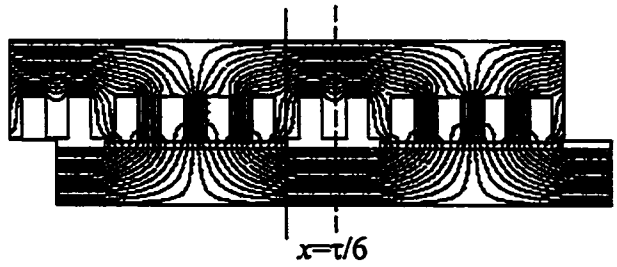

(b). When the magnet reaches the middle of the tooth

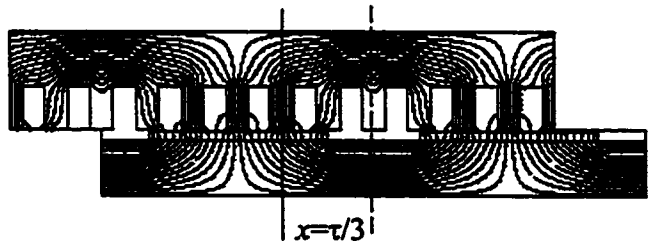

(c). When the tooth is covered by magnet

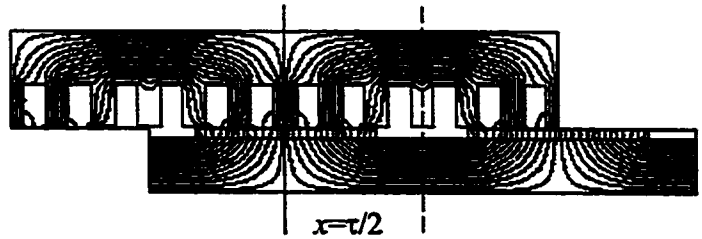

(d). When the tooth reaches the middle of the pole

Fig.3.1 Change of flux in a tooth of the linear PM motor

The calculated waveform by FEM for the normal component of the flux density in the

center of a tooth is shown in Fig.3.2. It can be seen from Fig.3.2 that the rise of the flux density follows almost a linear pattern except at the beginning and end of the change.

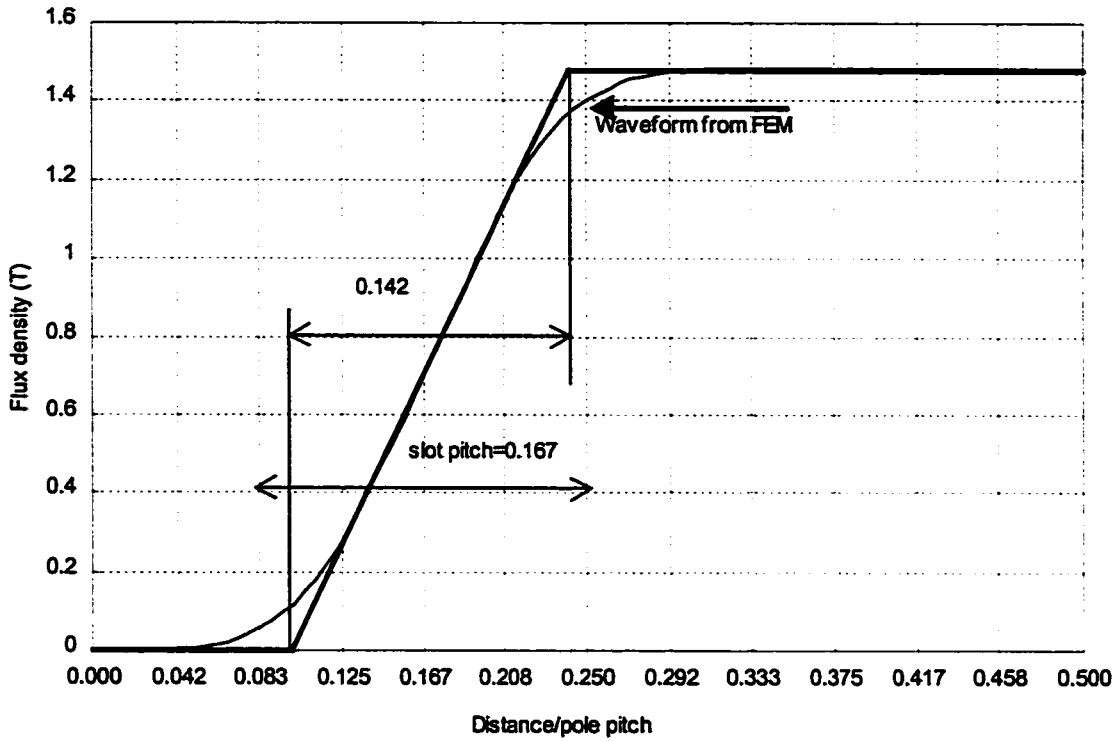

Fig.3.2 Waveform of the normal component of tooth flux density

If the slope of the linear part of the flux density waveform is taken and extended from zero to maximum flux density as shown in Fig.3.2, the distance needed for the flux density to rise is 0.142 pole-pitch or 0.852 slot-pitch.

In [8], it was suggested that the rise of the tooth flux density takes one tooth width or 0.5 slot-pitch for configurations with equal slot and tooth width. The approximated flux density waveform suggested in [8] is compared with the flux density waveform obtained by FEM as shown in Fig.3.3. It can be seen that the rise of flux density takes much longer time than suggested in [8].

Although the linear approximation in Fig.3.2 better reflects the rise pattern of the tooth flux density, the calculated tooth eddy current loss by this linear approximation is expected to

be larger than that calculated by FEM because the actual flux rises slower at the beginning and end of the change.

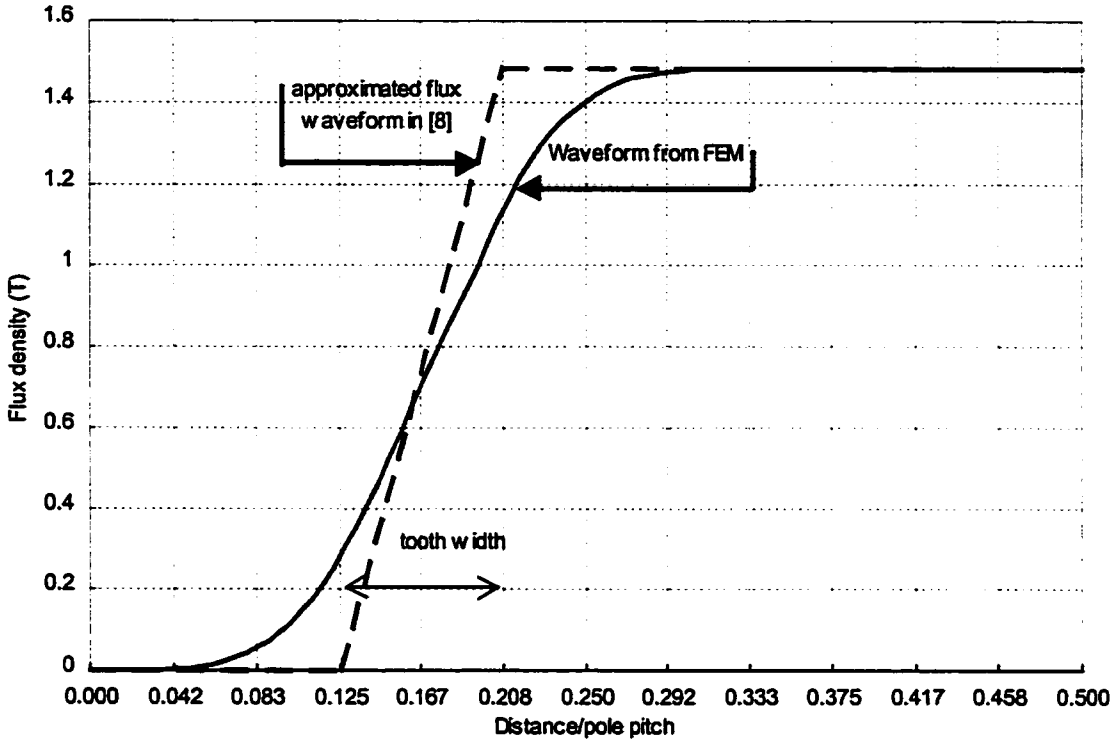

Fig.3.3 Comparison of tooth flux density waveform with that suggested in [8]

Fig.3.4 introduces the assumption that the observed flux density waveform from FEM rises in approximately the time needed for the magnet edge to traverse one slot pitch in contrast to a tooth width as assumed in [8]. The assumption can be tested as follows.

Suppose that the waveform of the normal component of the tooth flux density can be represented by a linear approximation as shown in Fig.3.4. This linear approximation produces the same eddy current loss as the actual flux density waveform. The rise time of flux density for this approximation can be obtained by comparing the eddy current loss calculated by FEM and the eddy current loss calculated by the linear approximation.

The rise time of the linear approximation is Δt and the change happens four times per period. The eddy current loss induced by the normal component of this approximation is:

$$P_{etr,APP} = \frac{2k_e}{T} V_t \int_0^T \left(\frac{dB_x}{dt}\right)^2 dt = \frac{2k_e}{T} \left(\frac{B_{th}}{\Delta t}\right)^2 (4\Delta t) V_t = \frac{8k_e}{T} \frac{B_{th}^2}{\Delta t} V_t \text{ (W)} \tag{3.1}$$

where V_t is the volume of the teeth, B_{th} is the plateau value of the normal component of tooth flux density, which is essentially the same as the magnitude of the tooth flux density.

A conclusion can also be drawn from (3.1) that the eddy current loss is inversely proportional to the rise time of the linear approximated flux density.

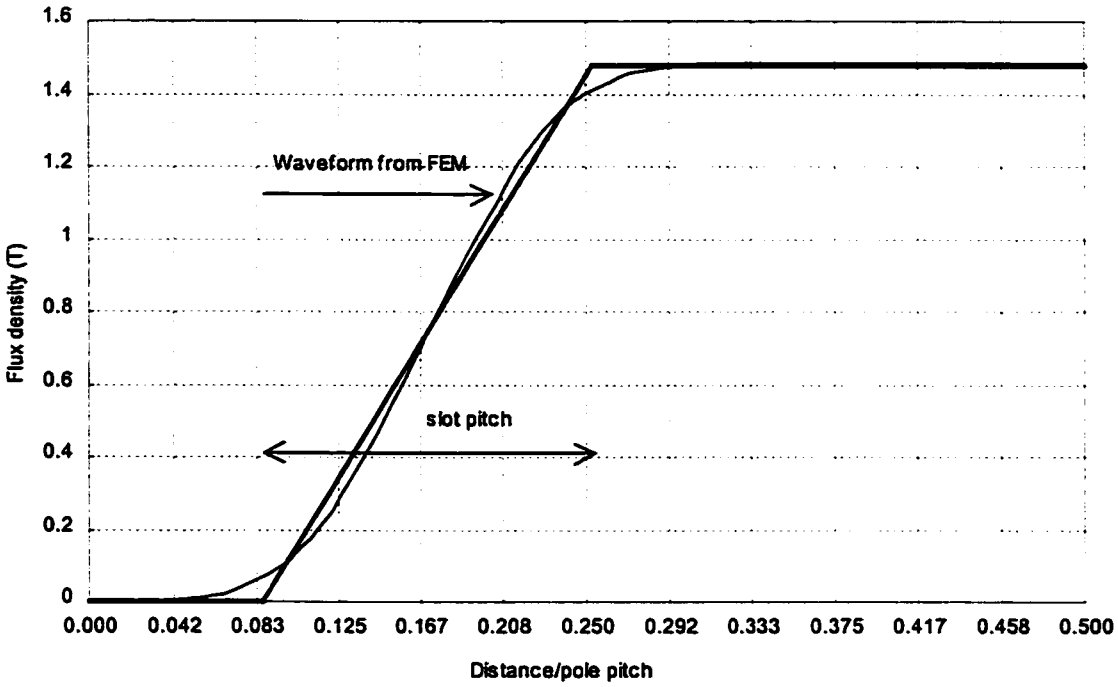

Fig.3.4 Approximation of tooth flux density waveform

The rise time for the linear flux can be determined by (3.1) using the eddy current loss calculated by FEM:

$$\Delta t = \frac{8k_e}{T} \frac{B_{th}^2 V_t}{P_{etr,FEM}} \tag{3.2}$$

where $P_{etr,FEM}$ is the eddy current loss induced by the normal component of tooth flux density calculated by FEM.

The distance Δx that the magnet travels during Δt can be obtained. Since it takes half a period for the magnet to traverse a pole-pitch, a half period in the time domain is equivalent to one pole-pitch in distance domain, e.g.,

$$\frac{\Delta x}{\tau} = \frac{\Delta t}{T/2} \tag{3.3}$$

Therefore, when expressed in the distance domain, the distance needed for the normal component of tooth flux density to rise from zero to maximum is

$$\Delta x = \tau \cdot \frac{16 k_e}{T^2} \frac{B_{th}^2 V_t}{P_{etr.FEM}} \tag{3.4}$$

In Table III-1, the distance needed for the normal component of tooth flux density to rise from zero to the plateau value is calculated by (3.4) and compared to that measured on Fig.3.2 and that suggested in [8]. There are 6 slots per pole. So one slot pitch is 0.167 pole-pitch. It can be seen from Table III-1 that the equivalent distance for the normal component of tooth flux density to rise from zero to the plateau value is approximately one slot pitch. Therefore, the suggestions in [8] are not appropriate.

Table III-1 Distance needed for tooth flux to rise from zero to plateau

Method	Obtained by (3.4)	Measured on Fig.3.2	Suggested in [8]
$\Delta x/\tau$	0.1600	0.1420	0.0833
$\Delta x/\lambda$	0.960	0.852	0.500

Table III-2 shows the eddy current loss induced by the normal component of tooth flux density calculated by different methods.

Table III-2 Eddy current loss induced by the normal component of tooth flux density

Method used	Use FEM	Use slot pitch	Use actual slope	Use sinusoidal	Suggested in [8]
Eddy current loss at 120Hz or 12.1m/s (W)	72.7	70.4	82.4	29.0	142.1
Error (%)	-	-3.1	13.4	-60.1	95.5

It can be seen from Table III-2 that

- When the distance needed for the tooth flux density to rise is assumed to be one slot pitch, the calculated loss is close to that calculated by FEM (error of 3.1%).
- When the distance needed for tooth flux density to rise is assumed to be the extension of the linear part of tooth flux waveform, the calculated loss is about 13% more than that calculated by FEM.
- When the flux density is assumed to be sinusoidal with the plateau flux density as its magnitude, the eddy loss is less than a half of that calculated by FEM.
- When the distance needed for tooth flux density to rise is assumed to be a tooth width, the calculated loss is almost twice of that calculated by FEM.

Therefore, it can be concluded from the above observations that:

- The waveform of the normal component of tooth flux density can be approximated by a linear trapezoidal waveform.
- The rise time of the normal component of tooth flux density is approximately the time needed for the magnet edge to traverse one slot pitch. Alternatively, the distance needed for the tooth flux density to rise from zero to plateau value is approximately one slot pitch.

3.3 Simplified Tooth Eddy Current Loss Model

3.3.1 Eddy Current Loss Induced by the Normal Component

As it has been shown in the last section, the waveform of the normal component of the tooth flux density in a surface-mounted PM synchronous motor can be approximated by a simple trapezoidal waveform as shown in Fig.3.5 for an open slot PM motor.

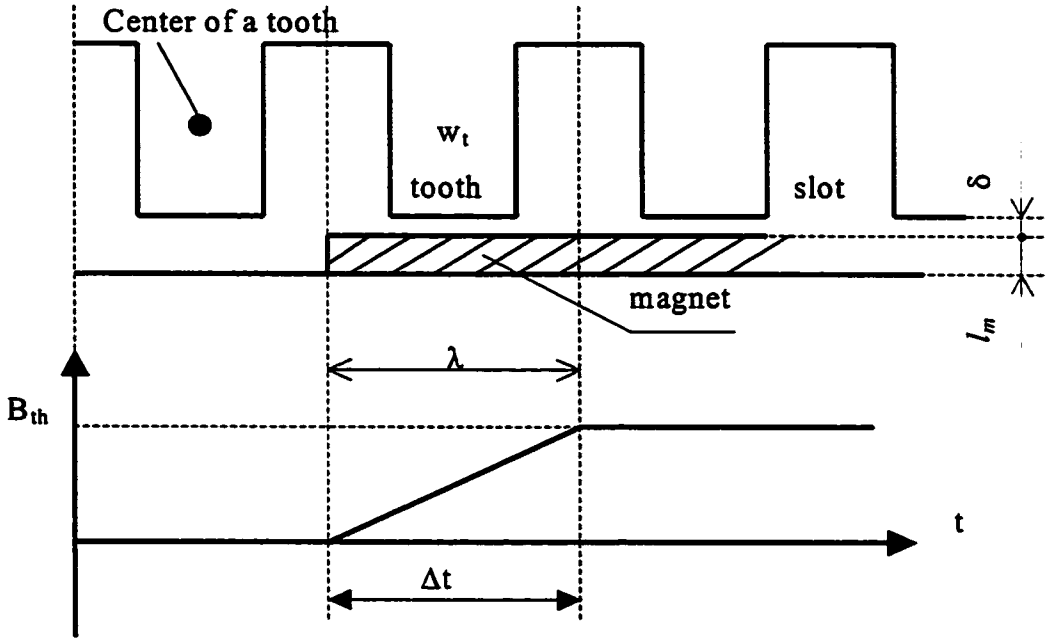

Fig.3.5 Approximation of the normal component of tooh flux density

The time interval for the approximated normal component of tooth flux density to rise from zero to plateau is approximately the time for the magnet edge to traverse one slot pitch. For an *m*-phase PM motor with *q* slots per pole per phase, there are *mq* slots per pole. Therefore, the time needed for the magnet edge to traverse one slot pitch is

$$\Delta t = \frac{T}{2} \frac{1}{mq} \tag{3.5}$$

Substituting (3.5) to (3.1), the eddy current loss induced by the normal component of

tooth flux density can be approximated for three-phase motors:

$$P_{etr} = 16mqk_e(fB_{th})^2 = \frac{12}{\pi^2}qk_e(\omega_s B_{th})^2 V_t \quad \text{(W)} \tag{3.6}$$

The total tooth eddy current loss can be further written as a function of speed n:

$$P_{etr} = \frac{qp^2}{300}k_e B_{th}^2 n^2 V_t \tag{3.7}$$

It can be inferred from (3.6) and (3.7) that:

- The eddy current loss induced by the normal component of the tooth flux density is proportional to the number of slots per pole per phase q for given frequencies. Increasing q will dramatically increase the tooth eddy current loss.

- For given torque and speed ratings, the tooth eddy current loss induced by the normal component is approximately proportional to the product of poles squared and slots per pole per phase.

3.3.2 Effect of Slot Closure

The previous model was based on an open-slot configuration. In order to test the linear assumption of the rise and fall of the normal component of tooth flux density, the effect of slot closure is now studied. Fig.3.6 illustrates the slot closure of an electrical machine. The opening at the surface of the slots is w_O. The relative closure γ can be defined as the ratio of slot closure to slot pitch:

$$\gamma = \frac{\lambda - w_t - w_o}{\lambda} \tag{3.8}$$

FEM was performed on the linear PM motor by varying slot closure but keeping other dimensions constant. The waveforms of the normal component of the tooth flux density at the center of the tooth are shown Fig.3.7 for different slot closure.

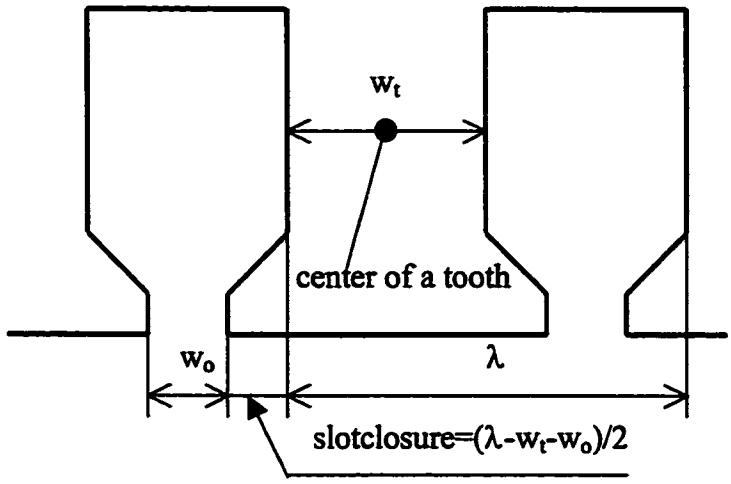

Fig.3.6 Illustration of slot closure

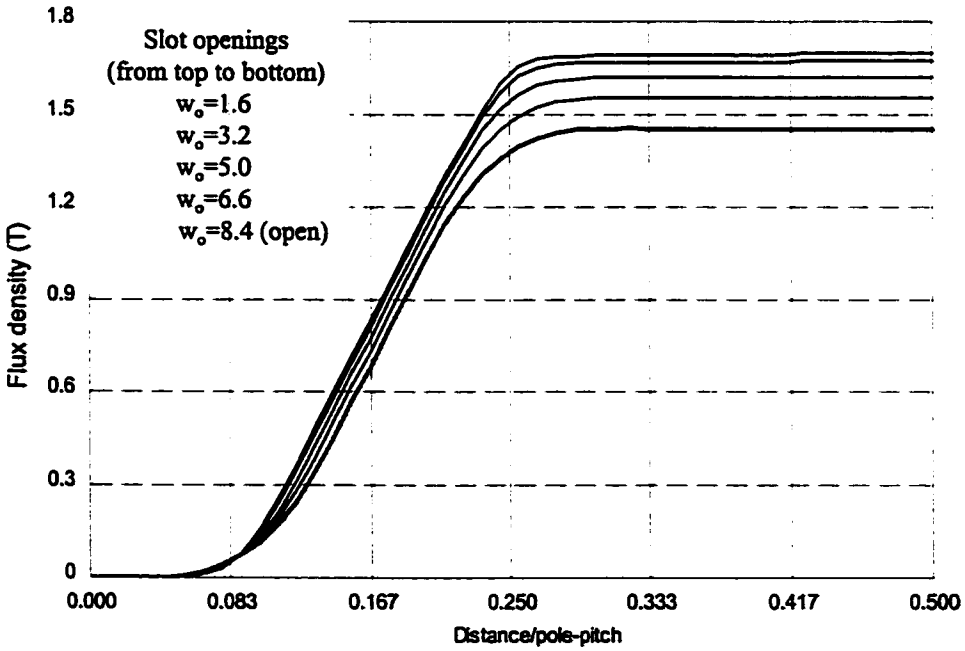

Fig.3.7 Effect of slot closure on tooth flux density at the center of a tooth

It can be seen from Fig.3.7 that when slot closure or slot opening changes, the achieved plateau value of the normal component of tooth flux density waveform also changes due to the change of effective airgap reluctance.

In order to compare the rate of rise of the normal component of tooth flux density against slot closure, the tooth flux density was normalized to the same value for different slot closure as shown in Fig.3.8. The normalized waveforms of the normal component of tooth flux density show that the slope is approximately independent of slot closure with only a slight decrease in slope as the slot is closed.

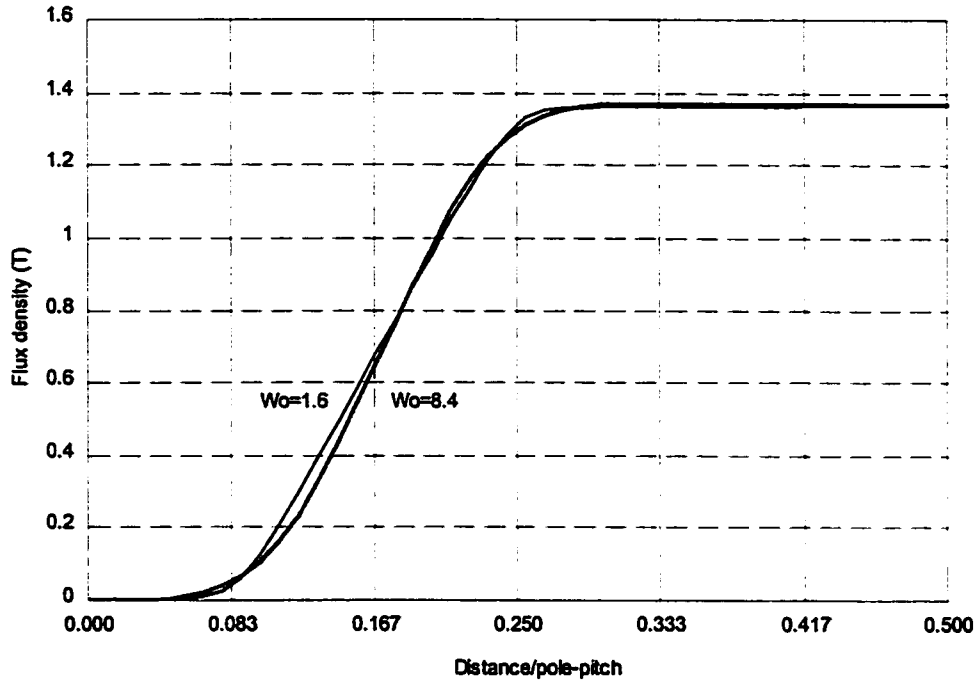

Fig.3.8 Tooth flux density waveform for different slot closure

The effect of slot closure was also studied on configurations by changing magnet thickness and airgap length. Based on normalized plateau flux density, the tooth eddy current losses were calculated by FEM for different slot closures and shown in Fig.3.9 for two cases with different magnet thickness of 3mm and 6mm. It can be seen that the tooth eddy current loss slightly increases as the slot closure decreases. The increase of eddy current loss is less than 3% when slot closure changes from 1.6mmm to 8.4mm based on normalized tooth flux density. This small increase of eddy current loss in the tooth is consistent with the small change of slope of the normal component of tooth flux density as seen from Fig.3.8. Therefore, it can be concluded that the approximation model is independent of slot closure.

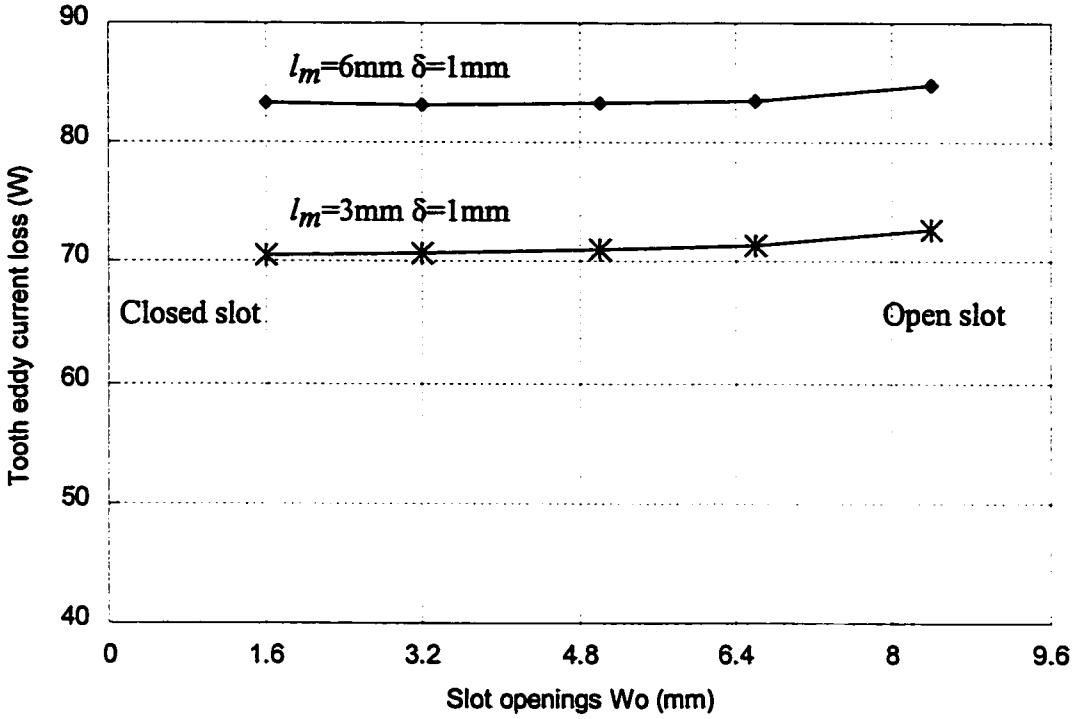

Fig.3.9 Effect of slot closure on tooth eddy current loss

3.3.3 Effect of Magnet Width

In the approximation model, tooth eddy current loss is assumed to occur only when there is a change in the normal component of tooth flux density when those teeth pass the magnet edges. It follows that the loss would be independent of the angular width of magnet.

In order to test whether the tooth eddy current is independent of the angular width of magnet, FEM analyses were performed on the linear PM motor such that the width of the magnets was changed by keeping the same number and shape of slots.

The first example was the linear PM motor with 2 slots per pole per phase. Fig.3.10 shows a quarter of a period (a half pole pitch) of the waveform of the normal component of the flux density in the center of a tooth when the magnet coverage was changed from α=0.167 to α=0.990. The parallel lines are drawn to show the slope of the flux.

It can be seen from Fig.3.10 that, when the magnet coverage is within the range of α=0.167 to α=0.833, the major part of the flux waveform follows a linear pattern with the same slope and same plateau. The linear approximation of the flux density needs 0.142 pole-pitch to rise from zero to plateau value. Although the slope is the same, the flux density does not reach the plateau value when the magnet coverage falls to α=0.167 or the magnet width is one slot-pitch.

The slope of the flux density waveform starts to increase when the magnet coverage is increased beyond α>0.833 or the space between the two magnets is less than one slot-pitch. The increase in slope of flux density suggests that the simplified tooth eddy current loss model is not valid beyond α>0.833.

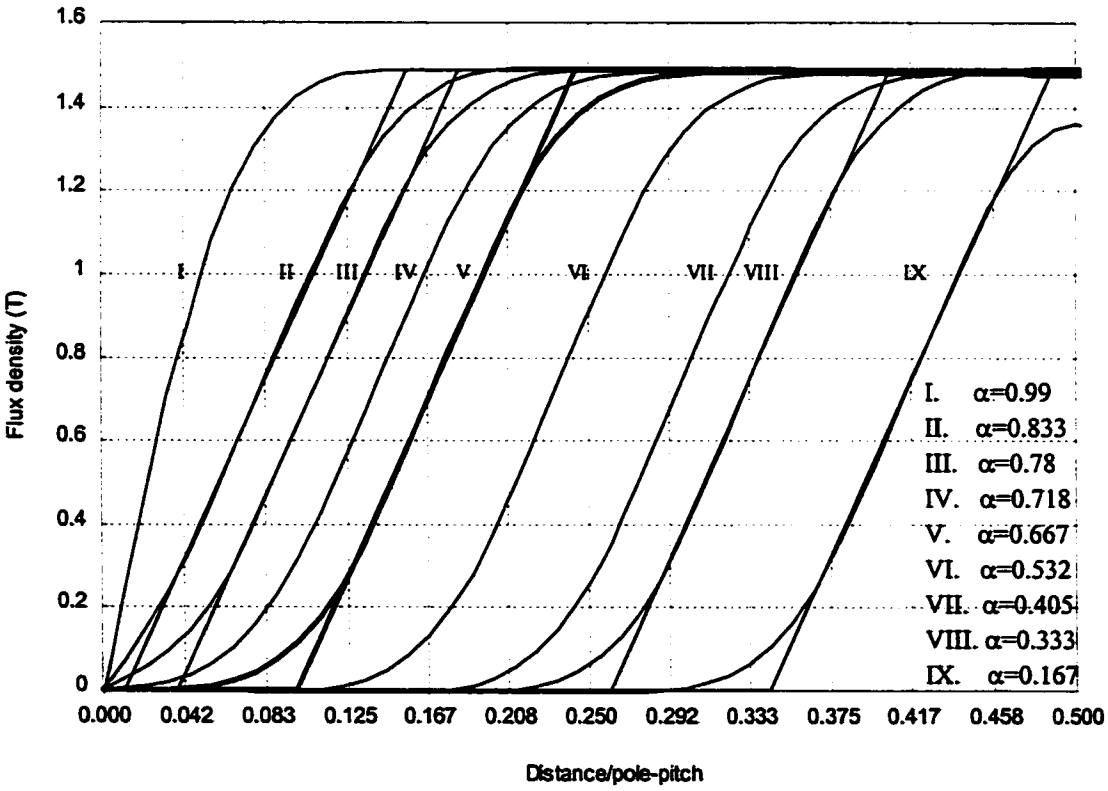

Fig.3.10 Waveform of the normal component of tooth flux density (q=2)

As a second example, FEM was performed on a linear PM machine with q=1 (3 slots

per pole). The waveforms of the normal component of the tooth flux density at the center of a tooth are shown in Fig.3.11.

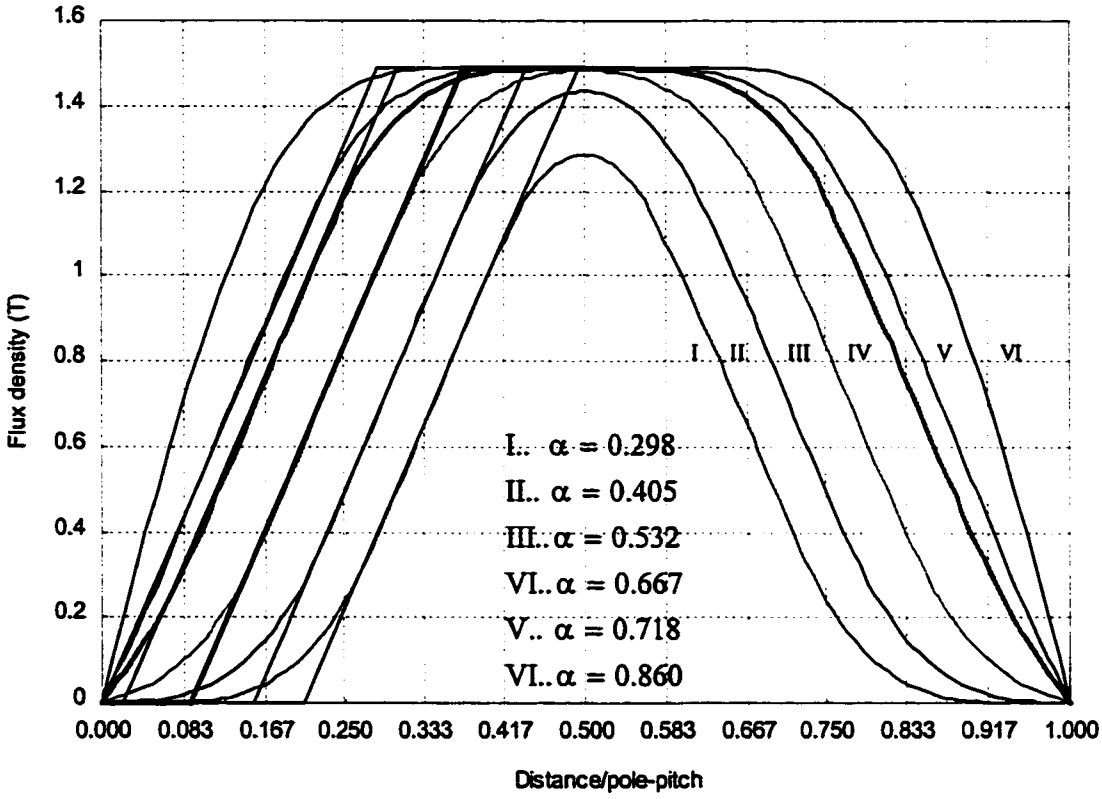

Fig.3.11 Waveform of the normal component of tooth flux density (q=1)

In Fig.3.11, five parallel lines are also drawn to show the slope of the linear part of the flux waveforms. It can be seen that, for different magnet widths, the flux waveform follows a linear pattern with the same slope except for the widest magnet coverage α=0.860. The distance needed for normal component of tooth flux density to rise at constant is again 0.284 pole-pitch (or 0.852 slot-pitch). For different magnet widths, the tooth flux density is seen to have the same plateau value except for the narrow magnet widths of α=0.298 and α=0.405.

It can be concluded from the above observations that over a wide range of magnet width, the slope of the linear part of tooth flux and the plateau value of the tooth flux density are constant. When the magnet width is less than about a slot pitch, the normal component of the

flux density in the tooth will not reach the plateau as other cases do. When the space between the two magnets is less than about a slot pitch, the slope of the normal component of tooth flux density is considerably increased.

The tooth eddy current losses for the linear PM motor with different magnet widths shown in Fig.3.10 were calculated using FEM and shown in Fig.3.12.

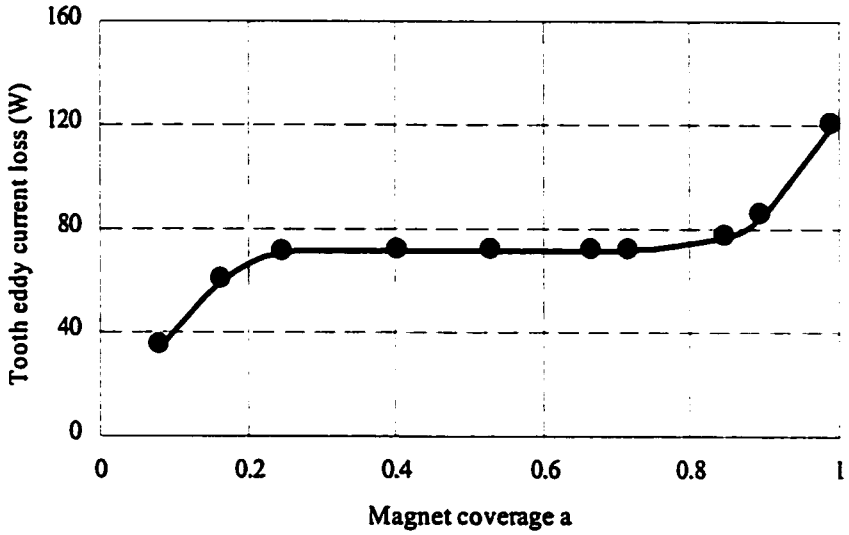

Fig.3.12 Tooth eddy current loss vs. magnet width (q=2)

The losses shown on Fig.3.12 further confirm that the tooth eddy current loss remains substantially constant as the magnet width is varied over a wide range.

For the impractical cases with a magnet coverage less than 0.25, the loss decreases because the flux density doses not reach a plateau.

When the space between the two magnets is less than about one a slot pitch, the eddy current loss is seen to be considerably increased. The effect of the adjacent magnets is to increase the slope of the normal component and eliminate the slow rise of flux density in the region near zero tooth flux density.

A significant conclusion about magnet width is that the tooth eddy current loss is

dramatically increased as shown in Fig.3.12 when magnet coverage approaches 1.0 because of the significant increase of the slope of tooth flux density as shown in Fig.3.10. The increase in loss is more than 50% with 180° magnets only for the normal component of tooth flux density. Therefore, motors with 180° magnets should be avoided in the design of a PM motor in contrast to that suggested in [33].

3.3.4 Effect of Slots Per Pole Per Phase with Fixed Slot Pitch

In order to confirm that the tooth eddy current loss is approximately proportional to the number of slots per pole per phase for given frequency, FEM was performed on a linearly arranged PM motor such that the number of slots per pole per phase is varied with fixed slot pitch λ. In other words, the pole pitch τ is changed according to the number of slots per pole as shown in Fig.3.13 (q is changed from 1 to 4). To simplify the analysis, the magnet coverage is kept constant at 0.667 and the open slot configuration is used.

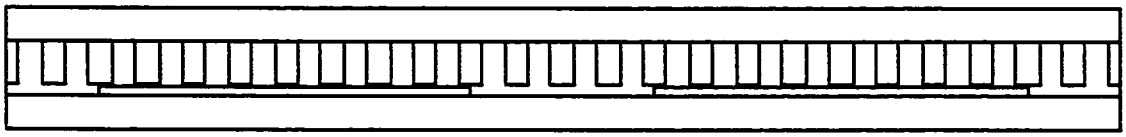

(a). q=4

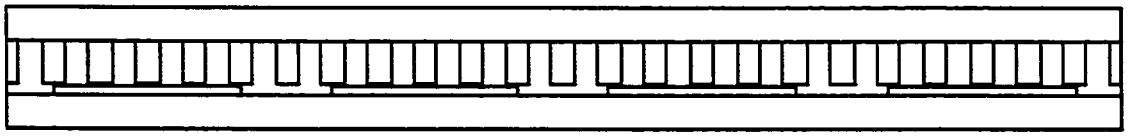

(b). q=2

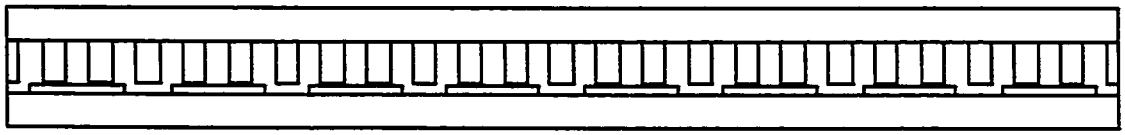

(c). q=1

Fig.3.13 Configuration of linear motors performed by FEM, varying q and p

On a linear machine with fixed frame, increasing q means the reduction of number of poles if the slot pitch is fixed. In order to be comparable, the tooth eddy current loss is calculated for fixed frequency and fixed speed respectively.

The waveforms of the normal component of the tooth flux density for q=1 and q=2 are shown in Fig.3.14 when plotted as a function of pole pitch. The distance needed for the flux to rise can be measured as listed in Table III-3.

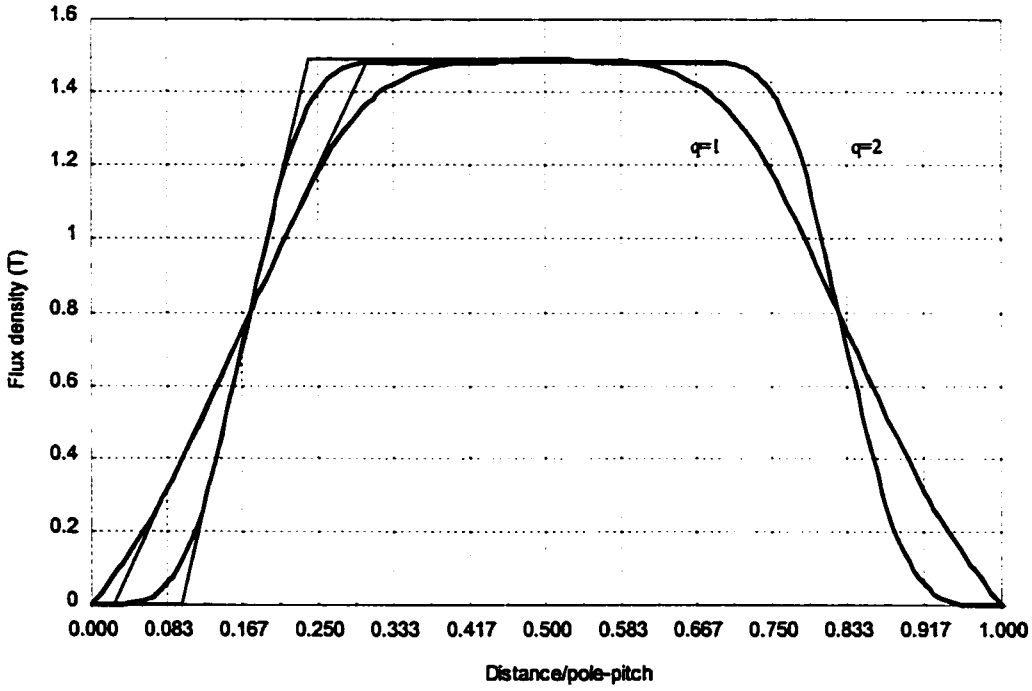

Fig.3.14 Tooth flux waveforms for different q with the same slot pitch when plotted as a function of pole-pitch

Table III-3 Distance needed for the normal component of tooth flux density to rise

Slots per pole per phase q	1	2	3	4
Distance needed (in pole-pitch)	0.284	0.142	0.095	0.071
Distance needed (in slot-pitch)	0.852	0.852	0.852	0.852

It can be seen from Table III-3 that, since the two cases have different pole-pitches, the distances are different for different q when expressed as a fraction of pole pitch. However, when expressed as a fraction of slot pitch, the distances needed for the normal component to rise from zero to plateau is seen to be the same. Therefore, it is desirable to plot the flux waveforms as functions of slot pitch as shown in Fig.3.15. It can then be seen that for the two cases, the waveforms of the tooth flux density have the same slope. It can also be seen from both Table III-3 and Fig.3.15 that the linear approximation to the rise of the normal component of the tooth flux density takes 0.852 slot-pitch no matter how many teeth per pole per phase.

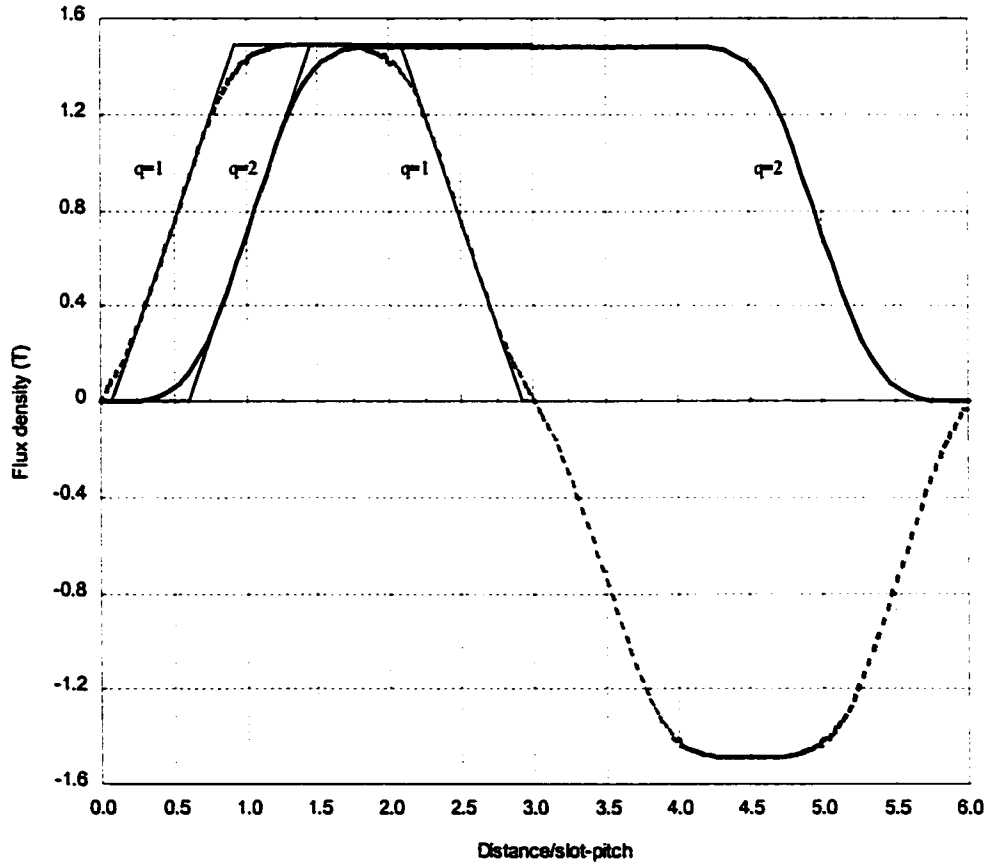

Fig.3.15 Tooth flux waveforms for different q with the same slot pitch when plotted as a function of slot pitch

Table III-4 shows the calculated tooth eddy current loss by FEM with fixed frequency. Row 4 of Table III-4 shows that the ratio of tooth eddy current loss the number of slots per pole

per phase (P_{etr}/q) is nearly constant. Therefore, equation (3.6) is validated: **the tooth eddy current loss is proportional to the number of slots per pole per phase for a given frequency.**

Table III-4 Eddy current loss in the teeth when changing the number of poles (f=60Hz)

Slot number per pole per phase q	1	2	4
Number of poles p	8	4	2
Eddy current loss by FEM (W)	18.1	36.4	72.9
P_{etr}/q	18.1	18.2	18.2
Speed (m/s)	3	6	12

The tooth eddy current loss is also calculated at fixed speed as shown in Table III-5. It is shown in Table III-5 that the ratio of tooth eddy current loss to the product of number of poles squared and the number of slots per pole per phase (P_{etr}/qp^2) is nearly constant. Therefore, equation (3.7) is validated: **the tooth eddy current loss is proportional to the product of poles squared and the number of slots per pole per phase for a given speed.**

Table III-5 Eddy current loss in the teeth when changing the number of poles (v=6m/s)

Slot number per pole per phase q	1	2	4
Number of poles p	8	4	2
p^2q	64	32	16
Eddy current loss by FEM P_{etr} (W)	72.4	36.4	18.2
P_{etr}/p^2q	1.131	1.133	1.139
Frequency (Hz)	120	60	30

The conclusions made from Table III-4 and Table III-5 are true for a given number and size of slots when the number of poles is to be selected as shown in Fig.3.13. The effects of

number of slots per pole per phase for motors with a given number of poles will be studied in Section 3.3.6.

3.3.5 Effect of Airgap Length and Magnet Thickness

It is shown in Section 3.2 that, for the linear PM motor, using slot pitch as the distance needed for the rise of the normal component of tooth flux density gave quite good estimation of the eddy current loss induced by the normal component of tooth flux density. In this section, the effect of variations of airgap length and magnet thickness is investigated. For each combination of the two dimensions, a correction factor k_q is evaluated based on FEM loss analysis.

Suppose that after introducing the correction factor k_q, the approximated eddy current loss is the same as that obtained by FEM, then

$$P_{etr.APP} = k_q \cdot \frac{12}{\pi^2} q k_e (B_{th}\omega_s)^2 V_t = P_{etr.FEM} \tag{3.9}$$

Therefore,

$$k_q = \frac{\pi^2 P_{etr.FEM}}{12 q k_e (B_{th}\omega_s)^2 V_t} \tag{3.10}$$

Correction factor k_q is first developed on the linear PM motor with equal slot and tooth width. A series of FEM analyses were performed such that for a given ratio of magnet thickness l_m over airgap length δ, both the magnet thickness and the airgap length were varied. Then, this procedure is repeated for different ratios of magnet thickness to airgap length. Slot pitch was kept constant at all times.

The correction factor k_q was calculated for a wide range and plotted on Fig.3.16. It can be see from Fig.3.16 that, with constant slot pitch,

- Given the ratio of magnet thickness to airgap length, proportionally increasing

airgap length and magnet thickness will decrease k_q.

- Given airgap length and slot pitch, increasing magnet thickness will decrease k_q.

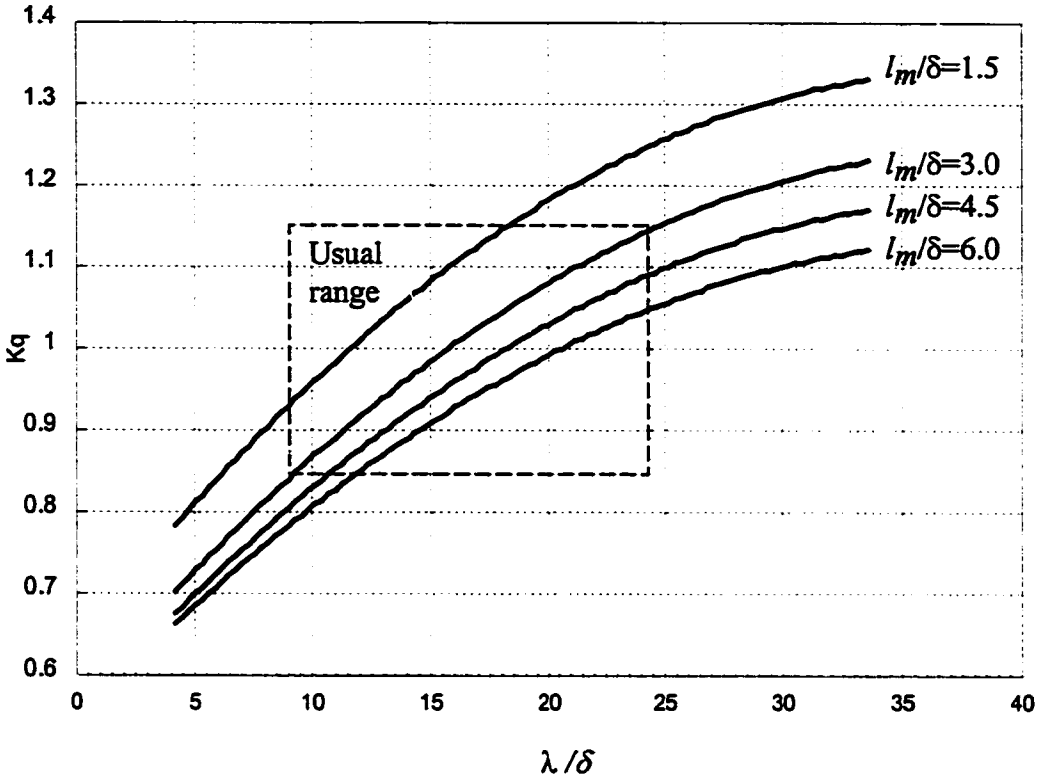

Fig.3.16 Relationship of k_q vs. magnet thickness and airgap length

Fig.3.16 is plotted for a very wide range of dimension variations. In an actual PM motor design, the variation of the dimensions is usually constrained in a small range. Typically, airgap length in small machines is 0.5mm to 2.0mm. To make good use of tooth density, l_m/δ is usually larger than 2.5 and λ/δ is usually within the range of 8 to 24. Therefore, the variation of k_q for PM motors described above is in the range of 0.85 to 1.15.

3.3.6 Effect of Slots Per Pole Per Phase with Fixed Pole Pitch

In section 3.3.4 it was shown that the tooth eddy current loss is proportional to the number of slots per pole per phase q for given frequency. In that case, both the ratio of magnet thickness to airgap length and the ratio of tooth width to airgap length were kept constant.

Therefore, each case has a same factor k_q.

In this section, the effect of the number of slots per pole per phase with fixed pole pitch will be studied. On the linear arranged PM motor with open slots, the slot pitch is varied such that the pole pitch and number of poles are kept constant while changing the number of slots per pole per phase as shown in Fig.3.18.

Varying q by fixing pole pitch will require a change to the slot pitch. Note that in the previous section, slot pitch was kept constant when deriving k_q. The fact is, when slot pitch changes, both the ratio of magnet thickness to airgap length and the ratio of tooth width to airgap length will change. In this section, the effectiveness of k_q will also be tested against slot pitch by keeping a constant magnet thickness and airgap length.

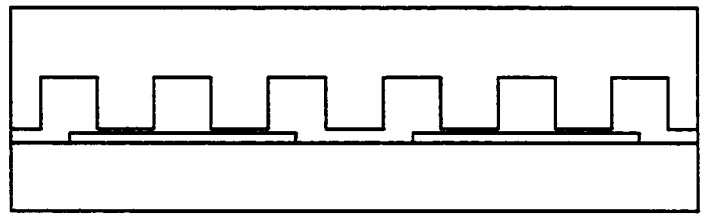

(a) q=1

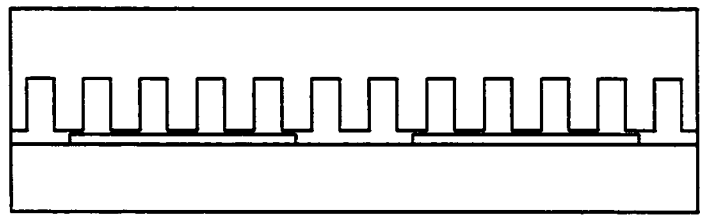

(b) q=2

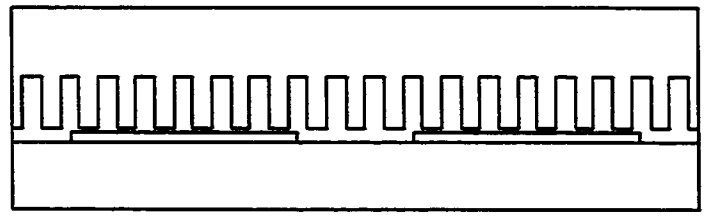

(c) q=3

Fig.3.17 Changing of the number of slots per pole per phase with fixed pole pitch

The flux waveforms of the normal component of the flux density in the center of a tooth are shown in Fig.3.18. It can be seen from Fig.3.18 that when the pole pitch is kept constant and the slot pitch is inversely proportional to the number of slots per pole per phase q, the rise time of the linear part of tooth flux density decreases when q increases. The larger the q, the less time is needed for the magnet edge to traverse one slot pitch as shown in Table III-6. It can be clearly seen from Table III-6 that the decrease in the time interval is not proportional to q. A correction factor is necessary.

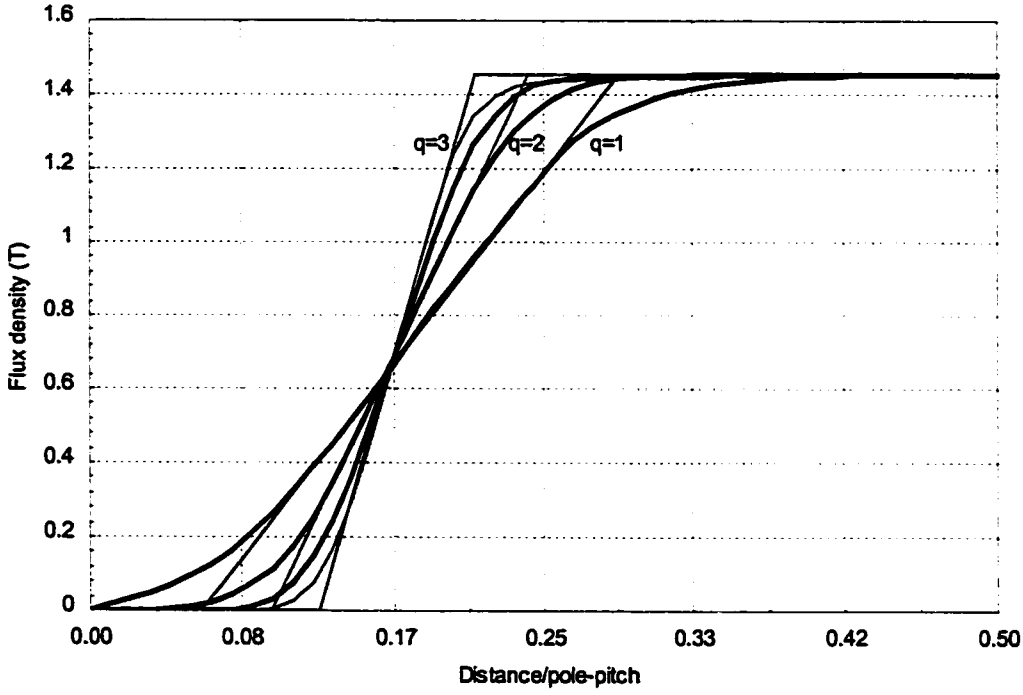

Fig.3.18 Normal component of tooth flux density for different q with variable slot-pitch

Table III-6 Distance needed for tooth flux density to rise at constant slope

Slot per pole per phase q	1	2	3	4
Distance (in pole pitch)	0.230	0.142	0.101	0.087

Although the magnet to airgap length ratio was kept constant, the ratio of tooth width

over airgap length was changed when the tooth width was changed. Therefore, the correction factor k_q is different for each case. Constant k_q can be determined for each case on Fig.3.16. By using (3.9), the eddy current loss induced by the normal component of tooth flux density can be determined. These results are listed in Table III-7. It can be seen from Table III-7 that the approximated tooth eddy current losses have good agreement with those calculated by FEM. Therefore, it can be concluded that the variation of k_q is also valid when varying the slot pitch.

Table III-7 Tooth eddy current loss vs. number of slots per pole per phase at 120Hz

Slot number per pole per phase q	1	2	3	4
k_q from Fig.3.16	1.23	1.03	0.89	0.815
Eddy current loss by FEM (W)	43.7	72.7	94.5	114.8
Tooth eddy loss by approximation model (W)	43.3	72.5	94.0	114.8
Error (%)	0.8	0.2	0.5	0.1

3.3.7 Effect of Tooth Width with Fixed Slot Pitch

The previous investigation was based on equal slot and tooth width. In this section, the effect of unequal tooth and slot width will be studied. The analysis was performed such that the tooth width was varied but the slot pitch was kept constant. Both the volume of the teeth and tooth flux density vary with tooth width by keeping a constant slot pitch. Table III-8 shows the comparison between the tooth eddy current loss calculated by the approximation model and that calculated by FEM. It can be seen from Table III-8 that when tooth width is changed from 36% to 74% slot-pitch, the error between the tooth eddy current loss calculated by the approximation model and that calculated by FEM is generally less than 5%. Therefore, varying tooth width within fixed slot pitch has little effect to the approximation model assuming other dimensions are kept constant.

Table III-8 Tooth eddy current loss vs. tooth width at 120Hz

Tooth width (mm)	6.4	8.4	10.4	12.4
Tooth-width/slot-pitch (%)	38	50	62	74
Tooth flux density (T)	1.5453	1.4528	1.2077	1.1047
Tooth volume ($x10^{-3}m^3$)	0.2627	0.3447	0.4268	0.5089
Tooth eddy current loss by FEM (W)	63.6	72.7	61.6	60.9
Eddy current loss by approximation model (W)	60.7	70.4	60.3	60.1
Differences (%)	-4.6	-3.1	-2.2	-1.2

3.3.8 Eddy Current Loss Induced by Circumferential Component

So far, only the normal/radial component of tooth flux has been considered for the estimation of eddy current loss in the stator teeth. Since the circumferential/longitudinal component follows a more complex pattern, it is difficult to linearly approximate the longitudinal component of the tooth flux density and the eddy current loss induced by this component.

When the eddy loss induced by the circumferential flux is considered, the total eddy current loss in the teeth can be expressed as:

$$P_{et} = P_{etr} + P_{etc} = P_{etr}(1 + \frac{P_{etc}}{P_{etr}}) = k_c P_{etr} \tag{3.11}$$

where P_{etc} is the eddy current loss induced by circumferential component of the tooth flux density and k_c is a correction factor.

First, for the linear PM motor with open slots, the eddy loss induced by circumferential

or longitudinal flux in the teeth is compared with the eddy current loss induced by the normal component. It was found that the eddy current loss induced by the longitudinal component of tooth flux density is approximately 15% of that induced by the normal component of tooth flux density and is constant over a wide range of magnet coverage.

Second, the correction factor k_c was tested when changing the magnet width, magnet thickness and airgap length for the open slot linear PM motor. It was found that the correction factor k_c is not affected by the magnet width nor magnet thickness but affected by airgap length.

Finally, the influence of slot closure on k_c was studied. When the slot closure is increased, the longitudinal flux in the shoe area of the teeth increases significantly as shown in Fig.3.19. The eddy current loss induced by the longitudinal flux also significantly increases with the increase of slot closure.

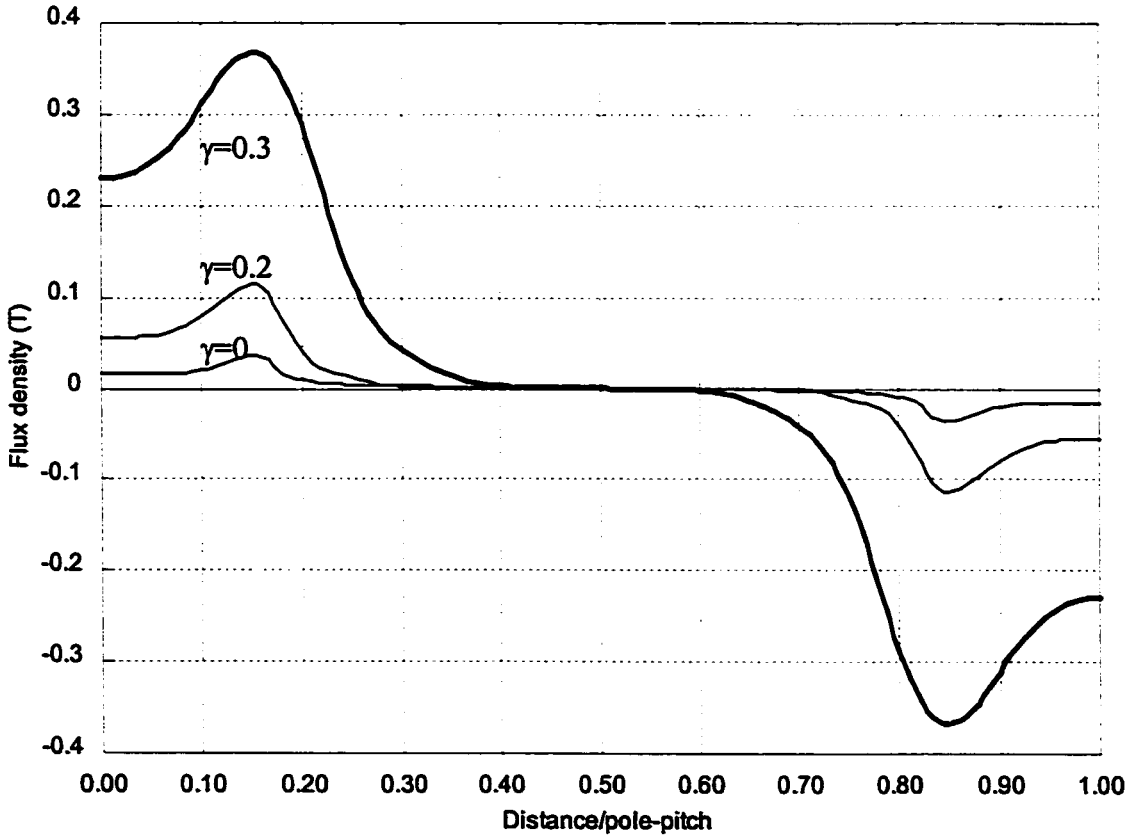

Fig.3.19 Longitudinal component of tooth flux density in the shoe area

It was found from the FEM results that k_c is a function of relative slot closure γ and the ratio of slot-pitch to airgap length. The correction factor k_c is graphed in Fig.3.20 for different slot closure and slot-pitch to airgap-length ratio.

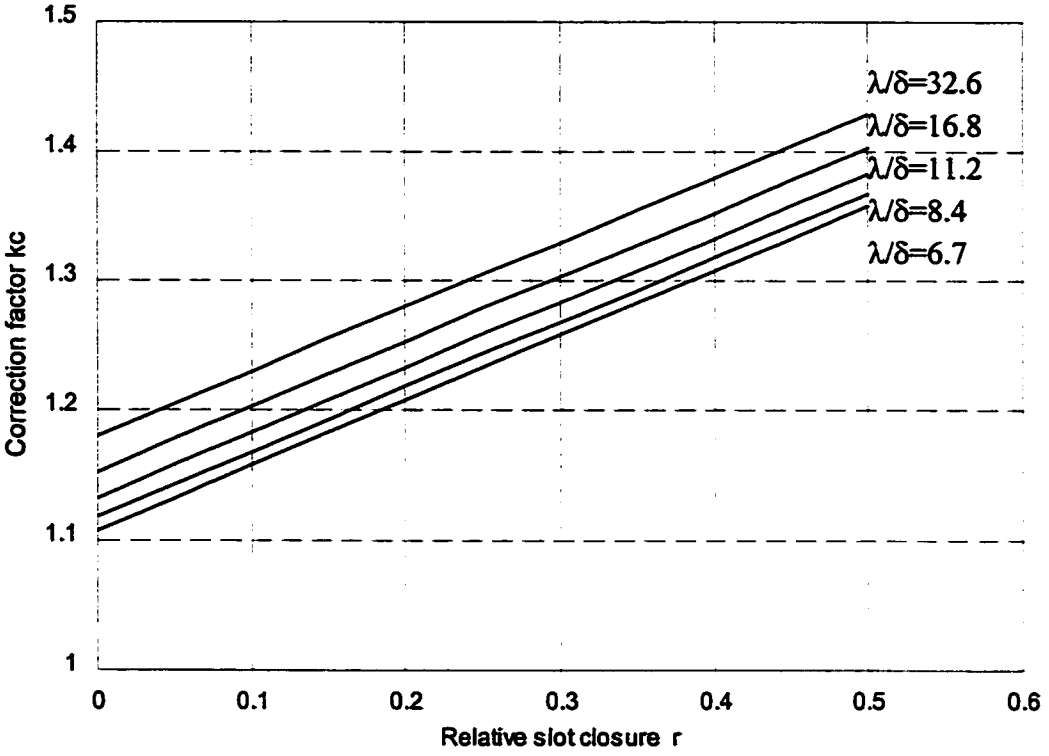

Fig.3.20 Correction factor k_c with regard to slot closure, airgap and tooth width

3.3.9 Simplified Expression of Tooth Eddy Current Loss

The total eddy current loss in the stator teeth of a PM synchronous motor can be approximated as:

$$P_{et} = \frac{12}{\pi^2} q k_q k_c k_e (\omega B_{th})^2 V_t \tag{3.12}$$

where k_q and k_c are correction factors which can be obtained through Fig.3.16 and Fig.3.20 respectively.

Therefore, the tooth eddy current loss is proportional to the number of slots per pole per phase for a given frequency.

When expressed as a function of speed, the tooth eddy current loss can be approximated as:

$$P_{et} = \frac{qp^2}{300} k_q k_c k_e B_{th}^2 n^2 V_t \tag{3.13}$$

Therefore, the tooth eddy current loss is proportional to the product of number of slots per pole per phase and the square of number of poles for a give speed.

3.3.10 Case Studies on Tooth Eddy Current Loss

The developed tooth eddy current loss model was applied to some cases to evaluate the tooth eddy current loss. The predicted tooth eddy losses are compared to those calculated using FEM method. Listed in Table III-9 are some of the calculation examples.

Case I: The 4-Pole PM Motor

The 4-pole motor was analyzed using the developed tooth eddy current loss model and FEM. Fig.3.21 shows the waveform of the radial component of the tooth flux density of the 4-pole PM synchronous motor of Fig.2.7 obtained by FEM at the center of a tooth. The linear part of the waveform was extended to show the slope of the flux density.

It can be measured from Fig.3.21 that the distance needed for the linear part of the normal component of the tooth flux density to rise from zero to the plateau value is 0.128 pole-pitch or 1.15 slot-pitch.

From the dimensions of the motor, it can be calculated that $l_m / \delta = 3.15$, $\lambda / \delta = 5.1$ $\gamma = 0.186$. From Fig.3.16, k_q can be found to be 0.72. From Fig.3.20, k_c can be found to be 1.18. The tooth eddy current loss of this motor was calculated by the approximation model (3.12) as 18.02W while that calculated by FEM is 17.3W (3.9% discrepancy). The proposed tooth eddy

current loss model gave a good approximation of the tooth eddy current loss.

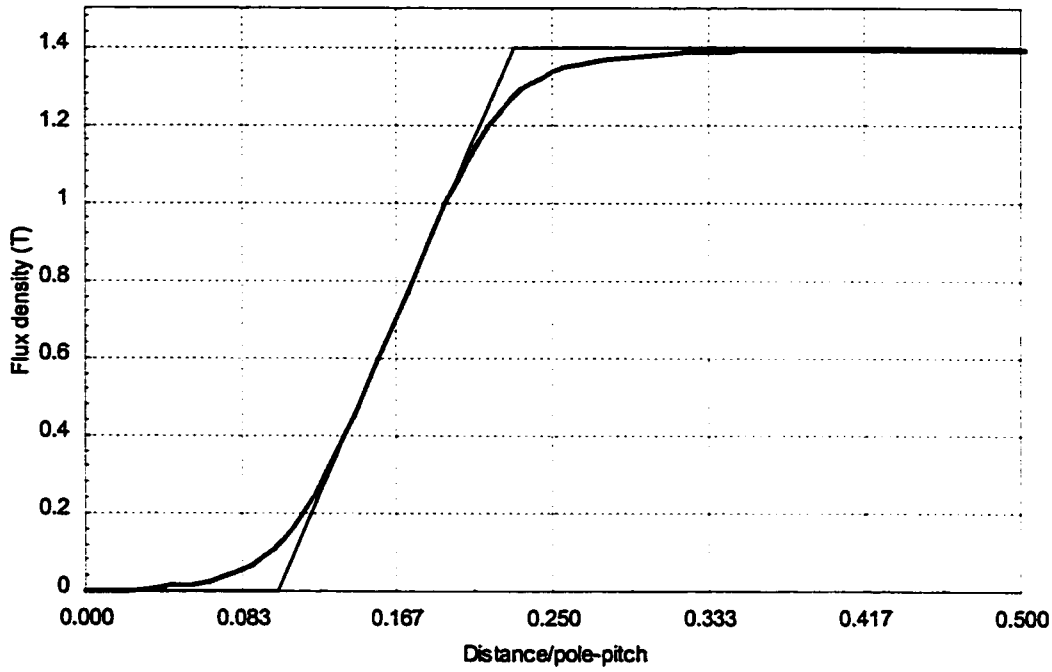

Fig.3.21 Radial component of tooth flux density of the 4-pole PM motor

Case II: The 8-Pole PM Motor

The waveform of the radial component of the tooth flux density of the 8-pole PM synchronous motor of Fig.2.8 is obtained by FEM and shown in Fig.3.22.

The distance needed for the linear part of the normal component of tooth flux density to rise from zero to maximum is 0.3 pole-pitch or 0.9 slot-pitch. In other words, the measured time on Fig.3.22 for the rise time of tooth flux is 1.38ms. The time interval for the magnet edge to traverse one slot pitch 10.2mm is 1.39ms at 1800rpm (or 120Hz).

From the dimensions of this motor, we have $l_m / \delta = 4.3$, $\lambda / \delta = 25.2$ $\gamma = 0.356$. From Fig.3.16, it can be found that k_q=1.1. From Fig.3.20, it can be found that k_c=1.33.

The tooth eddy current loss calculated by the approximation model (3.12) is 8.04W while that obtained by FEM is 8.22W (-2.2% discrepancy).

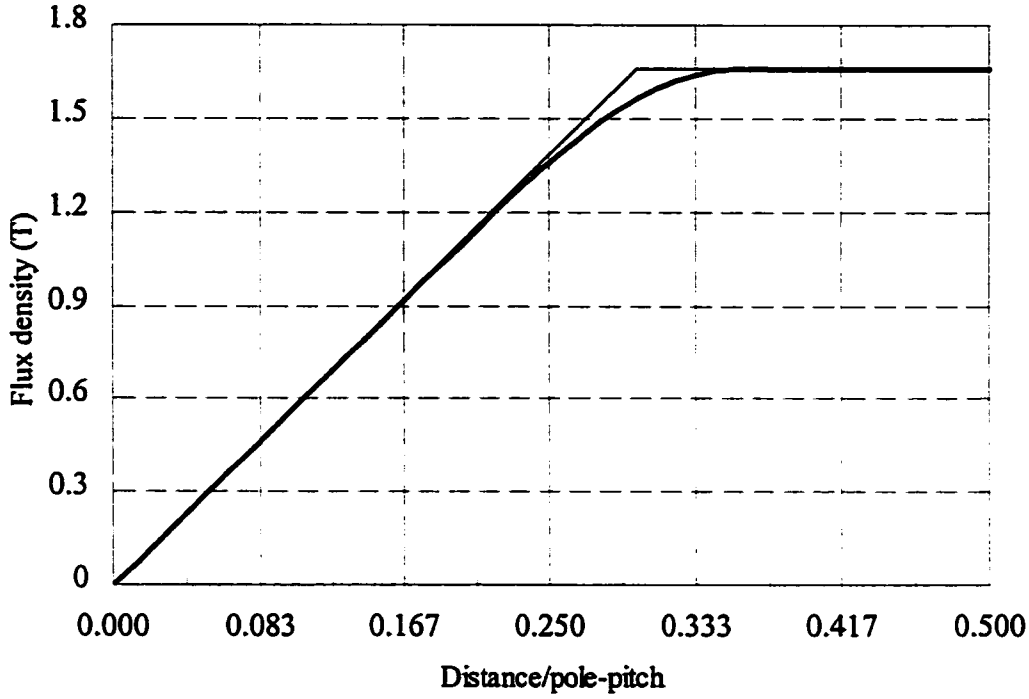

Fig.3.22 Radial component of tooth flux density of the 8-pole PM motor

Case III: A Linear Motor with Open Slot

The linear PM motor of Fig.2.4 with open slot was investigated with FEM and the approximation model. The motor has an airgap length of 1mm, magnet thickness of 3mm, equal slot and tooth width of 8.4mm and 2 slots per pole per phase. From the dimensions of the motor, the correction factors can be found from Fig.3.16 and Fig.3.20 respectively ($l_m/\delta = 3$, $\lambda/\delta = 16.8$, $\gamma = 0$, k_q=1.03 and k_c=1.15). The approximated tooth eddy current loss is 83.4W comparing with 83.7W obtained by FEM (-0.4% discrepancy).

Case IV: Varying Slot Closure and Magnet Thickness

Based on the configurations in Case III, the open slot was change to partly closed slot w_O=1.6mm, and magnet thickness was changed from 3mm to 6mm but keeping other dimensions the same. From the dimensions of the motor, $l_m/\delta = 6$, $\lambda/\delta = 16.8$, $\gamma = 0.405$, k_q and k_c are found to be 0.93 and 1.33 respectively. The tooth eddy current loss is 127.3W

calculated by the approximation model and 122.2W calculated by FEM (4.2% discrepancy).

Case V: Varying Slot Closure, Magnet Thickness and Airgap Length

Based on the configurations in Case IIII, the slot openings were changed from open to 3.2mm, magnet thickness was changed from 3mm to 10mm and airgap length was changed from 1mm to 3.2mm. From the dimensions of the motor, $l_m/\delta = 3.13$, $\lambda/\delta = 5.25$, $\gamma = 0.31$. Both k_q and k_c are different from those in Case III. With k_q=0.72 and k_c=1.24, the tooth eddy current loss can be approximated by (3.12) as 78.5W, while that obtained by FEM is 75.9W (4.3% discrepancy).

Case VI: Varying Slot Width

Based on Case III, the tooth width and the slot width were changed from 8.4mm to 4.2mm but keeping other dimensions constant. Both k_q and k_c are different from those in Case III. From the dimension of the motor, $l_m/\delta = 3$, $\lambda/\delta = 8.4$, $\gamma = 0$. With k_q=0.81 and k_c=1.11, the approximated tooth eddy current loss has an error of 4% when compared with that obtained by FEM (4.0% discrepancy).

Summary

All the above six examples are listed in Table III-9 for comparison. It can be seen from Table III-9 that the tooth eddy current loss calculated using the proposed approximation model is in good agreement with those calculated using the FEM method. The error is always within a ±5% error band.

Table III-9 Eddy current loss in the teeth calculated by FEM and proposed model

	Case I	Case II	Case III	Case IV	Case V	Case VI
Motor type	Rotary	Rotary	Linear	Linear	Linear	Linear
Slot pitch λ (mm)	10.2	13.88	16.8	16.8	16.8	8.4
Tooth width w_t(mm)	5.3	6.94	8.4	8.4	8.4	4.2
Slot openings w_o (mm)	3	2	Open	1.6	3.2	Open
Magnet thickness l_m(mm)	6.3	2.35	3	6	10	3
Airgap length δ (mm)	2	0.55	1	1	3.2	1
Number of poles p	4	8	8	8	8	8
Slots per pole per phase q	3	1	2	2	2	4
Tooth flux density B_{th} (T)	1.2398	1.5238	1.4528	1.6927	1.5447	1.5653
Angular frequency ω(rad/S)	377	754	754	754	754	754
Eddy loss coefficient k_e	0.07	0.0196	0.07	0.07	0.07	0.07
Tooth volume V_t (x10^{-3}m^3)	0.3802	0.1746	0.3447	0.3712	0.3807	0.3447
Coefficient k_q	0.72	1.1	1.03	0.95	0.72	0.81
Coefficient k_c	1.18	1.33	1.15	1.21	1.25	1.11
Eddy loss in the teeth by FEM (W)	**17.3**	**8.2**	**83.7**	**122.2**	**75.9**	**141.4**
Eddy loss in the teeth by proposed model (W)	**18.0**	**8.0**	**83.4**	**127.3**	**79.1**	**147.0**
Discrepancy (%)	3.9	-2.2	-0.4	4.2	4.3	4.0

3.4 Waveforms of Yoke Flux Density

It was assumed in [8] that the yoke flux density can be approximated by a trapezoidal waveform and the eddy current loss in the yoke can be approximated using only the magnitude of the average yoke flux density. In order to test these assumptions, FEM was performed on the linear arranged PM motor and the waveforms of the yoke flux density were obtained.

3.4.1 Waveforms of the Longitudinal Component of Yoke Flux Density

Fig.3.23 shows the waveforms of the longitudinal component of the yoke flux density of the linear PM motor calculated by FEM obtained above a tooth. The flux densities were obtained at the following locations in the yoke: (I). 1/3 yoke thickness from the surface of the stator. (II). Middle of the yoke. (III). 1/3 yoke thickness above the teeth.

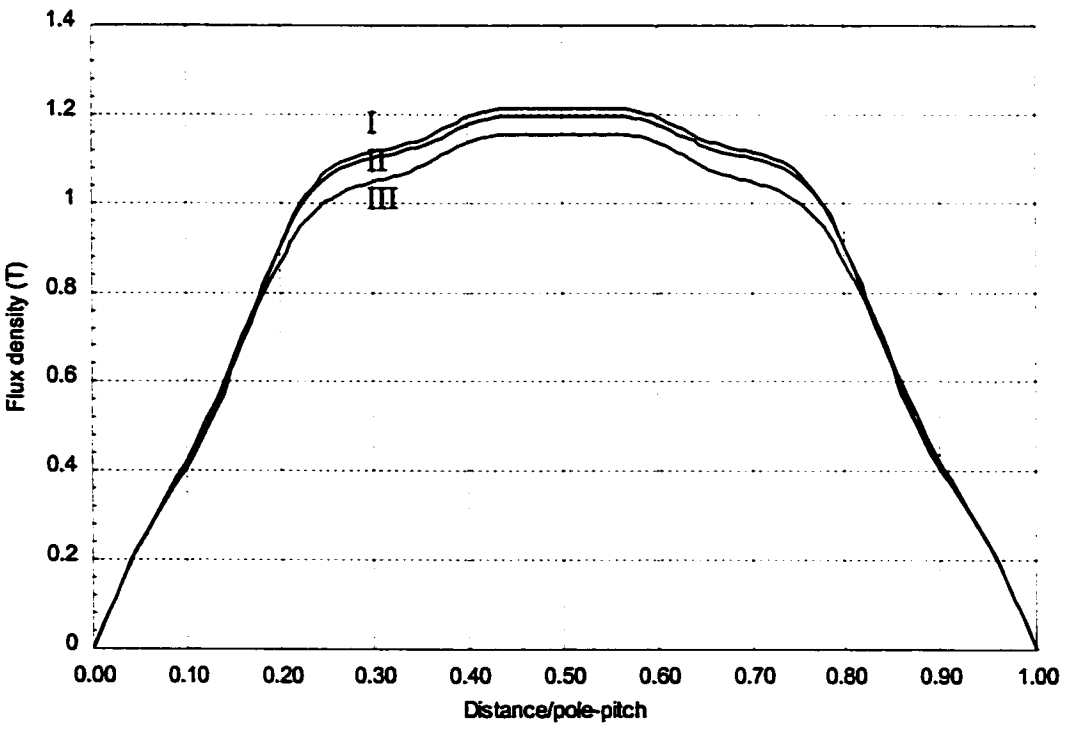

Fig.3.23 Waveforms of the longitudinal component of yoke flux density (above a tooth)

Fig.3.24 shows the waveforms of the longitudinal component of the yoke flux density of the linear PM motor calculated by FEM obtained above a slot. The flux densities were obtained at the following locations in the yoke above a tooth: (I). 1/3 yoke thickness from the surface of the stator. (II). Middle of the yoke. (III). 1/3 yoke thickness above the teeth.

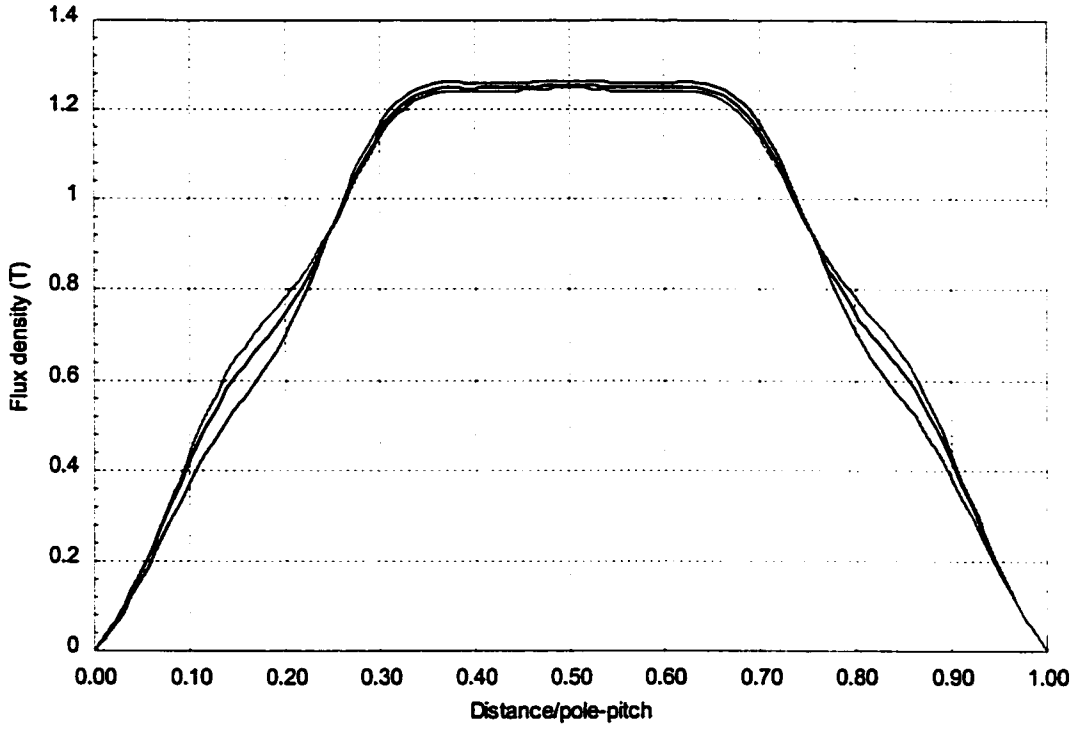

Fig.3.24 Waveforms of the longitudinal component of yoke flux density (above a slot)

It can be seen from Fig.3.23 that the longitudinal component of the yoke flux density approximately follows a linear trapezoidal waveform. The plateau value of this component is approximately evenly distributed over the thickness of the yoke.

The original assumption made in [8] assumed that the longitudinal component of yoke flux density increases approximately linearly from the middle point of the magnet to the edge of the magnet and it remains approximately constant in the yoke sector which is not above the magnet. The time needed for the rise of the longitudinal component of the yoke flux density from zero to plateau or fall from plateau to zero is approximately the time interval for half of the magnet width to traverse.

In order to determine the rise/fall time of the flux density, an approximated trapezoidal waveform of the longitudinal component of yoke flux density was plotted in Fig.3.25 with the average flux densities obtained above the slot and above the tooth.

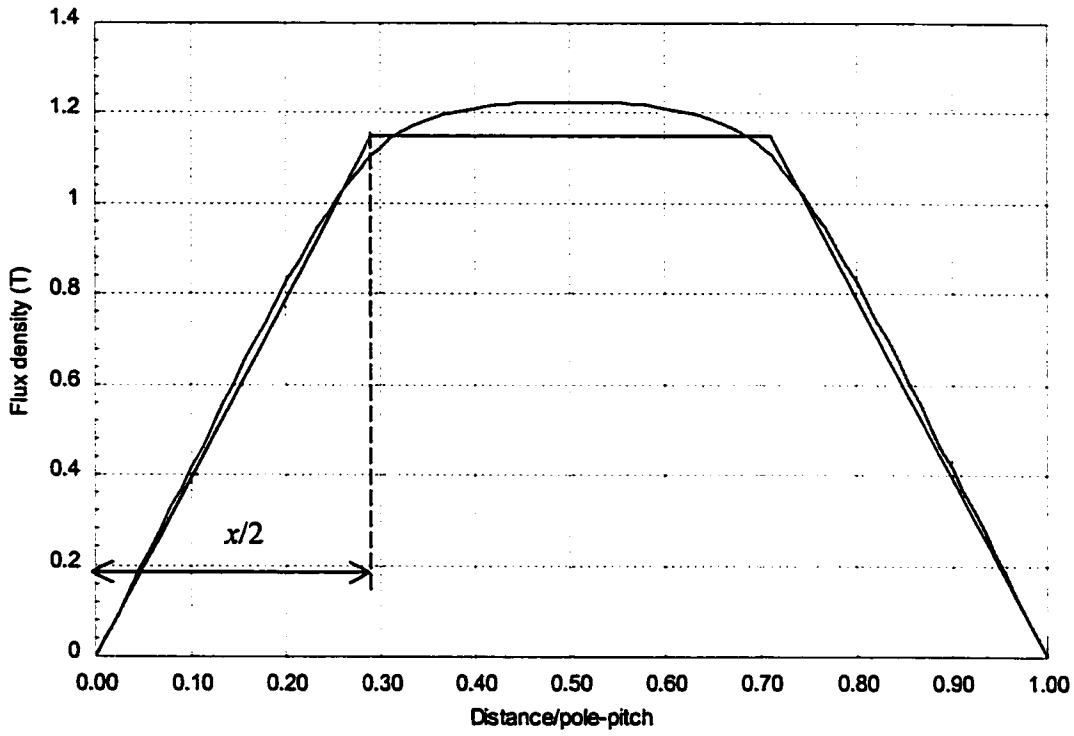

Fig.3.25 Approximation of the longitudinal component of yoke flux density

It can be seen from Fig.3.25 that the plateau of the waveform is longer than the space between the two magnets. The length of the plateau is 0.42 pole-pitch and the distance needed is 0.29 pole-pitch for the flux density to rise from zero to plateau or 0.58 pole-pitch from negative plateau to positive plateau. The space between the two magnets is 0.333 pole-pitch. The difference between these two is 0.087 pole-pitch. Recall that one slot-pitch of this machine is 0.167 pole-pitch. The length of the plateau is approximately the sum of the space between the two magnets and a half slot pitch. Based on this observation, distance x can be expressed as:

$$x = 1 - (1 - \alpha + \frac{1}{2}\frac{\lambda}{\tau}) = \alpha - \frac{1}{6q} \tag{3.14}$$

If the rise time of the linear part of yoke flux density were used to evaluate the eddy current loss induced by the longitudinal component of yoke flux density, the results would be larger than that calculated by FEM. This is due to the fact that the actual flux density rises slower at the beginning and the end of the change and that the longitudinal flux density is lower near the teeth than in other part of the yoke.

Suppose that the waveform of the longitudinal component of the yoke flux density can be represented by a linear trapezoidal waveform and this approximation produces the same eddy current loss as the actual waveform does. Using a similar procedure to that of the teeth in Section 3.2, the equivalent distance x for this approximation can be obtained by using (3.2):

$$\frac{x}{2} = \tau \cdot \frac{16 k_e}{T^2} \frac{\hat{B}_c^2 V_y}{P_{eyc,FEM}} \tag{3.15}$$

where $\hat{B}_c$ is the plateau value of the longitudinal component of yoke flux density, V_y is the volume of the yoke and $P_{eyc,FEM}$ is the eddy current loss of the longitudinal component calculated by FEM.

In Table III-10, the distance needed for the longitudinal component of yoke flux density to rise from zero to plateau value was calculated by (3.15) and compared to that measured on Fig.3.25 and that suggested in [8]. The distance obtained by (3.15) is about 4.4% less than the magnet width.

Table III-10 Distance x needed for yoke flux to rise

Method	Obtained by (3.15)	Measured on Fig.3.25	Suggested in [8] (magnet width)
Distance in pole-pitch	0.638τ	0.58τ	0.667τ

Table III-11 shows the eddy current loss induced by the longitudinal component of yoke flux density calculated by different methods.

Table III-11 Eddy current loss induced by the longitudinal component of yoke flux density

Method	FEM	Use magnet coverage	Use actual slope	Sinusoidal
Eddy current loss (W) at 120Hz or 12.1m/s	73.3	70.1	80.6	57.7
Error (%)	0.0	-4.4	10.0	-21.3

It can be seen from Table III-11 that

- When the distance needed for longitudinal yoke flux density to rise from negative plateau to positive plateau is assumed to be magnet coverage as suggested in [8], the calculated loss is close to that calculated by FEM (error of -4.4%).

- When the distance needed for longitudinal yoke flux density to rise is assumed to be the extension of the linear part of yoke flux waveform, the calculated loss is about 10% more than that calculated by FEM.

- When the flux density is assumed to be sinusoidal with the plateau flux density as its magnitude, the eddy loss is 21.3% less than that calculated by FEM.

Therefore, it can be concluded from the above observations that:

- The waveform of the longitudinal component of yoke flux density can be approximated by a linear trapezoidal waveform.

- The time needed for the longitudinal component of yoke flux density to rise from negative plateau to positive plateau is approximately the time needed for one point in the yoke to traverse a magnet width. Alternatively, the distance needed for the yoke flux density to rise from negative plateau to positive plateau is approximately the magnet width.

3.4.2 Waveforms of the Normal Component of Yoke Flux Density

Fig.3.26 shows the waveforms of the normal component of yoke flux density for the linear motor obtained by FEM. The flux densities were obtained at four locations in the yoke: 1/3 yoke thickness from the surface of the stator (I), middle of the yoke (II), 1/3 yoke thickness above the teeth (III) and 1mm from the teeth (IV). The waveform of the normal component of tooth flux density (V) is also shown in the same graph for comparison.

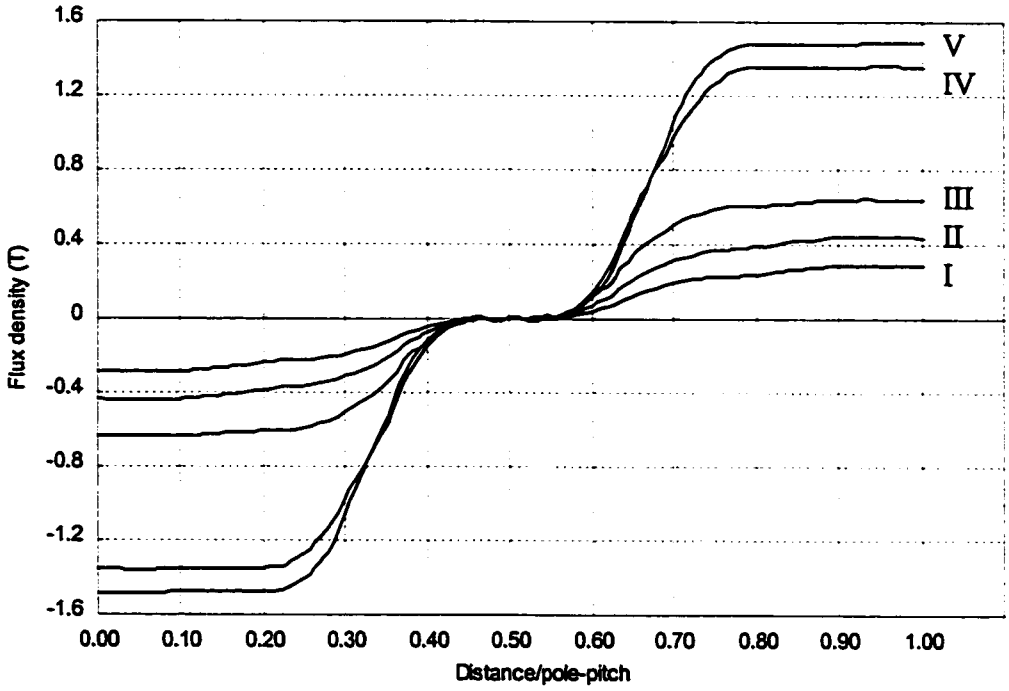

Fig.3.26 Normal component of yoke flux density of the linear motor

It can be seen from Fig.3.26 that

- The normal component of yoke flux density is seen to have similar waveform as that of the normal component of tooth flux density, particularly in the region just above the tooth (curve IV on Fig.3.26) as would be expected. The value of the plateau is dependent on the tooth flux density and motor dimension.

- The plateau value of the normal component of yoke flux density is different at each

layer of the yoke. It is maximal near the tooth and drops dramatically penetrating further into the yoke. It approaches zero near the surface of the motor.

3.4.3 Analytical Solutions to Yoke Flux Density

In order to develop the relationship between the normal component and the longitudinal component of yoke flux density, the flux distribution is shown again in Fig.3.27.

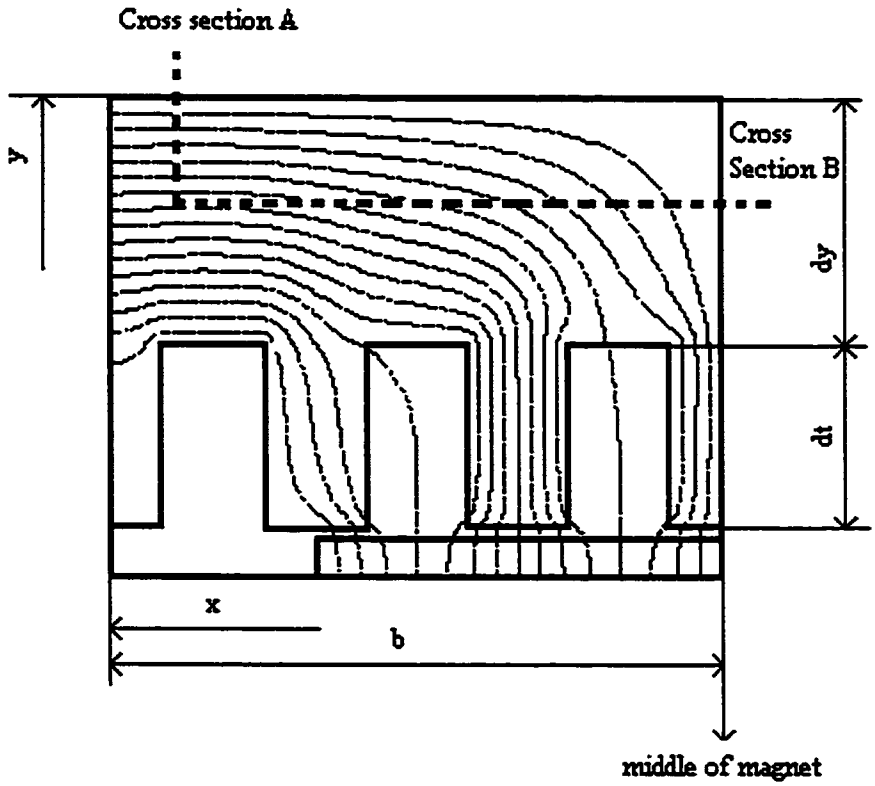

Fig.3.27 Flux distribution in the yoke

In the section of the yoke not above the magnet, the total flux is assumed to be constant and mainly contributed by the longitudinal component ($\hat{B}_c d_y$). In the section of the yoke above the magnet, the total flux is contributed by both longitudinal and normal components of the flux density.

Since it has been shown that the normal component of yoke flux density follows a

trapezoidal waveform similar to that in the teeth as shown in Fig.3.28 with different plateau at each layer, the rise time of the linear approximated flux is one slot-pitch divided by correction factor k_q.

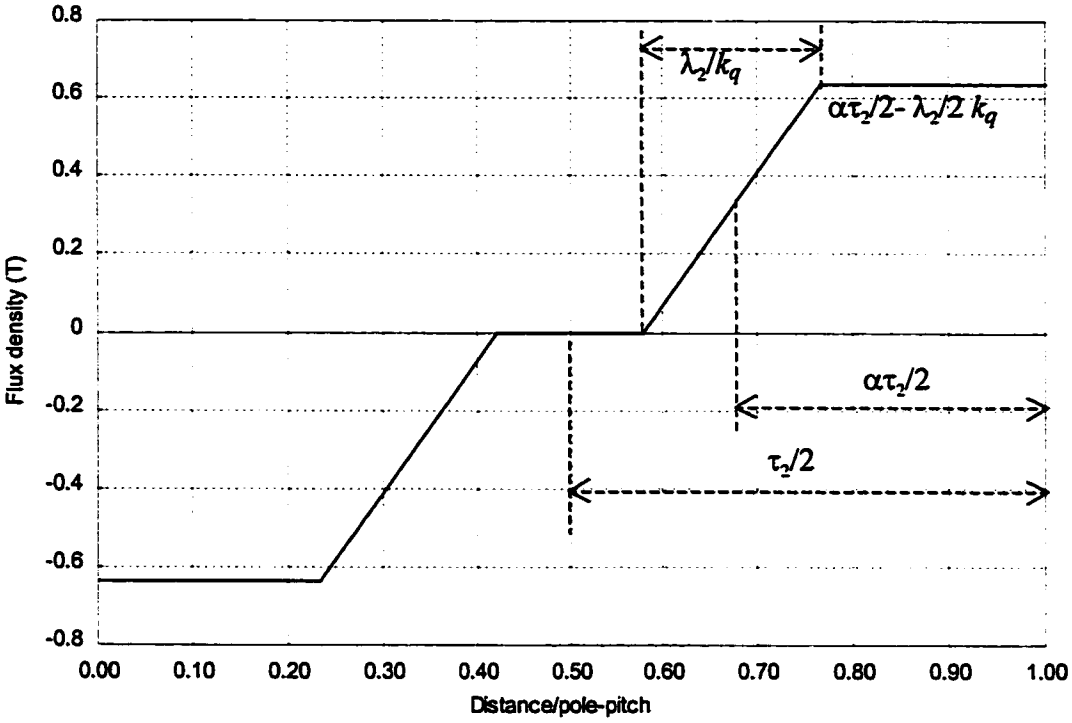

Fig.3.28 Approximated normal flux density waveform in the yoke

The flux supplied by the magnet is assumed to be in the normal direction when it passes through the teeth. Part of the flux turns into longitudinal direction on its way penetrating further into the yoke. In the yoke, the flux that crosses the horizontal layer (cross section B on Fig.3.27) must be equal to that passes through the vertical layer (cross section A on Fig.3.27), assuming no flux linkage. Therefore, from Fig.3.27 and Fig.3.28

$$y\hat{B}_c = \int_0^{\phi} B_r(y)dx = \int_0^{\lambda_2/k_q} B_r(y)dx + \hat{B}_r(y)\left(\frac{\alpha\tau_2}{2} - \frac{\lambda_2}{2k_q}\right) \tag{3.16}$$

where y is the distance from the edge of the yoke along the vertical layer, $B_r(y)$ and $\hat{B}_r(y)$ are the instantaneous value and plateau value of the normal component of yoke flux density at

distance y from the surface in the yoke, τ_2 and λ_2 are projected pole pitch and projected slot pitch which are measured in the yoke. For linear motors, τ_2 is the same as τ and λ_2 is the same as λ. In rotary machines λ_2 and τ_2 can be expressed as:

$$\lambda_2 = \frac{2\pi(r + d_t + y)}{3pq} \tag{3.17}$$

$$\tau_2 = 3q\lambda_2 \tag{3.18}$$

where d_t is the height of teeth, r is the inner radius of the stator.

Since B_r is linear in the integral part, (3.16) can be further simplified:

$$\frac{\hat{B}_r(y)}{\hat{B}_c} = \frac{2y}{3\alpha q\lambda_2} \tag{3.19}$$

The above analytical solution is based on an average basis. In order to validate the analytical solution, the normal component of yoke flux density was obtained at the area above a tooth and the other above a slot respectively. Fig.3.29 shows the normal component of yoke flux density as a function of yoke depth calculated by FEM and by the analytical method. It can be seen that

- The normal component of yoke flux density is not evenly distributed near the teeth/slots area. In the yoke where it is above the teeth, the flux density is higher than the flux density in the area where it is above the slots.
- Equation (3.19) gives a good estimation of the normal component of yoke flux density up to 2/3 of the of the yoke depth.
- Since eddy current loss is proportional to the square of flux density, it may not accurate when it is employed to evaluate the eddy current loss using (3.19).

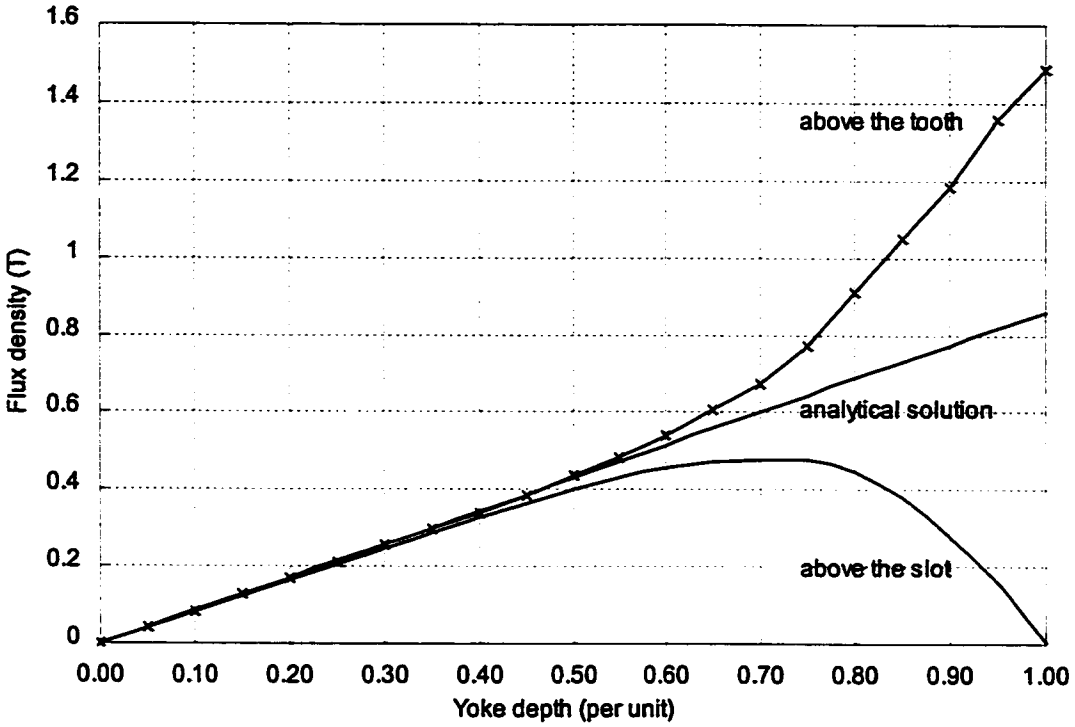

Fig.3.29 Normal component of yoke flux density as a function of yoke depth

Based on the above observation, the expression for the normal component of yoke flux density is then redeveloped for the yoke above a tooth and the yoke above a slot respectively.

In the yoke above a tooth

$$\frac{\hat{B}_{rt}(y)}{\hat{B}_c} = \begin{cases} \dfrac{2y}{3\alpha q \lambda_2} & 0 \le y \le \dfrac{2}{3} d_y \\ \dfrac{4(2y - d_y)}{3\alpha q \lambda_2} & \dfrac{2}{3} d_y \le y \le d_y \end{cases} \tag{3.20}$$

In the yoke above a slot:

$$\frac{\hat{B}_{rt}(y)}{\hat{B}_c} = \begin{cases} \dfrac{2y}{3\alpha q \lambda_2} & 0 \le y \le \dfrac{2}{3} d_y \\ \dfrac{4(d_y - y)}{3\alpha q \lambda_2} & \dfrac{2}{3} d_y \le y \le d_y \end{cases} \tag{3.21}$$

where $\hat{B}_{rt}(y)$ and $\hat{B}_{rs}(y)$ are the plateau values of the normal component of yoke flux density above a tooth and above a slot respectively.

3.5 Simplified Yoke Eddy Current Loss Model

3.5.1 Eddy Current Loss Induced by the Longitudinal Component

It has been shown that the waveform of the longitudinal component of the yoke flux density of a linear machine or the circumferential component of the yoke flux density of a rotary machine can be approximated as a trapezoidal waveform as shown in Fig.3.30. The longitudinal component of the flux density at any point in the yoke starts to rise when the middle of the magnet passes this point. It reaches plateau value when the rear magnet edge reaches this point. It keeps constant when this point passes the space between the two poles. Then it starts to decrease when it hits the front edge of following magnet. The flux density reaches zero again when it reaches the middle point of this magnet then it increases in the other direction.

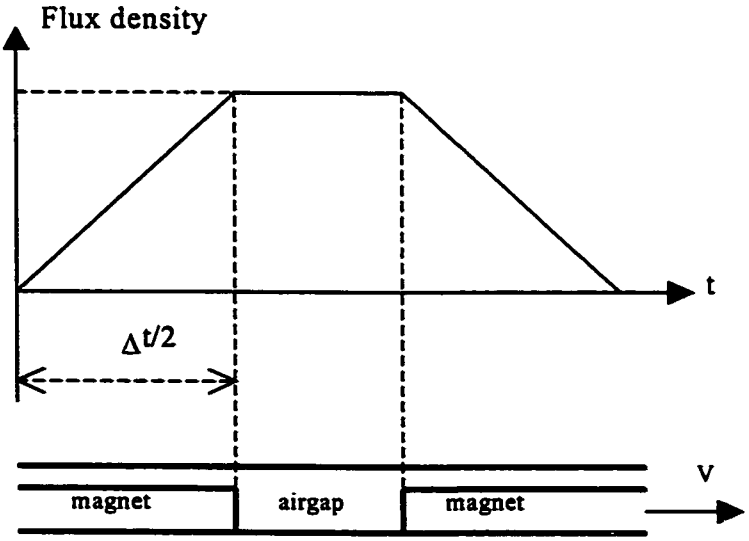

Fig.3.30 Approximation of the circumferential component of yoke flux density

For rotary machines, the time interval required for the magnet of width w_m to pass one point in the stator yoke, (e.g the circumferential component of the yoke flux density changing from $-\hat{B}_c$ to $\hat{B}_c$ or from $\hat{B}_c$ to $-\hat{B}_c$) is

$$\Delta t = \frac{w_m}{2r\omega_s/p} = \frac{\alpha\pi}{\omega_s} \tag{3.22}$$

where α, the magnet coverage, is defined as the ratio of magnet width over pole-pitch:

$$\alpha = \frac{w_m}{\tau} = \frac{w_m}{2\pi r/p} = \frac{pw_m}{2\pi r} \tag{3.23}$$

The time rate of change of circumferential component of the yoke flux density is

$$\frac{dB}{dt} = \frac{2\hat{B}_c}{\Delta t} = \frac{2\omega_s \hat{B}_c}{\alpha\pi} \tag{3.24}$$

The change of flux happens twice in one period. The total yoke eddy current loss induced by the longitudinal/circumferential component flux is

$$p_{eyc} = 2k_e\left(\frac{dB}{dt}\right)^2 \cdot \frac{2\Delta t}{T} V_y = \frac{1}{\alpha}\frac{8}{\pi^2} k_e \omega_s^2 \hat{B}_c^2 V_y \quad (\mathrm{W/m^3}) \tag{3.25}$$

It can be inferred from (3.25) that the eddy current loss induced by the circumferential component of yoke flux density is inversely proportional to the magnet coverage. It is not related to the number of slots per pole per phase or any dimensions of the motor.

3.5.2 Effect of Slot Closure

In order to test the derived approximation equation of yoke eddy current loss, the effect of geometrical variations of the linear PM motor was studied. The yoke eddy current losses calculated by the approximation model are compared with those calculated by FEM.

First, FEM was performed on the linear motor by varying the slot closure but keeping

other dimensions unchanged. The calculated yoke eddy current loss by FEM and the approximation model is shown in Table III-12.

It can be seen from Table III-12 that yoke eddy current loss increases when slot closure increases due to the increase of yoke flux density. The yoke eddy current loss calculated by the approximation model is in accordance with that calculated by FEM for different slot closure. The error is within 5%. Therefore, the effect of slot closure on the approximation model can be neglected.

Table III-12 Effect of slot closure on yoke eddy curent loss at 120Hz

Slot openings (mm)	8.4 (open)	6.6	5.0	3.2	1.6
Yoke flux density (T)	1.2558	1.3330	1.3878	1.4325	1.4551
Yoke eddy current loss by FEM (W)	73.3	81.7	88.0	94.0	95.9
Yoke eddy current loss by Approximation model (W)	70.1	79.0	85.6	91.2	94.1
Difference (%)	-4.4	-3.3	-2.7	-3.0	-1.8

3.5.3 Effect of Magnet Coverage

In order to test that the yoke eddy current loss is inversely proportional to magnet coverage, the magnet coverage of the linear PM motor was varied from 0.532 to 0.833. In some cases, the yoke thickness of the motor was also changed according to the magnet coverage to keep a relatively constant yoke flux density.

For different magnet coverage, the eddy current loss was calculated by the approximation equation (3.25) and compared to that obtained by FEM as shown in Table III-13. It can be seen from Table III-13 that for the given range of magnet coverage, the difference between the estimated yoke eddy current loss by the approximation model and that calculated

by FEM is generally less than ±5%. Therefore, magnet coverage has little effect on the approximation model.

Table III-13 Effect of magnet coverage on yoke eddy curent loss at 120Hz

Magnet coverage α	0.833	0.718	0.667	0.532
Yoke flux density (T)	1.4665	1.2848	1.2558	1.2677
Yoke volume ($\times 10^{-3} m^3$)	0.9193	0.9882	0.9193	0.73544
Yoke eddy current loss by FEM (W)	74.2	73.5	73.3	69.9
Yoke eddy current loss by approximation model (W)	76.6	73.3	70.1	71.7
Difference (%)	3.2	-0.2	-4.3	2.5

3.5.4 Effect of Slots Per Pole Per Phase

Equation (3.25) shows that the eddy current loss induced by the circumferential yoke flux density is not effected by the number of slots per pole per phase q. In order to test this statement, the effect of the number of slots per pole per phase was studied. On the linear PM motor, within fixed slot pitch, the number of slots per pole per phase was changed and the slot pitch was changed accordingly. The yoke eddy current loss was calculated for each case by FEM and compared with that calculated by the approximation model as shown in Table III-14. It can be seen from Table III-14 that, although the yoke eddy current loss increases with q due to the increase of yoke flux density, the error between the yoke eddy current loss calculated by the approximation model and that calculated by FEM is less than 7%.

Two conclusions can be drawn from this test. First, the effect of number of slot per pole per phase on the approximation model is negligible. Secondly, with equal slot and tooth width, slot pitch has little effect on the approximation model.

Table III-14 Effect of number of slots with fixed pole pitch and variable slot pitch at 120Hz

Slots per pole per phase q	4	3	2	1
Yoke flux density (T)	1.3374	1.3094	1.2558	1.1243
Yoke eddy current loss by FEM(W)	85.33	81.06	73.3	57.1
Yoke eddy current loss by approximation model (W)	79.5	76.2	70.1	56.2
Difference (%)	-6.8	-6.0	-4.3	-1.6

3.5.5 Effect of Magnet Thickness

In order to test if the approximation model is affected by magnet thickness, the magnet thickness of the linear PM motor was varied from 2.5mm to 6mm. The yoke eddy current loss induced by the circumferential component calculated by FEM and by the approximation model is shown in Table III-15. It can be seen from Table III-15 that the error between the yoke eddy current loss calculated by the approximation model and that calculated by FEM is less than 5% when magnet thickness changes in a wide range. Therefore, the approximated yoke eddy current loss model is effective for different magnet thickness assuming other dimensions are kept constant.

Table III-15 Effect of magnet thickness on yoke eddy current loss at 120Hz

Magnet thickness (mm)	2.5	3	3.5	4	5	6
Yoke flux density (T)	1.1292	1.2132	1.2816	1.3379	1.4251	1.4895
Yoke eddy current loss by FEM (W)	64.0	73.3	81.4	88.3	99.6	108.2
Yoke eddy current loss by Approximation model (W)	60.8	70.1	78.3	85.3	96.8	105.7
Difference (%)	-5.0	-4.3	-3.8	-3.4	-2.8	-2.3

3.5.6 Effect of Airgap Length

In order to test whether the approximated yoke eddy current loss model is affected by airgap length, the airgap length of the linear PM motor was varied from 0.5mm to 2.5mm. The yoke eddy current loss induced by the circumferential component calculated by FEM and calculated by the approximation model is shown in Table III-16.

Table III-16 Effect of airgap length on yoke eddy current loss at 120Hz

Airgap length (mm)	0.5	1	1.5	2	2.5
Yoke flux density (T)	1.4120	1.2558	1.1278	1.0227	0.9316
Yoke eddy current loss by FEM (W)	94.9	73.3	58.1	47.1	39.0
Yoke eddy current loss by approximation model (W)	88.7	70.1	56.6	46.5	38.6
Difference (%)	-6.6	-4.3	-2.6	-1.3	-1.1

It can be seen from Table III-16 that, although the yoke eddy current loss decreases as the airgap length is increased due to the decrease of flux density, the error between the loss calculated by the approximation model and that calculated by FEM is within 7%. Therefore, the effect of airgap length on the approximated yoke eddy current loss model can be neglected.

3.5.7 Effect of Tooth Width with Fixed Slot Pitch

Equation (3.25) also shows that the approximated yoke eddy current loss model is not affected by tooth width. In order to test this statement, the tooth width of the linear PM motor was varied from 4.4mm to 12.4mm for a fixed slot pitch of 16.8mm. The yoke eddy current loss induced by the circumferential component calculated by FEM and by the approximation model is shown in Table III-15. It can be seen from Table III-15 that the yoke eddy current loss increases with tooth width due to the increase of flux density and the increase of tooth volume.

However, the error between the loss calculated by the two methods is within 6%. Therefore, the influence of tooth width on the approximated yoke eddy current loss model can be neglected.

Table III-17 Effect of tooth width on yoke eddy current loss at 120Hz

Tooth width (mm)	6.4	8.4	10.4	12.4
Yoke flux density (T)	1.1259	1.2132	1.2701	1.3003
Yoke eddy current loss by FEM (W)	64.3	73.3	79.4	82.7
Yoke eddy current loss by approximation model (W)	60.4	70.1	76.9	80.6
Difference (%)	-6.0	-4.3	-3.2	-2.5

3.5.8 Eddy Current Loss Induced by the Normal Component

It has been shown that the waveform of the normal component of the yoke flux density has the same waveform as that of the normal component of tooth flux density. Therefore, the approximation formula derived for the tooth eddy current loss density (normal component only) can be used to approximate the eddy current loss density induced by the normal component of yoke flux density at each layer of the yoke:

$$p_{eyr} = \frac{12}{\pi^2} q k_q k_e \omega_s^2 \hat{B}_r^2(y) \qquad (\mathrm{W/m^3}) \qquad (3.26)$$

Since at each layer of the yoke the normal component of flux density has a different plateau, it is desirable to integrate the loss over the whole yoke to get the total eddy current loss. The plateau of the normal component of yoke flux density changes linearly with the depth of yoke as shown in Fig.3.29and at each layer of the yoke the flux density follows the linear pattern shown in Fig.3.28.

By using (3.26), (3.20) and (3.21), the average eddy loss density induced by the normal

component of yoke flux density.

$$p_{eyr} = \frac{1}{2d_y}\left[\frac{12}{\pi^2} q k_q k_e \omega_s^2 \int_0^{d_y} \hat{B}_{rs}^2(y)dy + \frac{12}{\pi^2} q k_q k_e \omega_s^2 \int_0^{d_y} \hat{B}_{rt}^2(y)dy \right] \tag{3.27}$$

The projected slot pitch λ_2 in (3.20) and (3.21) is also a function of y for rotary machines. In order to simplify the integration, assume that projected slot pitch λ_2 can be obtained as a constant at the middle of yoke, then:

$$p_{eyr} \approx \frac{64 k_q d_y^2}{27 q \pi^2 \alpha^2 \lambda_2^2} k_e \omega_s^2 \hat{B}_c^2 = k_y p_{eyc} \tag{3.28}$$

where k_y is the ratio of eddy current loss induced by the two component of yoke flux density.

$$k_y = \frac{8 k_q d_y^2}{27 \alpha q \lambda_2^2} \tag{3.29}$$

The corrected expression (3.29) was found to be approximately accurate for a wide range of configuration variations on the linear PM motor. Table III-18 shows the calculated k_y for four cases used in Section 3.5.4.

Table III-18 Test of correction factor k_r

Slots per pole per phase q	4	3	2	1
P_{eyr}/P_{eyc} by FEM	0.43	0.39	0.33	0.23
k_y calculated by (3.29)	0.51	0.42	0.33	0.19

3.5.9 Simplified Expression of Yoke Eddy Current Loss

Summing the eddy current losses induced by normal and longitudinal components, the total eddy current loss in the yoke is derived:

$$P_{ey} = P_{eyc} + P_{eyr} = \frac{1}{\alpha}\frac{8}{\pi^2} k_e k_r \omega_s^2 \hat{B}_c^2 V_y \quad \text{(W)} \tag{3.30}$$

where k_r is a correction factor for the eddy current loss induced by the normal component of yoke flux density:

$$k_r = 1 + k_y = 1 + \frac{8 k_q d_y^2}{27 \alpha q \lambda_2^2} \tag{3.31}$$

Therefore, yoke eddy current loss is inversely proportional to magnet coverage for given operational frequency. When expressed as a function of speed, the yoke eddy current loss is:

$$P_{ey} = \frac{p^2}{450\alpha} k_e k_r n^2 \hat{B}_c^2 V_y \quad \text{(W)} \tag{3.32}$$

Therefore, yoke eddy current loss is proportional to the poles squared divided by magnet coverage for a given speed.

3.5.10 Case Studies on Yoke Eddy Current Loss

The developed approximation model was applied to some cases to estimate the yoke eddy current loss. The results are compared to those calculated by FEM method. Listed in Table III-19 are the same examples used to calculate tooth eddy current loss.

Case I: The 4-Pole PM Motor

The waveforms of the two components of the yoke flux density at middle yoke of the 4-pole PM motor calculated by FEM are shown in Fig.3.31. It can be seen that the linear part of the circumferential component of yoke flux density takes 0.3 pole-pitch to rise from zero to the plateau. The rise time calculated by (3.14) is 0.306 pole-pitch. These results coincide with each other.

The normal component of yoke flux density takes 0.13 pole-pitch to rise from zero to plateau. Recall that the normal component of tooth flux density of this motor takes 0.128 pole

pitch to rise from zero to plateau. It therefore confirms that the normal component of yoke flux density has the same shape as that of the normal component of tooth flux density.

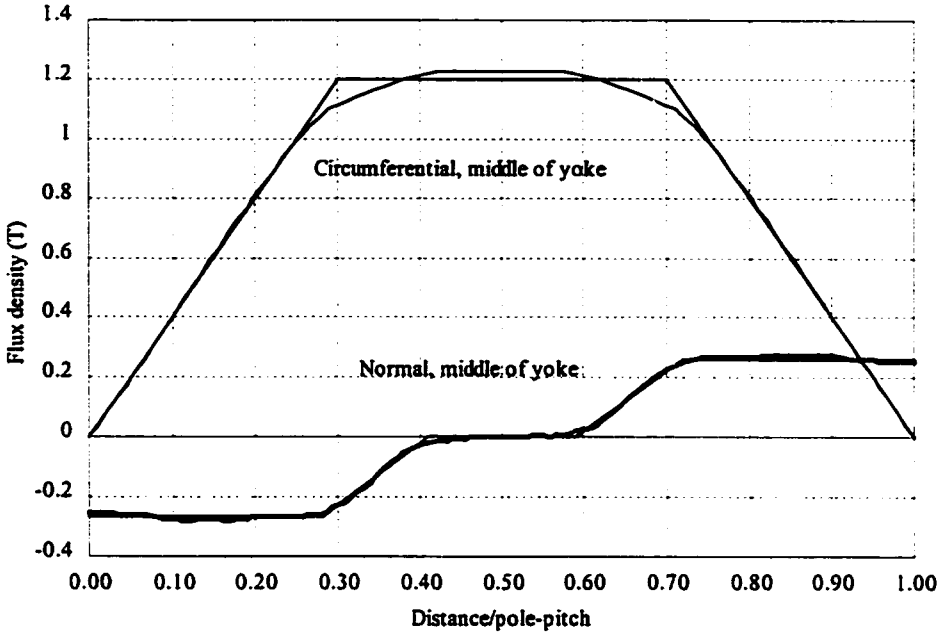

Fig.3.31 Yoke flux waveform of the 4-pole PM motor

By using the dimensions of the motor and k_q=0.72 from Table III-9, correction factor k_r can be found to be 1.14. The yoke eddy current loss of this motor is 18.07W calculated by FEM while the predicted yoke eddy current loss by the proposed model is 19.03W (discrepancy (5.3% discrepancy).

Case II: The 8-Pole PM Motor

The waveforms of the two components of the yoke flux density at middle yoke of the 8-pole PM motor are shown in Fig.3.32. Since there is only one slot per pole per phase, there is more distortion in the flux waveforms. However, these waveforms still follow the approximated pattern.

It can be seen that the linear approximated circumferential component of yoke flux density takes 0.25 pole-pitch to rise from zero to plateau. The measured rise time Fig.3.32

coincides with that calculated by (3.14).

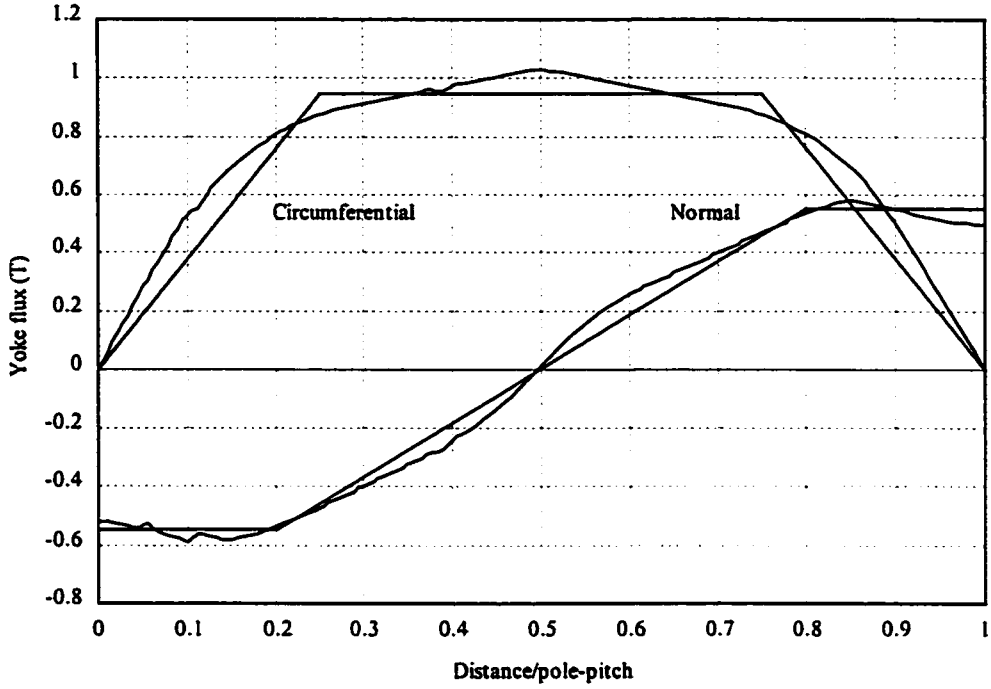

Fig.3.32 Yoke flux waveform of the 8-pole PM motor

The normal component of yoke flux density takes 0.3 pole-pitch to rise from zero to plateau. Recall that the normal component of tooth flux density of this motor also takes 0.3 pole-pitch to rise from zero to plateau.

By using the dimensions of the motor and k_q=1.1 from Table III-9, correction factor k_r can be found to be 1.11. The predicted loss is 5.81W by the proposed approximation model comparing to 5.75W calculated by FEM (-1.1% discrepancy).

Case III: A Linear Motor with Open Slot

The linear PM motor of Fig.2.4 is investigated with FEM and the approximation model. From the dimensions of the motor, the correction factors can be found as k_r=1.33. The approximated yoke eddy current loss is 94.3W comparing with 97.4W obtained by FEM (discrepancy –3.2%).

Case IV: Varying Magnet Coverage and Yoke Thickness

Based on Case III, the magnet coverage α was change from 0.659 to 0.532 and yoke thickness was changed from 20mm to 16mm but keeping other dimensions the same. k_r is found to be 1.26. The yoke eddy current loss is 90.3W calculated by the approximation model and 90.8W calculated by FEM (-0.5% discrepancy).

Case V: Varying Slot Closure, Magnet Thickness and Airgap Length

Based on Case III, the slot opening was changed from 8.4mm to 3.2mm, magnet thickness was changed from 3mm to 10mm and airgap length were changed from 1mm to 3.2mm. Correction factor k_r was found to be 1.23. The yoke eddy current loss can be approximated as 97.0W, while that obtained by FEM is 93.2W (4% discrepancy).

Case VI: Varying Slot Width

Based on Case III, the tooth width and the slot width were changed from 8.4mm to 4.2mm but keeping other dimensions constant. Correction factor k_r was found to be 1.51. The approximated tooth eddy current loss has an error of 1.6% when compared with that calculated using FEM.

Summary

All of the above examples are listed in Table III-19 for comparison. It can be seen from Table III-19 that the yoke eddy current loss calculated by the proposed approximation model are generally acceptable when comparing with the FEM results. The error is always within ±6%.

Table III-19 Eddy current loss in the yoke calculated by FEM and proposed model

	Case I	Case II	Case III	Case IV	Case V	Case V
Machine type	Rotary	Rotary	Linear	Linear	Linear	Linear
Slot pitch (mm) λ_2	14.6	19.2	16.8	16.8	16.8	8.4
Tooth width (mm)	5.3	6.94	8.4	8.4	8.4	4.2
Magnet thickness (mm)	6.3	2.35	3	3	10	3
Magnet coverage	0.667	0.667	0.659	0.532	0.667	0.667
Airgap length (mm)	2	0.55	1	1	3.2	1
Number of poles	4	8	8	8	8	8
Slots per pole per phase q	3	1	2	2	2	2
Inner radius of the stator r (mm)	58.5	53	-	-	-	-
Tooth height d_t (mm)	19.1	17	15	15	15	15
Yoke thickness d_y (mm)	17.4	10	20	16	20	20
Yoke flux B_c (T)	1.2827	1.1995	1.2558	1.2677	1.403	1.3374
Yoke volume V_y (x10^{-3}m^3)	0.8382	0.2687	0.9193	0.7354	0.9193	0.9193
Correction factor k_q	0.72	1.1	1.03	1.03	0.72	0.81
Correction factor k_r	1.14	1.11	1.33	1.26	1.23	1.51
Total yoke eddy current loss by FEM (W)	**18.1**	**5.6**	**97.4**	**90.8**	**93.2**	**122.0**
Total yoke eddy loss by proposed model (W)	**19.0**	**5.8**	**94.3**	**90.3**	**97.0**	**120.1**
Discrepancy (%)	5.3	1.1	-3.2	-0.5	4.0	-1.6

3.6 Simplified Hysteresis Loss Model

When time stepped FEM is performed, the hysteresis loss in the stator yoke and the stator teeth can be easily calculated using (2.29).

The teeth and yoke hysteresis loss can also be calculated using the following equation respectively:

$$P_{ht} = k_h \omega_s B_{th}^{\beta} V_t = \frac{\pi np}{60} k_h B_{th}^{\beta} V_t \tag{3.33}$$

$$P_{hy} = k_h \omega_s B_y^{\beta} V_y = \frac{\pi np}{60} k_h B_y^{\beta} V_y \tag{3.34}$$

where B_t and B_y are the average of plateau flux densities of all elements in the teeth and the average of plateau flux densities of all elements in the yoke respectively.

Table III-20 shows the comparison of calculated hysteresis loss by using FEM and by using average flux density for the linear arranged PM motor at 120Hz with hysteresis loss constant k_h=44 and β=1.9. It can be seen that the error between the two methods is negligible.

Table III-20 Hysteresis losses calculated by FEM and by average flux density at 120Hz

	Flux density (T)	Volume ($x10^{-3}m^3$)	Hysteresis loss by FEM (W)	Hysteresis loss by average flux density (W)
Teeth	1.4528	0.3447	23.31	23.25
Yoke	1.2558	0.9193	47.07	47.01

Chapter 4

Measurement of Iron Losses in PM Synchronous Motors

In order to validate the proposed iron loss models, the losses of two existing PM motors were measured.

4.1 Loss Measurement of PM Synchronous Machines

Loss measurement in electrical machines has been a difficult task for electrical industry. The electrical industry is spending an enormous amount of money to improve the accuracy of the testing equipment in order to measure motor efficiency within ±0.5% [34].

When measuring machine losses, it is necessary to employ precise instruments and calibration in order to achieve higher accuracy. It is also desirable to collect repeated samples of the data at each point to compute an average value.

4.1.1 No-load Loss Measurement of PM Synchronous Machines

No load losses of a PM synchronous motor include stator iron losses, mechanical losses (windage and friction losses), and stator copper loss. For surface-mounted PM synchronous

motors, rotor iron loss is negligible. For inset and buried PM synchronous motors, the rotor iron loss must also be considered.

In IEEE STd 115-1995 [35] it states that the core loss at each value of armature voltage is determined by subtracting the friction and windage loss from the total power input to the machine being tested.

When a PM synchronous machine is operated as a motor, without any mechanical device connected to its shaft, the measured input power, with copper loss subtracted, represents the combination of no load iron losses and friction and windage loss of the machine.

Alternatively, when a PM synchronous motor is driven by a DC motor, with the stator circuit of the permanent magnet motor opened, the measured shaft torque multiplied by the speed represents the combination of no load iron losses and friction and windage loss.

4.1.2 Load Loss and Motor Efficiency

The losses of a loaded PM machine include copper losses, iron losses, windage and friction losses and stray losses.

It is known that stray losses are due to leakage flux, mechanical imperfection of the airgap, non-sinusoidal current distribution, slotting and so on. It is commonly agreed that the investigation of stray load losses in rotating electrical machines is far from complete and the data available is subjected to a high degree of uncertainty [36].

In order to avoid the measurement of stray load loss, it is preferred to use direct input/output measurement [37]. Although the accuracy of direct input/output measurement test has been challenged by many authors and is expensive and time consuming, it is still the most accepted and will be the major method in measuring motor efficiency in the next few years to come [37].

When a PM synchronous machine is operated as a motor with a mechanical load connected to its shaft, by directly measuring the shaft torque and input power, the efficiency and

total loss can be determined.

PM synchronous motors for variable-speed drives are usually designed without damping cage. Therefore, a PM motor has to be operated with closed loop control. A PWM wave is inevitable in the control of variable-speed PM synchronous motors. The measurement of PWM waves is beyond the capability of traditional electrical instruments. The effectiveness of PWM wave measurement will be addressed in this chapter.

4.2 Implementation of the Control of a PM Synchronous Motor

In order to measure the iron losses of a PM synchronous motor when running it as a motor, a control system was implemented.

4.2.1 System Description

The system consists of a surface-mounted PM synchronous motor built within a 2hp induction motor frame, a VSI and an absolute position encoder. A MC68332 microcontroller is used to generate the gating. Fig.4.1 shows the block diagram of the control system of the PM synchronous motor drive system. A sinusoidal current was implemented to control the motor. Both torque control and spend control were implemented.

4.2.2 Mathematical Model of PM synchronous Motors

The developed torque of a PM synchronous motor can be expressed as:

$$T_q = \frac{p}{2}(\psi_d I_q - \psi_q I_d) \tag{4.1}$$

where I_d, I_q, ψ_d and ψ_q are d-axis current, q-axis current, d-axis flux linkage and q-axis flux linkage respectively.

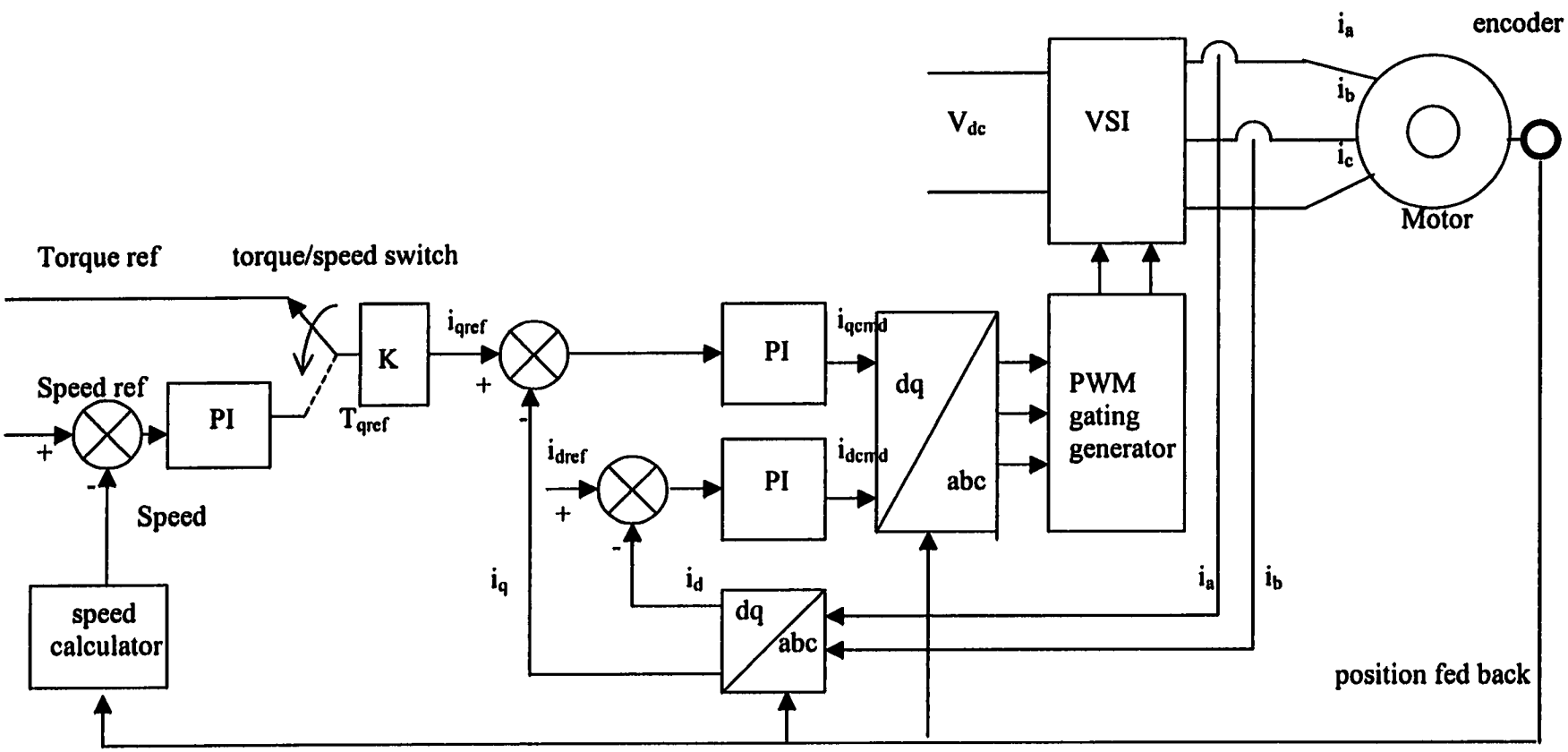

Fig.4.1 Closed loop control of a PM synchronous motor drive system

In a balanced system with the phase-a current leading rotor *d*-axis by θ degrees, the torque can be written as:

$$T_q = \frac{p}{2}\psi_m I_a \sin\theta \tag{4.2}$$

where I_a and ψ_m are magnitude of stator current and flux linkage of each phase respectively.

Since the flux is constant for PM motors, the control of torque can be achieved by controlling either the amplitude of the stator current or the angle θ. It can be seen that when fixing θ torque is proportional to the stator current. Especially when θ=90°, torque reaches maximum with the same supply current.

Surface-mounted cylindrical PM synchronous motors have essentially similar direct-axis and quadrature-axis synchronous reactance. Therefore, the equivalent circuit can be shown in Fig.4.2.

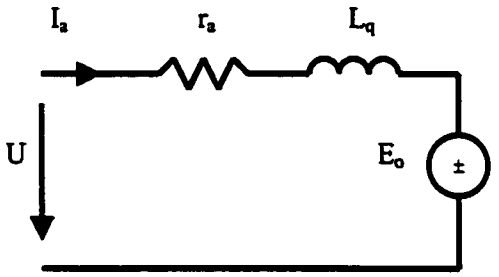

Fig.4.2 Equivalent Circuit of PM synchronous motors

4.2.3 Transfer Function

From Fig.4.2, the equivalent circuit equation can be written as:

$$U = E_o + I_a r_a + L_q \frac{dI_a}{dt} \tag{4.3}$$

where E_o is the induce phase back emf, r_a is the stator phase resistance, L_q is the quadrature-axis inductance and U is the magnitude of phase voltage.

For PM machines, the excitation is fixed, therefore, back emf E_o and torque equation (4.2) can be expressed as:

$$E_o = C_e \omega_s = 2\pi C_e f \tag{4.4}$$

$$T_q = C_m I_a = C_e I_a \tag{4.5}$$

where C_e and C_m are the machine constants.

If the friction is neglected, all of the torque is used to develop acceleration:

$$T_q = J\frac{d\omega}{dt} \tag{4.6}$$

where J is the inertia of the drive system, ω is the mechanical speed of the motor.

The Laplace transformation of (4.3) through (4.6) yields the transfer function of the motor:

$$G(S) = \frac{\omega(S)}{U(S)} = \frac{1}{C_e}\frac{1}{T_m T_e S^2 + T_m S + 1} \tag{4.7}$$

where T_m and T_e are the mechanical and electrical constants respectively:

$$T_m = \frac{r_a J}{C_m C_e}, \qquad T_e = \frac{L_q}{R_a} \tag{4.8}$$

Since T_e is much smaller than T_m, (4.7) can be further written as:

$$G(S) = \frac{1}{C_e}\frac{1}{(T_m S + 1)(T_e S + 1)} \tag{4.9}$$

Based on normalized parameters, the transfer function of the motor is shown in Fig.4.3 where

$K_a = Z_{base} / R_a$ and Z_{base} is the base reluctance.

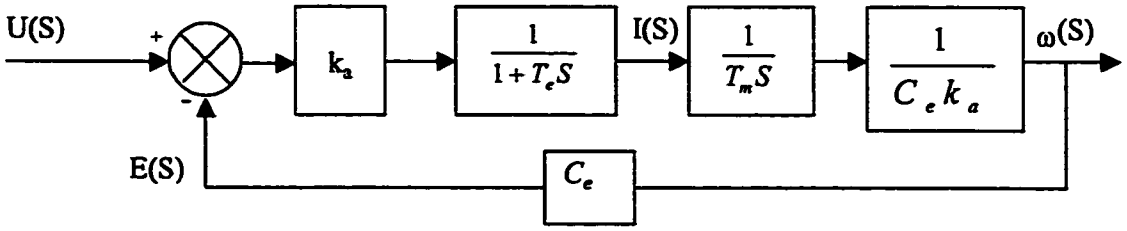

Fig.4.3 Simplified transfer function of a PM synchronous motor

4.2.4 Speed Limit for Current Control

The maximal output voltage of the inverter is limited by the DC link voltage. This voltage limit will set a limit to the maximal speed of the motor. The rms value of the line-line voltage U_{LL} of the inverter can be expressed as

$$U_{LL} = \frac{\sqrt{3}}{2\sqrt{2}} m_a U_d = 0.612 m_a U_d \tag{4.10}$$

where m_a is the modulation ratio and U_d is the DC link voltage.

The phasor diagrams of a PM synchronous motor are shown in Fig.4.4 for maximum torque operation and flux weakening operation respectively. The follow equation can be derived from the phasor diagram shown in Fig.4.4:

$$(E_o + I_a R)^2 + (I_a X_q)^2 = U^2 \tag{4.11}$$

Then the speed limit of maximum torque operation can be derived:

$$n_{max} = \frac{60}{p} \cdot \frac{\sqrt{(I_a r_a k_e)^2 + [C_e^2 + (2\pi I_a L_q)^2][0.1253 U_d^2 - (I_a r_a)^2]} - 2 I_a r_a C_e}{C_e^2 + (2\pi I_a L_q)^2} \tag{4.12}$$

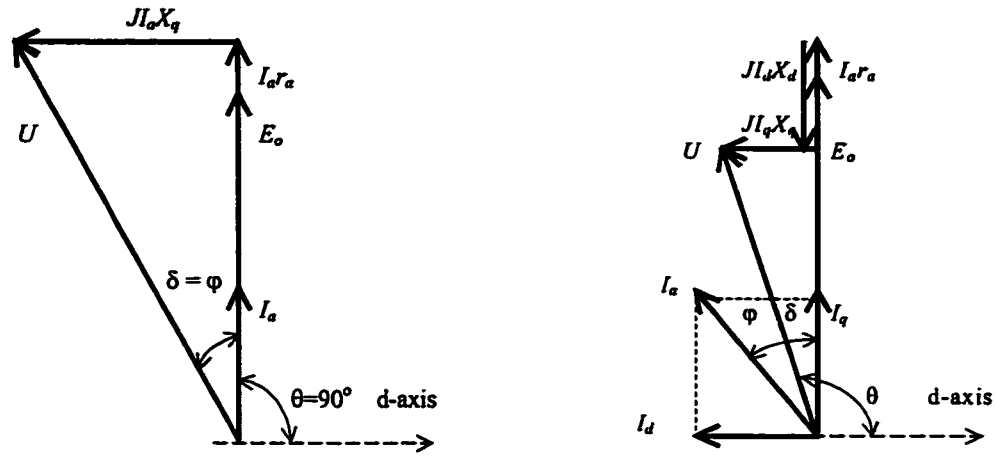

(a). Maximum torque operation (b). Flux weakening operation

Fig.4.4 Phasor diagrams of a PM synchronous motor

4.2.5 Torque and Speed Control

The transfer function of the control system is shown in Fig.4.5.

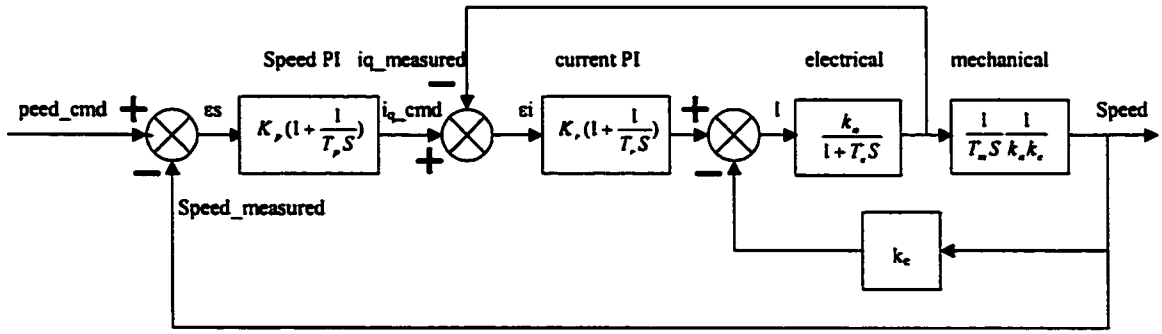

Fig.4.5 Block diagram of the speed loop

The speed of the motor is measured and compared to the given speed. The error signal of the speed is fed to the speed PI and a current command is generated. The current command is compared to the measured stator current and the error signal is fed to the current PI. A voltage command is then generated and forwarded to generate the gating signal.

4.2.6 Current and Speed Responses

The electrical and mechanical time constants of the 8-pole PM motor are listed in Table IV-1. The simulated and measured current responses are shown in Fig.4.6 and Fig.4.7 respectively. The simulated and measured speed responses are shows in Fig.4.8 and Fig.4.9 respectively.

Table IV-1 Time constants of the 8-pole motor

Electrical time constant T_e	12.6ms	Mechanical time constant T_m	1.5s
Time constant of current PI T_I	5ms	Time constant of speed PI T_p	1.04s
Gain of current regulator K_I	0.2	Gain of speed regulator k_p	0.3
Current sampling period T_i	0.5s	Speed sampling period T_s	3ms

It can be seen from Fig.4.6 and Fig.4.7 that both the simulated and measured current response has a first overshoot happening at 3.7ms with the maximum current reaching 24A and 23.6A respectively. Both simulated and measured current reach a steady state current at 19.2A.

While the simulated current response has only one overshoot, the measured current response has some damped oscillation. This is due to the sampling delay of the control system as well as high order time constants which were neglected in the transfer function of the motor control system.

It can be seen from Fig.4.8 that the simulated speed response has an overshoot at 2.2s with maximum speed 1225rpm and period of 2.5s, second undershoot at 4.5s with speed 940rpm. The steady state speed is 992rpm. It can be seen from Fig.4.9 that the measured speed responses has an overshoot at 2.3s with maximum speed 1220rpm and period 2.5s, second undershoot at 4.9s with speed 928rpm. The steady state speed is also 992rpm.

Therefore, it can be concluded that the simulated speed responses are in good agreement with the measured speed response.

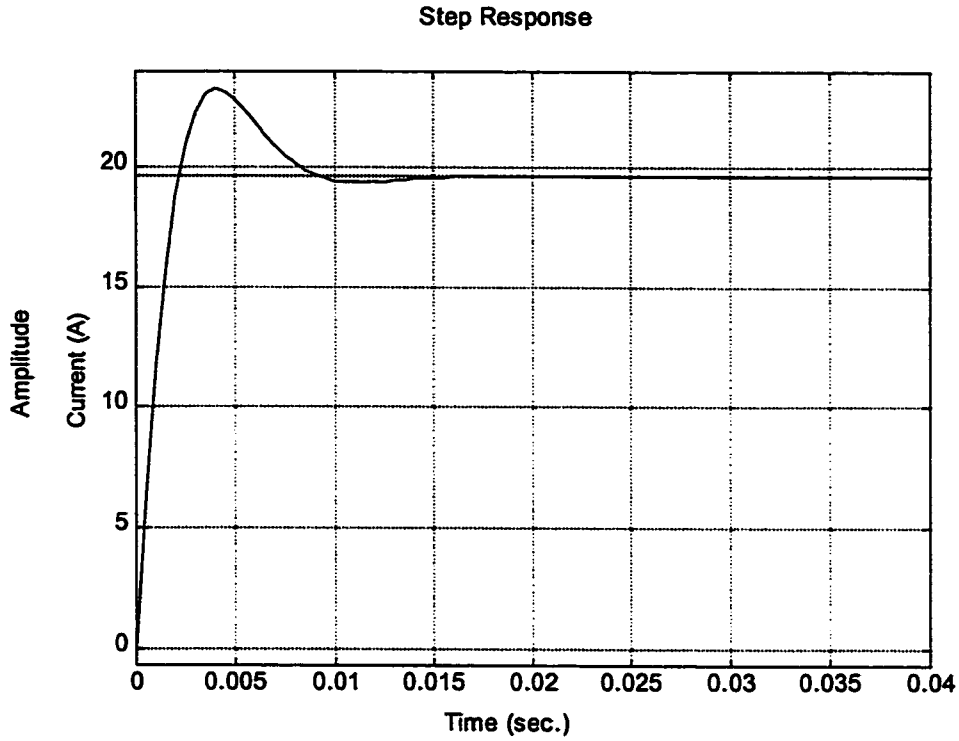

Fig.4.6 Simulated current response of the 2.5hp motor with blocked shaft

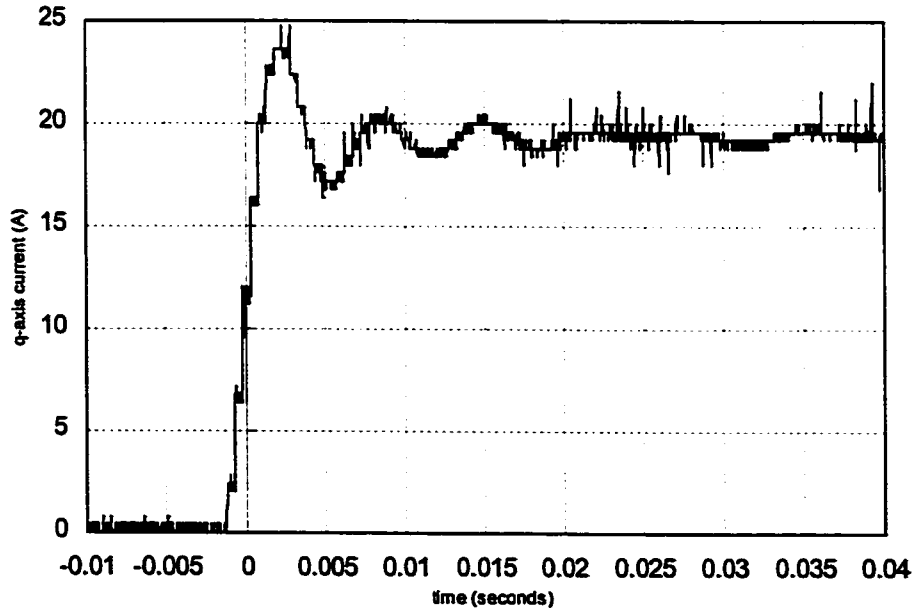

Fig.4.7 Measured current response of the 2.5hp motor with blocked shaft

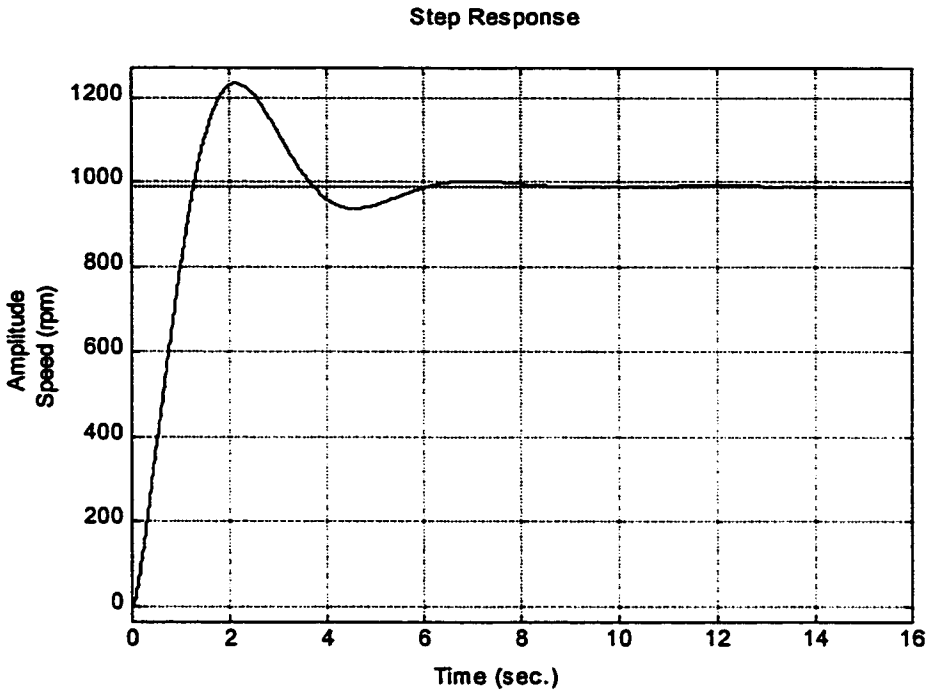

Fig.4.8 Simulated speed response of the 2.5hp motor

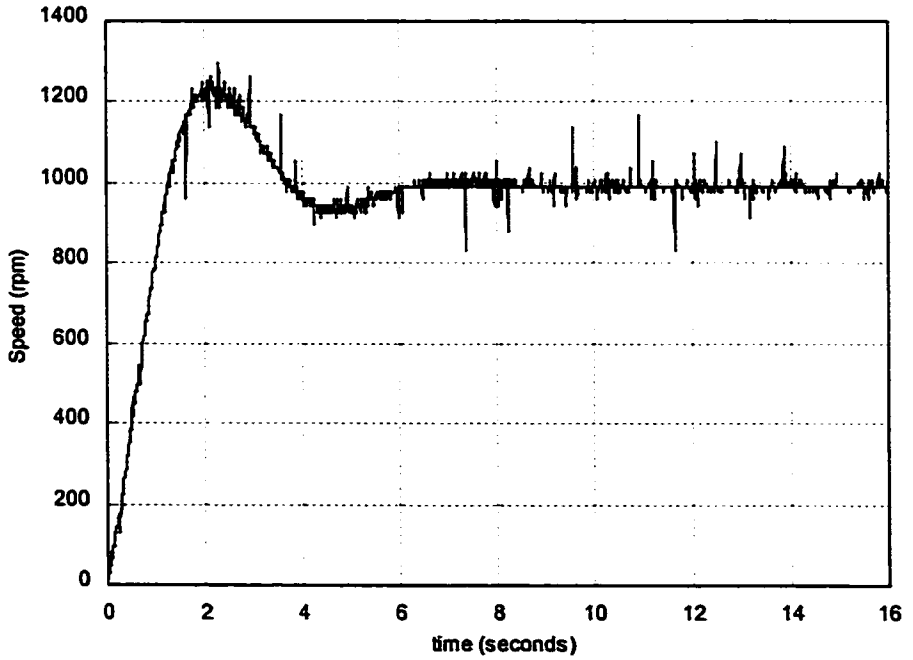

Fig.4.9 Measured speed response of the 2.5hp motor

4.3 Measurement of Voltage, Current and Power

While doing the experiments of PM synchronous motors, it was found that measured voltage, current and power by different instruments have significant discrepancies. The instruments employed include traditional meters (Voltmeter, Ammeter and Wattmeter), digital multimeters, digital power meters and direct sampling using a computer.

The discrepancy is generated by PWM waves since PM motors are often fed by PWM waveforms. A PWM wave is a series of pules with different widths. Traditional meters are designed for continuous waveforms whereas PWM waves are discontinuous. Therefore, traditional designed electrical meters can not give precise readings of the quantities of PWM waves. In order to overcome this difficulty, computer data acquisition as well as applying of filters is suggested to perform the measurements.

4.3.1 Computerized Data Acquisition

Since the accuracy of standard voltmeter and ammeter is not adequate for the measurements of PWM waves, it is necessary to use instantaneous values of voltage and current to calculate their RMS values and power. With fast A/D devices and microprocessors, the supply voltage and current of a PM synchronous motor can be converted to digital signals. The current sensor and the voltage sensor should have very low distortion and band width. The rms value, real power and power factor can be derived from these instantaneous values using computer simulation software such as Matlab.

4.3.2 Measurement of Current

Since the control strategy assures a sinusoidal current wave form, the phase current only consists mainly the fundamental. Fig.4.10 shows the measured phase current waveform of the 2.5hp PM motor at 1080rpm.

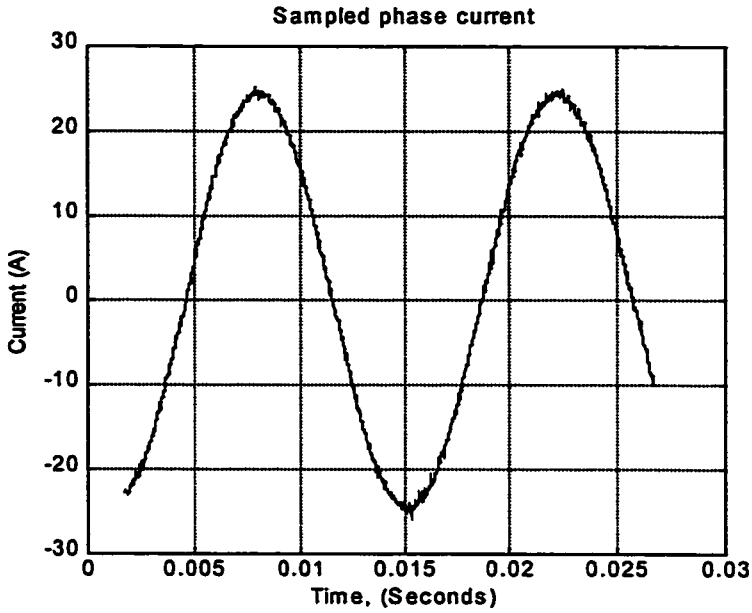

Fig.4.10 Sampled phase current

4.3.3 Measurement of Supply Voltage

A LC filter between the VSI and the PM motor can filter out most of the high frequency harmonics supplied to the PM motor. Fig.4.11 shows the filter used in the 2.5hp PM motor. Fig.4.12 shows the measured phase voltage waveform and filtered phase voltage (the thick line) waveform at 1080rpm and 17A. The measured amplitude of 8kHz (twice the switching frequency) at point A is only about 1% of that measured at the output of the VSI.

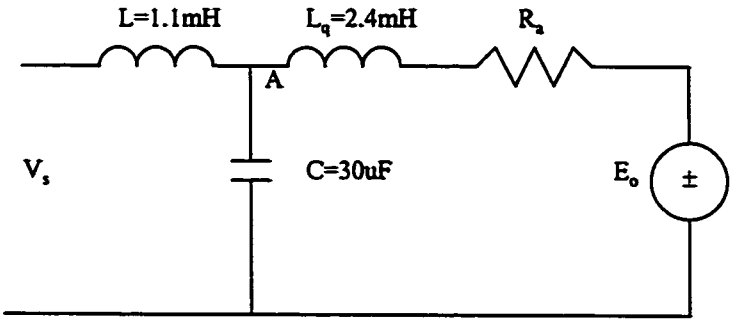

Fig.4.11 Filter design

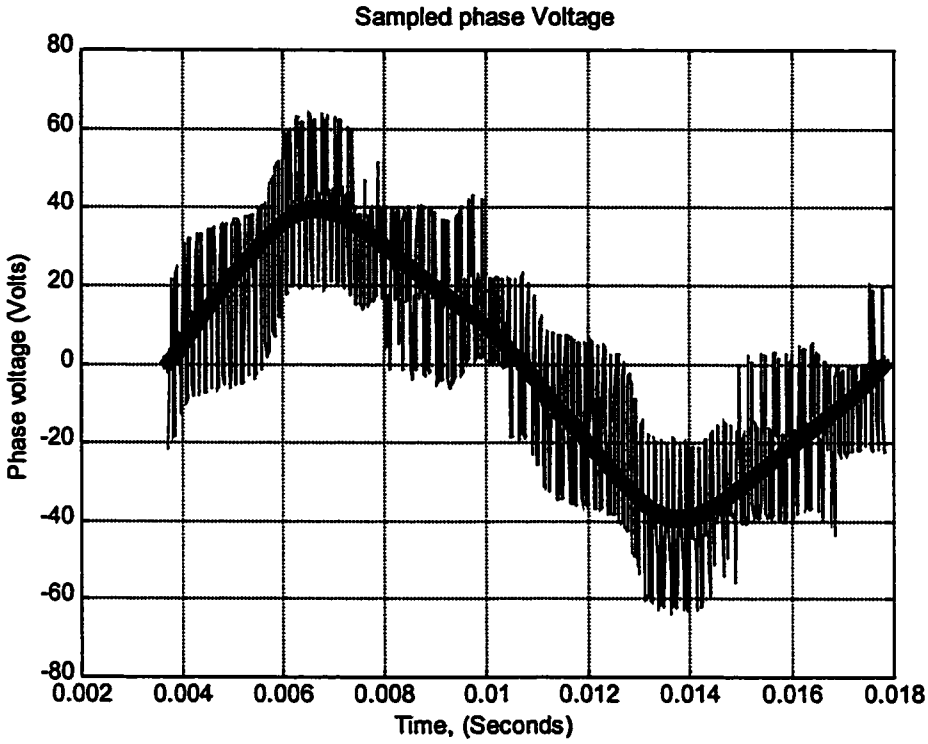

Fig.4.12 Measured phase voltage

4.4 Validation of Measurements Using Phasor Analyses

A Phasor diagram is a powerful tool for analysing synchronous motors. Since a phasor analysis is based on the fundamental quantities of voltage and currents, it is possible to validate the measured values of voltage, current and power using phasor diagram.

From the phasor diagram shown in Fig.4.4(a),

$$U\sin\delta = I_a X_q \tag{4.13}$$

$$\cos\varphi = \cos\delta = \frac{P_1}{mUI_a} = \frac{E_o + I_a r_a}{U} \quad or \quad U\cos\delta = E_o + I_a r_a \tag{4.14}$$

Therefore,

$$U = \sqrt{(I_a X_q)^2 + (E_0 + I_a r_a)^2} \tag{4.15}$$

Since current is sinusoidal and $X_d = X_q$ in surface mounted PM synchronous motors, measured current, reactance and resistance are accurate. All measured electrical quantities of the motor must satisfy (4.15). Table IV-2 shows a group of data measured on a PM motor with different meters.

Table IV-2 Measurements of the 8-pole PM motor

	I (A)	U (V)	P (W)	F (HZ)	φ	θ
Measured by multimeter	17.0	60.6	1620	58.5	58.4	-
Measured by computer	17.1	34.6	1616	58.3	24.1	24.1

Other measurements are: X_q = 2.4mH, r_a=0.176Ohm, E_o=28.6V. The phase voltage can be calculated using the data in Table IV-2 and (4.15). The calculated phase voltage is 35V and power angle is 25.4 degrees. Therefore, the measured values by computer are consistent with each other. The measured voltage by multimeters is not consistent with other measurements. Therefore, it can be concluded that the PWM waveform caused the multimeters and voltmeter function improperly.

4.5 Decomposition of Iron Losses and Mechanical Losses

In PM synchronous motors, the iron losses and mechanical losses are always present simultaneously. The mechanical losses in permanent magnet motors, which include windage and friction losses, must be known before the iron losses can be obtained. There are three ways to perform this task: with the help of an induction motor rotor; with the help of a replica of a nonmagnetic stator; and perform the measurement before the magnets have been assembled to the rotor.

4.5.1 With the Help of the Rotor of an Induction Machine

A PM synchronous motor is usually built within the same frame as a standard induction motor. If the stator of a PM motor has the same dimension as that of an induction machine, the rotor of the induction motor can be inserted and the windage and friction losses measured.

In this procedure, the bearing friction will essentially be the same but not necessarily the windage loss. This is because the airgap will be different and the surface-mounted PM rotor does not have a smooth surface.

4.5.2 With the Help of a Nonmagnetic Stator

Tseng et al suggested an iron loss measurement method by replacing the stator with a non-magnetic replica made of hard plastic with exactly the same geometrical dimensions as the original stator [10]. When the original stator is assembled, the measured losses include the stator iron losses and mechanical losses. When the magnetic rotor is assembled with the non-magnetic replica, the measured loss only includes the mechanical loss. Therefore, the difference between the two will be the stator iron losses and rotor iron loss.

In this procedure, the bearing friction loss can be different if the dummy stator has a different weight. Besides, manufacturing a dummy stator for large PM motors is not practical.

4.5.3 Measuring before Magnets Assembled

A practical and accurate method is to measure the mechanical loss before the magnets are assembled. It is preferable to assemble the PM motor with no magnetized magnets mounted on the surface of the rotor to simulate the magnetic rotor. In this procedure, the dummy motor has exactly the same configuration as the PM motor without iron loss.

4.6 Loss Measurement of the 8-pole Motor

4.6.1 Description of the Motor

A 2.5hp surface-mounted PM synchronous motor was constructed inside a standard 145T induction motor frame. Both the stator laminations and windings were redesigned. The ratings of the original induction motor and the redesigned PM motor are given in Table IV-3 [38]. The key distinguishing characteristics of the motor are:

- The machine was designed with 8 poles and 1 slot per pole per phase.
- M19 grade steel with 0.65mm laminations was used to construct the rotor.
- M15 grade low loss steel sheet with 0.35mm thickness laminations was used to build the stator.
- The magnets were surface-mounted.
- The rated power was increased from 2hp (induction) to 2.5hp (PM synchronous).

Table IV-3 Ratings of the original induction motor and the PM synchronous motor

Ratings and parameters	Induction motor	PM synchronous motor
Rated power	2hp	2.5hp
Voltage (line-line) (V)	575	183.6
Rated current (A)	2.2	7.0
Rated frequency (Hz)	60	120
Number of poles	4	8
Rated speed (rpm)	1735	1800

4.6.2 Measured Losses

The mechanical loss of the motor was measured before the magnets were assembled. The shaft torque was recorded when only the DC dynamometer was connected to the torque sensor at different speeds. Then the PM motor was connected without PM magnets on the rotor. The two motors were connected via the torque sensor and the torque for the same speed range was recorded. The net torque of the PM motor is derived by subtracting the torque of the DC dynamometer from the combined torque of the two motors. The windage and friction loss is then derived. The measured windage and friction loss of the motor is shown in Fig.4.13.

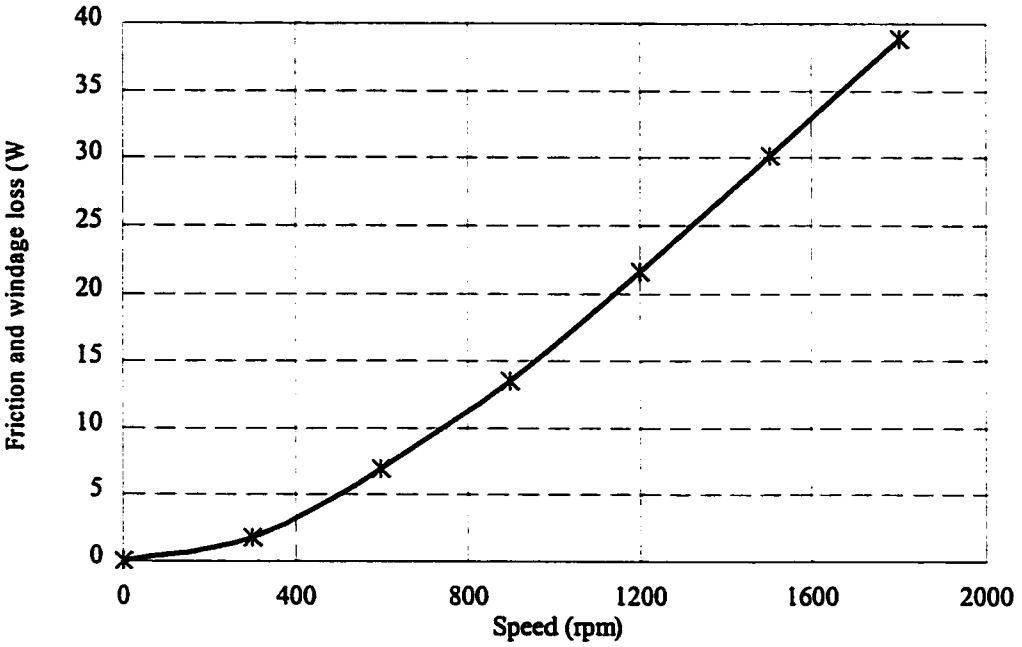

Fig.4.13 Measured friction and windage loss of the 8-pole PM motor

The PM motor was then assembled with magnets on the rotor. The no-load loss is determined by measuring the voltage and current supplied to the PM synchronous motor by an inverter with a near sinusoidal current using an inverter, without connecting any load to its shaft. The losses caused by the stator current fed to the PM motor are negligible at no load. The measured input power is mainly contributed by the stator iron losses and friction and windage losses.

The motor was also tested open-circuited, driven by a dynamometer. The torque-speed product represents the total loss of the motor. The measured iron losses by both methods are shown in Fig.4.14.

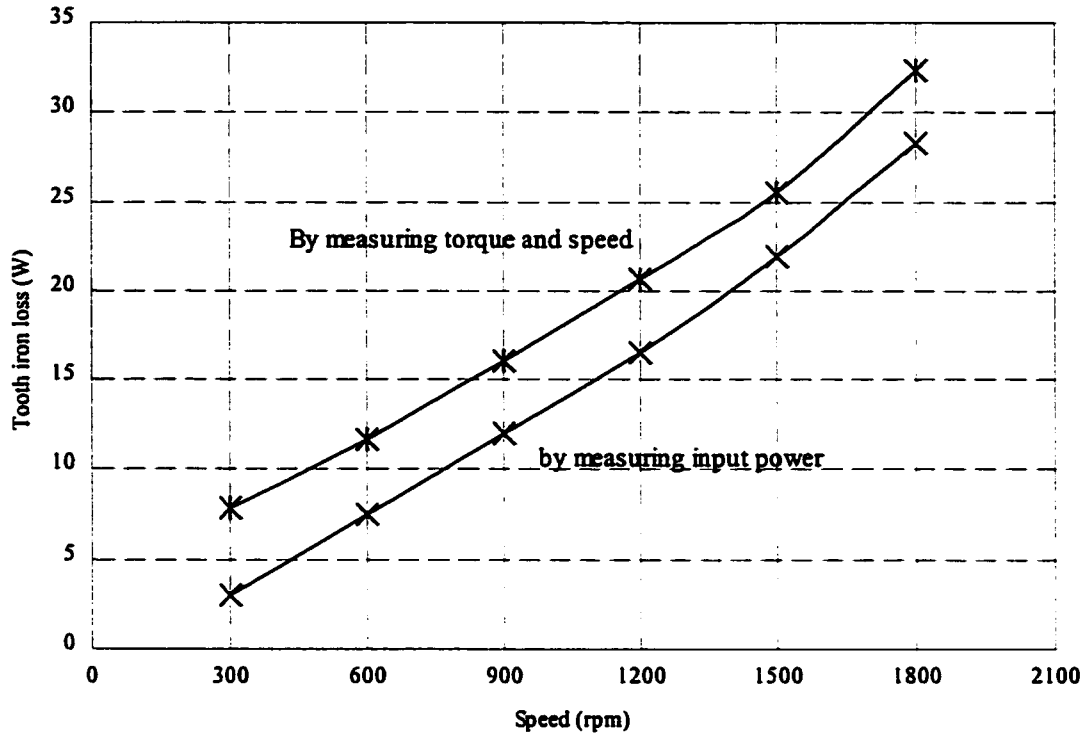

Fig.4.14 Measured iron losses of the 8-pole PM synchronous motor

It can be seen from Fig.4.14 that the measured iron losses using torque-speed product has a 4W offset comparing with those measured using electrical input power measurements.

The possible reason causing the discrepancy is the mechanical setup of the test system. First, measurement of torque is usually less precise than measurements of electrical quantities. Secondly, the DC dynamometer which drives the PM motor has very large inertia compared to the PM motor. Thirdly, there was usually a small offset in the torque readings caused by the torque ripple of the PM motor. Nevertheless, the measurements of iron losses are within 0.2% of the rated power.

4.6.3 Simulated Iron Losses

In order to test the proposed loss model, FEM analyses were performed on the PM motor. The coefficients needed to calculate the iron losses are shown in Table IV-4 [38, 39]. Each component of the iron losses at different speeds was calculated by FEM as shown in Table IV-5 and was calculated by proposed model as shown in Table IV-6.

Table IV-4 Parameters needed to calculate the iron losses (W)

Tooth volume V_t	$0.1737 \times 10^{-3} m^3$	Tooth flux density B_{th}	1.6118T
Yoke volume V_y	$0.2687 \times 10^{-3} m^3$	Yoke flux density B_{yk}	1.1995T
Eddy loss constant k_e	0.0196	Hysteresis loss constant k_h	22

Table IV-5 Iron losses predicted by FEM for the 8-pole motor(W)

SPEED(RPM)	300	600	900	1200	1500	1800
Teeth, eddy current loss	0.2	0.9	2.1	3.7	5.7	8.2
Teeth, hysteresis loss	1.2	2.4	3.6	4.8	6.0	7.2
Yoke, eddy current loss	0.2	0.6	1.4	2.6	4.0	5.8
Yoke, hysteresis loss	1.1	2.1	3.2	4.2	5.3	6.3
Total iron losses by FEM	2.7	6.0	10.3	15.3	21.0	27.5

Table IV-6 Iron losses predicted by simplified model for the 8-pole motor(W)

SPEED(RPM)	300	600	900	1200	1500	1800
Teeth, eddy current loss	0.2	0.9	1.9	3.5	5.4	7.8
Teeth, hysteresis loss	1.2	2.4	3.6	4.8	6.0	7.2
Yoke, eddy current loss	0.2	0.6	1.4	2.4	3.8	5.5
Yoke, hysteresis loss	1.1	2.1	3.2	4.2	5.3	6.3
Total iron losses by simplified model	2.7	6.0	10.1	14.9	20.5	26.8

It can be seen that the simulated iron losses by the two methods are in good agreement and the errors are within 3%.

4.6.4 Comparison of Iron Losses

In order to compare the measured and predicted iron losses, the measured and predicted iron losses of the motor at different speeds are shown in Fig.4.15.

It can be seen from Fig.4.15 that the iron losses predicted by both FEM and the simplified model are consistent with the measured iron losses over the whole speed range, the difference being always within 5%.

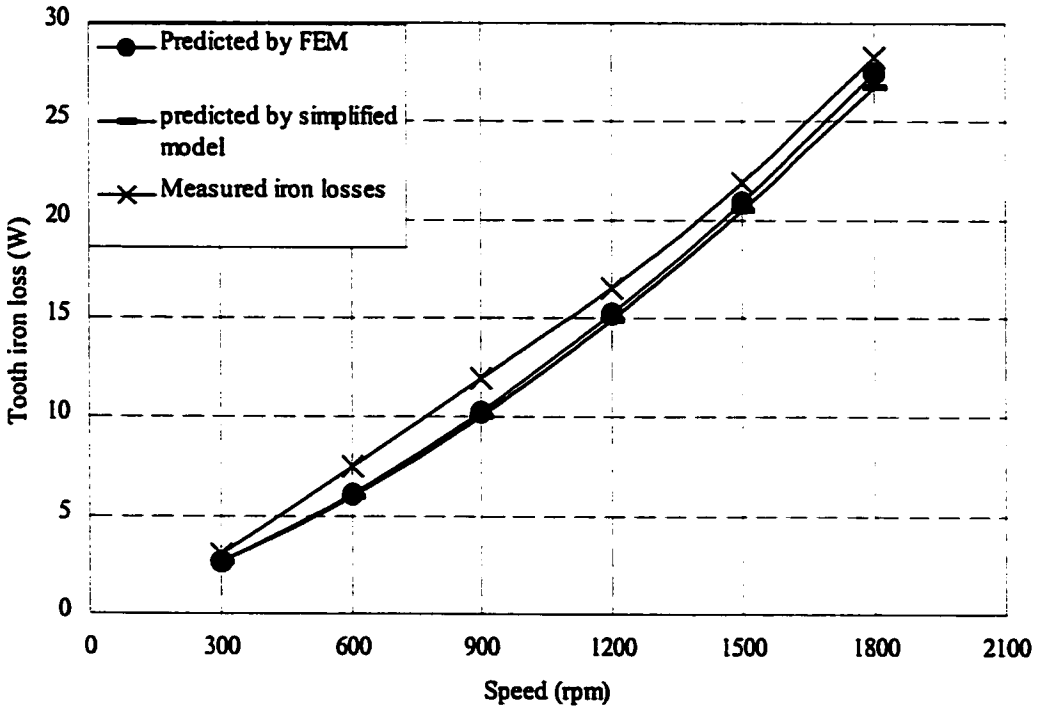

Fig.4.15 Comparison of calculated and measured loss of the 8-pole motor

4.7 Losses Measurement of the 4-Pole Motor

A 4-pole 5hp surface-mounted PM synchronous motor was also employed to do the experiment. The machine was built within the frame of a 5hp standard induction motor and the same stator was used for the PM motor. The original induction motor was totally enclosed fan cooled type motor. The ratings of both the induction motor and the PM motor are given in Table IV-7 [40]. The stator laminations are 0.65mm steel sheets with higher loss coefficients.

Table IV-7 Ratings of the 5hp induction motor and PM synchronous motor

Ratings and parameters	Induction motor	PM motor
Rated power (hp)	5	5
Voltage (line-line) (V)	208	183.6
Rated current (A)	16.7	16.7
Rated frequency (Hz)	60	60
Number of poles	4	4
Rated speed (rpm)	1742	1800

4.7.1 Simulated Iron Losses

The iron losses of this motor were calculated by FEM and the proposed model. The coefficients needed to predict the losses are listed in Table IV-8 [8, 39, 40]. Both k_e and k_h are different from that of the 8-pole motor due to the change of lamination thickness.

Table IV-8 Parameters and coefficients needed to predict iron losses (W)

Tooth volume V_t	$0.3802\text{x}10^{-3}\text{m}^3$	Tooth flux density B_{th}	1.3284T
Yoke volume V_y	$0.8382\text{x}10^{-3}\text{m}^3$	Yoke flux density B_{yk}	1.2827T
Eddy loss constant k_e	0.07	Hysteresis loss constant k_h	44

The predicted iron losses at different speeds by the two methods are listed in Table IV-9 and Table IV-10 respectively.

Table IV-9 Iron losses predicted by FEM for the 4-pole motor(W)

SPEED (RPM)	300	600	900	1200	1500	1800
Teeth, eddy current loss	0.5	1.9	4.3	7.7	12.0	17.3
Teeth, hysteresis loss	1.8	3.6	5.5	7.3	9.1	10.9
Yoke, eddy current loss	0.5	2.0	4.5	8.0	12.6	18.1
Yoke, hysteresis loss	3.7	7.5	11.2	14.9	18.6	22.4
Total iron losses by FEM	6.5	15.0	25.5	37.9	52.3	68.7

Table IV-10 Iron losses predicted by simplified model for the 4-pole motor(W)

Speed (rpm)	300	600	900	1200	1500	1800
Teeth, eddy current loss	0.6	2.3	5.2	9.3	14.5	20.9
Teeth, hysteresis loss	1.8	3.6	5.4	7.2	9.0	10.8
Yoke, eddy current loss	0.5	2.2	4.9	8.7	13.6	19.6
Yoke, hysteresis loss	3.7	7.4	11.2	14.8	18.6	22.3
Total iron losses by simplified model	6.6	15.5	26.7	40.1	55.7	73.6

It can be seen that the predicted iron losses of the motor are in good agreement. The errors are within 7% or less than 0.2% of the rated power.

4.7.2 Comparison to Measured Iron Losses

The mechanical loss of the motor was measured before the magnets were assembled. The measured mechanical losses at different speeds are shown in Table IV-11.

Table IV-11 Measured mechanical losses of the 4-pole PM motor (W)

Speed (rpm)	300	600	900	1200	1500	1800
Total mechanical loss	4.0	10.1	16.2	23.1	34.3	41.1

Then the iron losses were measured by feeding the motor with a inverter and driving the motor with a dynamometer respectively. The measured iron losses of the motor are shown in Fig.4.16 with predicted iron losses by proposed model and FEM method.

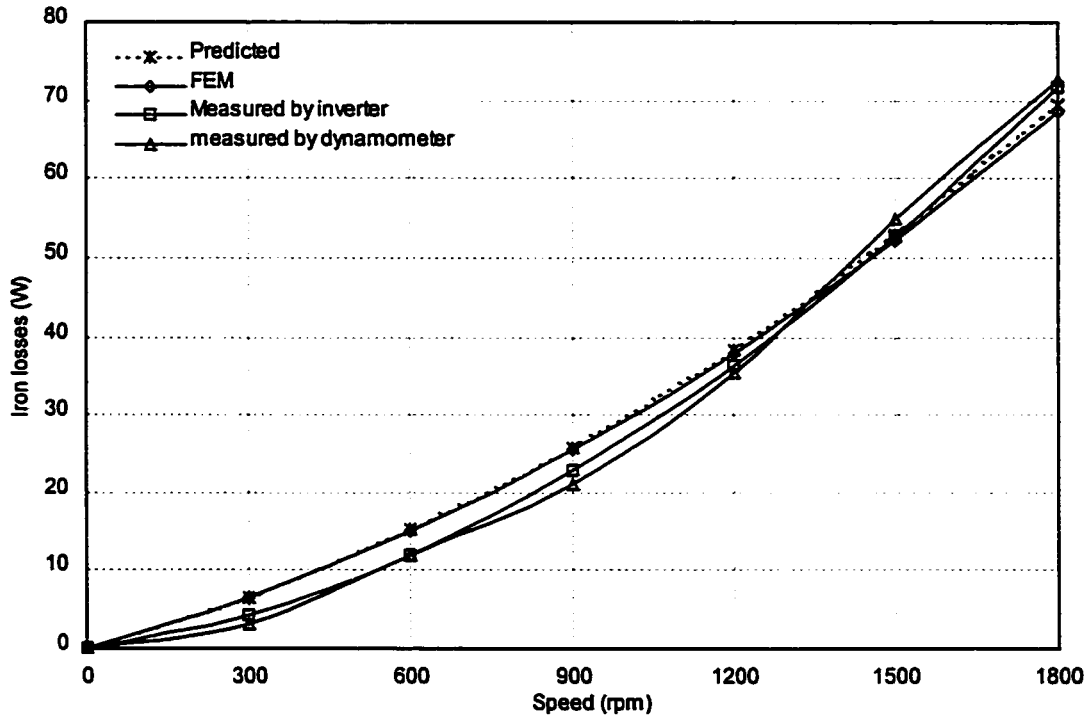

Fig.4.16 Comparison of calculated and measured losses of the 4-pole motor

It can be seen that the measured iron losses by both methods, the predicted iron losses by FEM and the predicted loss by simplified model are in good agreement. The difference is always within ±3.5% or less than 0.2% of the rated power.

4.8 Discussion

From the experimental data of the two PM synchronous motors, one can observe a good agreement between the iron losses predicted by the proposed model, the FEM results and the experimental data. The error is less than 0.2% of the rated power, which represents a great improvement over the conventional approach.

It can also be seen that the iron losses predicted by the proposed model are generally less than the measured iron losses. This discrepancy may be due to the fact that the rotor iron losses were not taken into account in the proposed iron loss model.

Both the proposed model and experimental results are quoted for the no-load condition only. When the motor is loaded, the iron losses will be induced not only by the PM field but also the field induced by the stator currents. The magnetic flux density in the stator teeth and stator yoke will be changed. The combined field may also cause minor loops of hysteresis. Hysteresis losses caused by minor loops can be predicted using the simple method proposed in [41].

Further more, not only the prediction of iron losses of PM motors, but also the measurement of iron losses, constitutes a quite difficult task. Different experimental methods yield different results [37].

As pointed out at the beginning of this chapter, the improvement of efficiency measurement of 0.5% in electrical machines with efficiency of 95% represents an error of 10% in the measured total losses. Therefore, the confidence in the loss measurement in electrical machinery industry is relatively low regardless the high effort in the process.

The FEM is also a numerical approximation of the magnetic field due to the limitation computing resources.

Even if the losses could be accurately predicted and measured, there would be practical difficulties. For example, iron losses are directly related to the characteristics of the

ferromagnetic steel sheets used in the motor, which are different for the same kind of material manufactured at a different time due to mechanical stresses and temperature.

The most important aspect, from the engineering point of view, is to explore the mechanism, tendency and first indication of the associated problems, bring down the complex problem into a manageable problem with sufficient accuracy, not so much to determine the exact values. The thesis study brings a closer yet simple prediction towards the insight of iron losses in PM synchronous machines.

Chapter 5

Minimization of Iron Losses in PM Synchronous Motors

5.1 Optimization of Electrical Machines

Electrical motor-driven equipment utilizes approximately 58% of the electrical energy consumed [42]. Among this electrical motor usage, 93% is consumed by induction motors with power ratings of 5.1hp and greater, 5% is consumed by induction motors with power ratings of 5hp or less. DC motors and synchronous motors consume only 2% of the total electrical motor usage [43]. From 1982 to 1992, the cost of electrical power has increased 120-150% [44]. This trend has forced many manufacturers to address the problem of improving the efficiency of electrical motors.

Since most of the electrical motor usage is induction motors, the focus has been placed on the optimization of induction machines. However, induction motors have their own limitations, e.g., the rotor slip loss always exists. This has lead to a search for alternative approaches. One important approach among them is to use variable speed PM synchronous motors.

With proper design, a PM machine will generally have higher energy efficiency than any

other type of rotating machines of equivalent power output. This is due to the elimination of field ohmic loss as compared to DC excited machines, and due to the elimination of the rotor loss as compared to induction motors. PM machines not only have the advantage of higher efficiency, but also have many other advantages such as less volume and weight, higher power factor and easier control.

There was very little interest in PM machines for drive systems two decades ago. It was only when new rare-earth PM material with their high energy products and low cost became available that industry recognized PM machines were not just low power devices of minimal commercial importance [45]. With the advances and cost reductions in modern rare-earth PM materials and power electronics, it is now possible to consider using motors in applications such as pumps, fans, and compressor drives, where the higher initial cost can be rapidly paid back by energy savings often within a year [46].

The overall optimization of a PM synchronous motor requires balance between the manufacturing cost, efficiency, power factor and torque capability. In most cases, these parameters conflict with each other and a compromise has to be made. The losses of a PM synchronous motor can be decomposed into four components, namely stator winding loss, iron loss, mechanical loss and stray load loss. These losses can be reduced either by using better quality materials, or by optimization of the motor design, or by both.

In this Chapter, some design approaches are proposed to reduce the iron losses of PM synchronous motors by maintaining a maximum torque and maximum efficiency. The proposed methods include proper design of magnets, slots and number of poles.

5.2 Design of Magnets

5.2.1 Magnet Edge Beveling

Beveling of magnets will change the slope of the teeth flux waveform. In order to test

this, FEM analysis were performed on a 4-pole motor with varying β of magnet edge as shown in Fig.5.1. The dashed line on Fig.5.1 is the original magnet with rectangular edges.

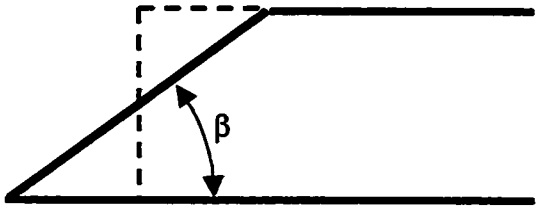

Fig.5.1 The beveling of magnet edge

In order to obtain consistent results, the magnet volume is kept constant when changing the magnet edge. Table V-1 shows the calculated iron losses of the motor by FEM for different magnet edges.

Table V-1 Tooth eddy current loss vs. magnet beveling at at 120Hz

Bevel degrees β	90° (no beveling)	75°	63°	51°	39°	27°
Tooth eddy current loss (W)	29.5	29.4	29.2	28.8	28.1	26.7
Tooth hysteresis loss(W)	14.5	14.4	14.4	14	14.4	14.4
Yoke eddy current loss (W)	20.6	20.6	20.6	20.5	20.5	20.3
Yoke hysteresis loss (W)	12.6	12.6	12.6	12.6	12.6	12.7
Total iron loss (W)	77.0	77.0	76.8	76.0	75.6	74.1
Total airgap flux per pole ($x10^{-3}$Wb)	1.3768	1.3770	1.3773	1.3777	1.3789	1.3820
Reduction of tooth eddy current loss (%)	-	-0.2	-1.0	-2.3	-4.8	-9.5
Total reduction of iron Losses(%)	-	-0.1	-0.4	-1.4	-1.9	-3.9

It can be seen from Table V-1 that when the bevel of the magnet edge is increased, the tooth current loss decreases. When the magnet is beveled at 27°, the tooth eddy current loss is

reduced by 9.5%; the total iron losses are reduced by almost 4% while the total airgap flux and other components of iron losses are kept nearly constant. Fig.5.2 shows the flux distribution of the investigated motor with non-beveled and beveled magnet edge respectively.

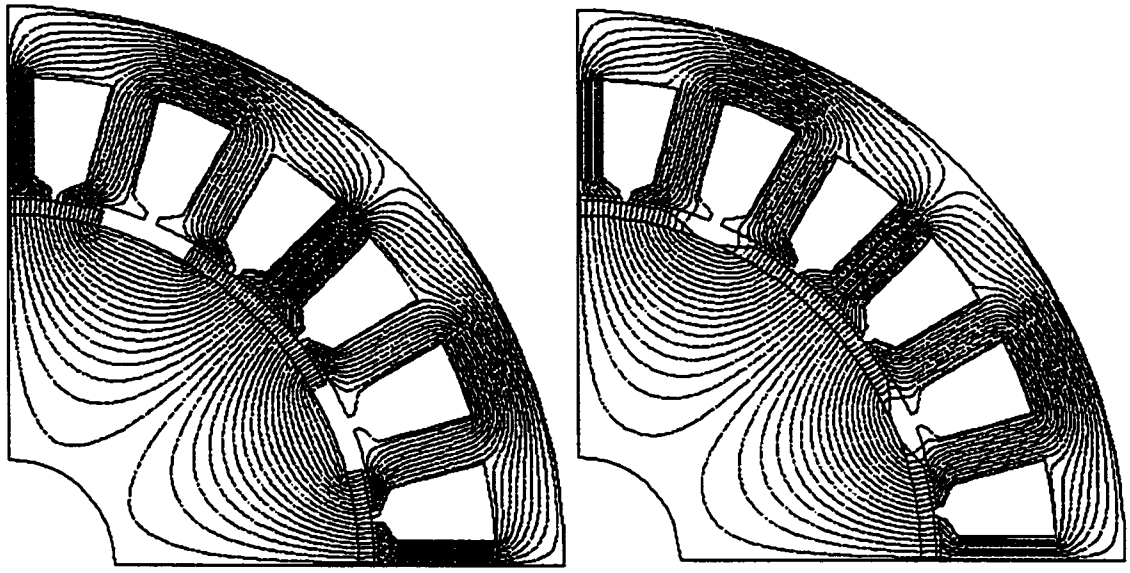

Fig.5.2 Flux distribution of the motor with un-beveled and beveled magnet edge

5.2.2 Shaping of Magnets

Based on the above observations, similar but alternative approaches can be employed to achieve the same effect as magnet edge beveling.

One method is to use curved magnets with the greatest thickness in the center and the thinnest at the two ends as shown in Fig.5.3(b). This will improve the curvature of the flux waveforms both in the teeth and in the yoke. Therefore, the eddy current loss can be reduced. The drawback of the method is that it will increase the difficulties and cost in manufacturing the magnets.

Another approach is to parallel magnetize the magnets or to gradient magnetize the magnets with the flux increasing from two ends to the middle of the magnets. The drawback of this approach is that the magnets are not fully utilized.

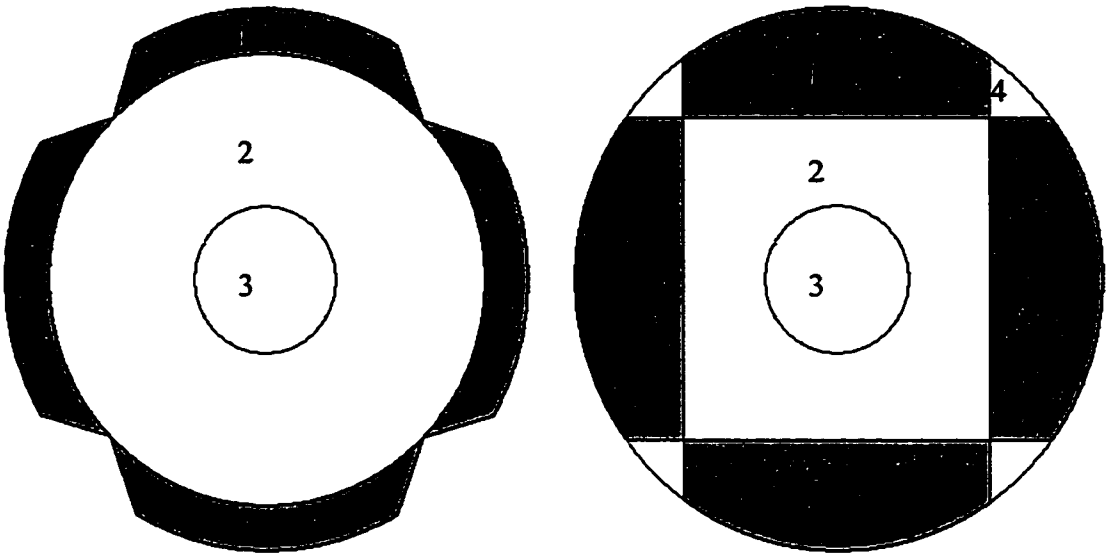

(a) Beveled magnets (b) Curved magnets

1—magnet 2—core 3—shaft 4—non-magnetic material

Fig.5.3 PM rotor with beveled or curved magnets

5.2.3 Magnet Width and Magnet Coverage

In Chapter 3, it has been shown that changing magnet width over a wide range does not change the maximum flux density achieved in the teeth, nor does it change the slope of the flux waveform in the teeth. However, when space between the two magnets is less than one slot pitch, the slope of tooth flux begins to increase. Especially when magnet coverage approaches 1.0, the slope of the normal flux in the teeth is dramatically increased thus tooth eddy current losses are significantly increased. Therefore, for a *m*-phase PM motor with *q* slots per pole per phase, the maximum magnet coverage to have maximum flux linkage but low tooth eddy current loss is

$$\frac{1}{mq} < \alpha < \frac{mq-1}{mq} \tag{5.1}$$

Since yoke eddy current loss is approximately inversely proportional to magnet

coverage, magnet coverage should be large enough in order to minimize yoke eddy current loss.

On the other hand, magnet width also has significant effects on cogging torque [47]. According to [47], the optimal magnet coverage to achieve the least torque cogging is:

$$\alpha = \frac{(n+0.14)\lambda}{\tau} = \frac{n+0.14}{mq} \tag{5.2}$$

where n is any integer which satisfies $\alpha<1$.

Combining (5.1) and (5.2), the optimal magnet coverage can be obtained. For example, for motors with two slots per pole per phase (m=3, q=2), magnet coverage that satisfies (5.1) and (5.2) is $\alpha=0.527$ or $\alpha=0.693$. In order to minimize yoke eddy current loss, the optimal magnet coverage is $\alpha=0.693$.

5.3 Design of Slots

5.3.1 Number of Slots

It was found in Chapter 3 that for a given supply frequency, tooth eddy current loss is proportional to the number of slots per pole per phase. Hence, it is beneficial to use fewer but wider teeth. The minimal possibility is to utilize 1 slot per pole per phase.

On the other hand, for a reasonably good approximation to a sinusoidal distribution of induced emf, the number of slots per pole per phase should be at least 2 [48].

5.3.2 Slot Closure

By increasing slot closure, the maximum value of airgap flux density can be increased if the same amount of magnet material is used. The flux distribution of the 8-pole PM motor with different slot closure is shown in Fig.5.4. The iron losses in Fig.3.9 also show that when

the airgap flux is kept constant, the iron losses are about the same for different slot closures.

Small slot openings are widely adopted in most motor designs. The reason is that although reducing slot openings does not reduce the stator iron losses of the motor, it increases output torque and reduces the rotor eddy current loss.

However, totally closed slots, as shown in Fig.5.4, will increase leakage flux in the shoes of the slots. This flux doesn't contribute to the generated torque but will increase the iron loss. Therefore, totally enclosed slots are not recommended.

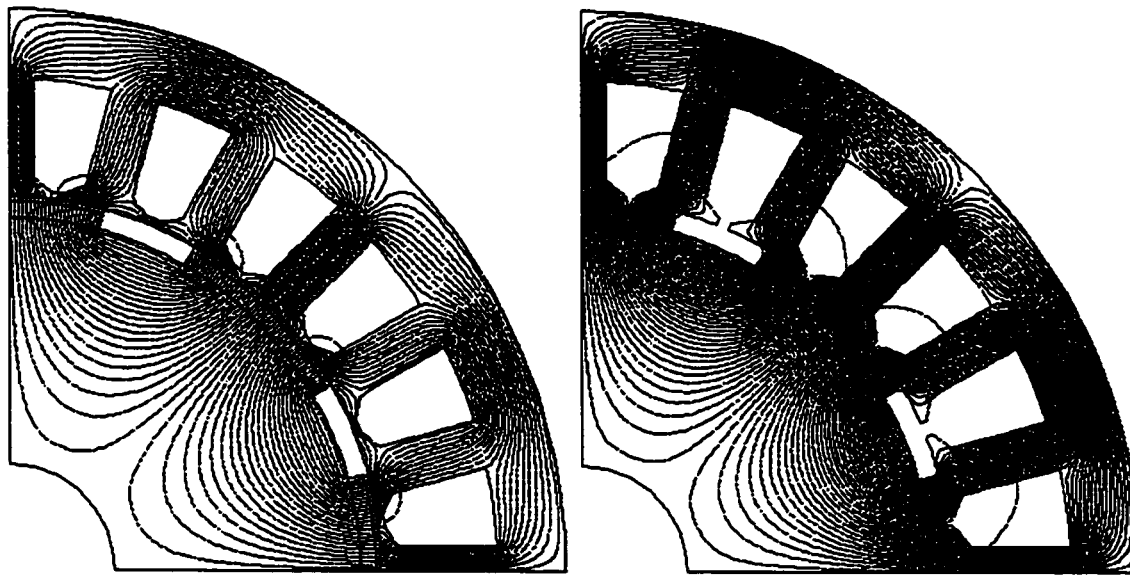

(a). Totally enclosed slots (b). Partly closed slots

Fig.5.4 Flux distribution with different slot closure

5.4 Number of Poles

Variable speed drives are free from the number of poles constraint imposed on ac motors operated at fixed frequency. The inverter can operate at frequencies from a few Hertz up to a few hundred Hertz. This allows the number of poles to be selected freely to achieve the best

motor design. By increasing the number of poles, the length of the end turn windings is reduced and thus the copper usage can be reduced and the stator copper loss is reduced. The thickness of the stator yoke is also reduced and therefore the usage of core material for the yoke is reduced. More power output or torque can be achieved with more poles for the same frame due to the reduction of yoke thickness and/or an increase in the inner radius of the stator.

Since the operating frequency increases proportionally to the number of poles in order to keep the desired speed, the eddy current loss increases despite the fact that the mass of the core material is reduced.

In order to have a reasonable comparison base, the following analysis assumes a given frame and speed. This assumption results in a fixed machine core length and a constant copper loss and friction and windage loss.

5.4.1 Iron Losses and Number of Poles

Total number of slots is usually limited by the frame size. When the total number of slots is fixed, the number of slots per pole per phase is inversely proportional to the number of poles. The tooth eddy current loss and tooth hysteresis loss can be written as:

$$P_{et} = \frac{pS}{900} k_q k_c k_e B_{th}^2 n^2 V_t \tag{5.3}$$

$$P_{ht} = \frac{\pi np}{60} k_h B_{th}^{\beta} V_t \tag{5.4}$$

where S is the total slots of the stator:

$$S = mpq \tag{5.5}$$

Therefore, both tooth eddy current loss and tooth hysteresis loss is proportional to number of poles.

Yoke volume can be expressed as a function of number of poles:

$$V_y = \pi r_j^2 - \pi(r_j - \frac{2}{p} d_{y2})^2 = \frac{4\pi d_{y2}}{p}(r_j - \frac{d_{y2}}{p}) \tag{5.6}$$

where r_j is the outer radius of the stator, d_{y2} is the yoke thickness of the motor with a 2-pole configuration.

Yoke eddy current loss and yoke hysteresis loss can be expressed as:

$$P_{ey} = \frac{\pi p n^2}{112\alpha} k_r k_e B_y^2 d_{y2}(r_j - \frac{d_{y2}}{p}) \tag{5.7}$$

$$P_{hy} = \frac{\pi^2 n}{15} k_h B_y^{\beta} d_{y2}(r_j - \frac{d_{y2}}{p}) \tag{5.8}$$

Therefore, yoke eddy current loss is proportional to number of poles while yoke hysteresis loss remains roughly constant when the number of poles is changed.

Take the original frame of the 4-pole PM motor as an example. The iron losses are calculated and listed in Table V-2 as functions of the number of poles. The total number of slots is S=36. The possible number of poles is 2, 4, 6, and 12. It can be seen from Table V-2 that the iron losses of the motor increase by 24W if the number of poles increases by a factor of two.

Table V-2 Iron loss as a function of number of poles

Number of poles	2	4	6	12
Operating frequency (Hz)	30	60	90	180
Tooth eddy current loss (W)	8.7	17.3	26.0	52.0
Yoke eddy current loss (W)	8.6	18.1	27.5	55.9
Tooth hysteresis loss (W)	5.5	10.9	16.3	32.7
Yoke hysteresis loss(W)	21.3	22.4	22.7	23.1
Iron losses (W)	44.0	68.7	92.6	163.7

5.4.2 Torque and Number of Poles

The torque of a PM motor is [18]

$$T_q = 2\pi r^2 l_{fe} B_{1g} K_{1\delta} \quad \text{(Nm)} \tag{5.9}$$

where B_{1g} and $K_{1\delta}$ are the rms values of the airgap flux and the linear current density on the stator inner periphery.

The linear current density can be expressed as a function of stator current [49]:

$$K_{1\delta} = \frac{mWI_a}{\pi r} \quad \text{(A/m)} \tag{5.10}$$

where W is the total number of turns for each phase, r is the inner radius of stator.

Therefore, motor torque is a function of rotor radius, airgap flux density and stator current. If constant airgap flux density and stator current are assumed, then

$$T = k_T r \quad \text{(Nm)} \tag{5.11}$$

Assume that the height of slots is kept constant. Than the inner radius of the stator can be expressed as a function of the number of poles:

$$r = r_j - \frac{2}{p} d_{y2} - d_t \tag{5.12}$$

It can be seen from (5.12) that when p is small, the increase of r is significant as p is increased. Therefore, torque can be significantly increased by increasing the number of poles assuming p is small.

Take the frame of the 4-pole PM motor as an example. The torque is

$$T = k_T(r_j - \frac{2}{p} d_{y2} - d_t) = 332 \times (0.095 - 0.0696/p - 0.0172) \tag{5.13}$$

The quantified torque of this motor as a function of the number of poles is shown in Table V-3 .

Table V-3 Torque as a function of number of poles

Number of poles	2	4	6	12
Torque (Nm)	14.3	20.0	22.0	23.9
Increase of torque (%)	--	40	10	8.6

It can be seen from Table V-3 that the torque increases by 40% and 10% respectively when the number of poles increases from 2 to 4 and from 4 to 6, while the torque only increases 8.6% when the number of poles increases from 6 to 12.

5.4.3 Optimal Number of Poles

The optimal number of poles may vary for different applications. The criteria are whether an optimal efficiency and a maximal torque are achieved. The motor efficiency is:

$$\eta = \frac{P_{out}}{P_{out} + p_{fw} + p_{cu} + p_{iron}} \tag{5.14}$$

Output power P_{out} and iron loss p_{iron} are functions of the number of poles p. Copper loss and friction loss are assumed constant. The optimal efficiency can be found by solving

$$\frac{d\eta}{dp} = 0, \qquad p = 2,4,6,8\cdots\cdots \tag{5.15}$$

Take the same example from the last section. The combined copper, friction and windage losses are 289W. The efficiency can be expressed as

$$\eta = \frac{4869 - 4356/p}{(4869 - 4356/p) + 289 + (20 + 12p)} \tag{5.16}$$

The torque and efficiency of the motor are listed in Table V-4. It can be seen that the choices of 4 and 6 poles are optimal amongst all possible choices.

Table V-4 Torque and efficiency as functions of the number of poles at 1800rpm

Number of poles	2	4	6	12
Torque (Nm)	14.3	20.0	22.0	23.9
Efficiency (%)	89.0	91.4	91.6	90.9

The choices for the number of poles are different for each application. It requires the balance of material usage, achieved maximal torque, efficiency and manufacturing cost. Usually the best choices are four, six and eight poles among all the possibilities for a PM motor design. In small machines, the number of poles is limited by the maximum number of slots which is limited by the minimum practical width of the stator teeth and slots.

Chapter 6

Conclusions

6.1 Contributions and Conclusions

The contributions of the thesis are:

(1). Developed refined approximation models of iron losses for surface-mounted PM synchronous motors taking into account details of the geometry of the design. Based on the models, the evaluation of iron losses of surface-mounted PM synchronous motors can be performed without the high effort of a time-stepped FEM. These models also give motor designers an easier but more precise tool to predict iron losses of surface-mounted PM synchronous motors in their initial design depending on the geometry of the design.

From the development of simplified iron loss models of surface-mounted PM synchronous motors, the following conclusions are made for tooth eddy current loss:

- For rectangular edged magnets, the flux density in the teeth of a PM synchronous motor is approximately uniform. The normal component of tooth flux density can be approximated by a trapezoidal waveform.

- For the approximated trapezoidal flux waveform of the normal component of tooth

flux density, the time needed to rise from zero to the plateau is approximately the time that a magnet edge traverses one slot pitch

- The eddy current loss in the teeth of a PM synchronous motor can be estimated by first considering the normal component of tooth flux density and then a correction factor for the circumferential component.

- For a given operating frequency, the tooth eddy current loss of a PM synchronous motor is proportional to the number of slots per pole per phase.

- For a given torque and speed rating, the tooth eddy current loss is approximately proportional to the products of number of poles squared and slots per pole per phase.

- The tooth eddy current loss is independent of the angular width of the magnet.

- Changing tooth width over a wide range within the same slot pitch will not change the tooth eddy current loss of a PM motor.

- The tooth eddy current loss is not affected by the slot closure.

- A correction factor can be introduced to reflect the effect of airgap length, slot pitch and magnet thickness of the motor.

The following conclusions can be made for yoke eddy current loss:

- The circumferential component of yoke flux density is approximately evenly distributed over the thickness of the yoke. It can be approximated by a trapezoidal waveform. The time needed for this component to rise from zero to the plateau is the time that a point in the yoke passes a half of the magnet width.

- The normal component of yoke flux density has the same waveform as that of the normal component of tooth flux density. The plateau value of the yoke flux density is linearly distributed over the thickness of the yoke with zero at the surface of the

yoke and maximum near the tooth.

- The eddy current loss in the yoke can be approximated by first considering the circumferential component and then a correction factor for the normal component.
- For a given frequency, yoke eddy current loss is proportional to the inverse of magnet coverage.
- For a given torque and speed rating, yoke eddy current loss is proportional to the number of poles squared.
- Major geometrical variations such as magnet thickness, airgap length, number of slot per pole per phase and tooth width of a PM synchronous motor have little effect on yoke eddy current loss.

(2). Performed measurements of iron losses of surface-mounted PM synchronous motors. Some methods were suggested to decompose the iron losses from the total no load losses of a PM synchronous motor. Measurement of PWM waves was discussed and phasor analyses were proposed to validate the measurements of a PM synchronous motor.

(3). Proposed general approaches to reduce iron losses of PM synchronous motors. The iron losses of a PM motor can be reduced by implementing one or more of the following recommendations:

- Beveled magnet edge, curved magnets and optimized magnet coverage will reduce the iron losses of surface-mounted PM synchronous motors.
- Using fewer but wider slots can reduce tooth eddy current loss.
- Using more poles can generally increase the torque of the motor. Optimal numbers of poles are 4, 6, or 8 depending on the application.

6.2 Future Work

Suggestions for the future studies are given below:

(1). Modeling of iron losses in PM synchronous motors with buried magnets, inset magnets and circumferential magnets.

(2). Determining the iron losses of loaded PM synchronous motors, including both calculations and experiments.

Reference

[1]. Bose B. K., *Power Electronics and Variable Frequency Drives: Technology and Applications*, IEEE Press, 1997

[2]. Bertotti G., Boglietti A., Chiampi M., Chiarabaglio D., Fiorillo F. and Lazzari M., "An Improved Estimation of Iron Losses in Rotation Electrical Machines", *IEEE Transactions on Magnetics*, 27(6) : pp5007-5009, 1991

[3]. Zhu J. G., Ramsden, V. S. and Watterson P. A., "Finite Element Calculation of Core Losses in Motors with Non-Sinusoidal Fields", *Proceedings of the international Conference on Electrical Machines*, ICEM92, Manchester, UK, pp1182-1186, 1992

[4]. Liu Z. J., Binns K. J. and Low T. S., "Analysis of Eddy Current and Thermal Problems in Permanent Magnet Machines with Radial Field Topologies", *IEEE Transactions on Magnetics*, 31(3) : pp1912-1915, 1995

[5]. Liu Z. J., Bi C. and Low T. S., "Analysis of Iron Loss in Hard Disk Drive Spindle Motors", *IEEE Transactions on Magnetics*, 33(5) : pp4089-4091, 1997

[6]. Jamil M. K.,and Demerdash N. A., "Harmonics and Core Losses of Permanent Magnet DC Motors Controlled by Chopper Circuits", *IEEE-Transactions on Energy Conversion*, 5(2) : pp 408-414, 1990

[7]. Deng F, "An Improved Iron Loss Estimation for Permanent Magnet Brushless Machines", *IEEE Transactions on Energy Conversion*, 14(4) : pp1391-1395, 1999

[8]. Slemon G. R. and Liu X., "Core Losses in Permanent Magnet Motors", *IEEE Transactions on Magnetics*, 26(5) : pp1653-1655, 1990

[9]. Deng F., "An Improved Iron Loss Estimation for Permanent Magnet Brushless Machines", *IEEE International Electrical Machine and Drives Conference Record*,

IEEE, New York, USA, pp1-3, 1997

[10]. Tseng K. J. and Wee S. B., "Analysis of Flux Distribution and Core Losses in Interior Permanent Magnet Motors", *IEEE Transactions on Energy Conversion*, 14(4) : pp969-975, December 1999

[11]. Gray G. G. and Martiny W. J., "Efficiency Testing of Medium Induction Motors: A Comment on IEEE Std 112-1991", *IEEE Transactions on Energy Conversion*, 11(3) : pp495-499, 1996

[12]. Amin B., "Contribution to Iron-Loss Evaluation in Electrical Machines", *European-Transactions-on-Electrical-Power-Engineering*, 5(5) : pp325-328, 1995

[13]. Sakamoto Y., Natsusaka M., Murakami K. and Abe N., "Experimental Studies on Iron Loss in a Parametric Motor", *IEEE-Translation-Journal-on-Magnetics-in-Japan*, 9(2) : pp36-42, 1994

[14]. James B. P. and Alzahawi B. A. T., "A High Speed Alternator for Small Scale Gas Turbine CHP Unit", *IEE 7th International Conference on Electrical Machines and Drives*, pp281-285, 1995

[15]. Honsinger V. B.., "The Fields and Parameters of Interior Type AC Permanent Magnet Machines", *IEEE Transactions on PAS*, 101(4) : pp867-876, 1982

[16]. Binns K. J. and Al-Din M. S. N., "Use of Canned Rotors in High-Fields Permanent Magnet Machines", *IEE Proceedings*, 139(5) : pp471-477, 1992

[17]. Mi C. and Ji X., "Effect of Ring Material on Airgap Flux of Permanent Magnet Machines", *Journal of Northwestern Polytechnical University*, 11(4) : pp447-450, 1993

[18]. Slemon G. R., "Design of Permanent Magnet AC Motors for Variable Speed Drives," Chapter 3, *Performance and Design of Permanent Magnet AC Motor Drives*, IEEE Press, New York, 1991

[19]. Rockwood G. H., "Calculation of Stray Load Losses", *Transactions of the AIEE*, Vol. 46 : pp1139-1147, 1927

[20]. Kosow I. L., *Electrical Machinery and Control*, Prentice-Hall, Inc., Englewood Cliffs, N. J., 1964

[21]. Slemon G. R., *Electrical Machines and Drives*, Addison Wesley Publications, Reading, Mass., 1992

[22]. Fiorillo F. and Novikov A., "An Improved Approach to Power Losses in Magnetic Laminations under Nonsinusoidal Induction Waveform", *IEEE Transactions on Magnetics*, 26(5) : pp2904-2910, 1990

[23]. Atallah K., Zhu Z. Q. and Howe D., "An Improved Method for Predicting Iron Losses in Brushless Permanent Magnet DC Drives", *IEEE-Transactions on Magnetics*, 28(5) : p 2997-2999, 1992

[24]. Gyselinck J., Dupre L., Vandevelde L. and Melkebeek J., "Calculation of Iron Losses in Electrical Machines Using the Preisach Model", *Proc 3rd Int. Workshop on Electrical and Magnetic Fields*, Liege, pp423-428, 1996

[25]. Salon S. J., *Finite Element Analysis of Electrical Machines*, Kluwer Acadamic Publishers, Boston/London/Dordrecht, 1995

[26]. Edward J. D. and Freeman E. M., *MagNet5.1 User Guide—Using the MagNet 5.1 Package from Infolytical*, Infilytical Corporation, 1995

[27]. Mi C. and Fu Y., "Computer-Aided Design and Optimization of Rare-Earth Permanent Magnet Synchronous Motors", *Small and Special Electrical Machines*, 1996(1), pp4-7, 1996

[28]. Ali K., Atallah K. and Howe D., "Prediction of Mechanical Stress Effects on the Iron Loss in Electrical Machines", *Journal-of-Applied-Physics*. 81(8) : pp4119-21, 1997

[29]. Yamada H., Magashima H. et al, "Rotational Core Losses of Induction Motor by Finite Element Method," *Electrical Engineering in Japan*, 103(6) : pp75-82,1983

[30]. Rabinovici R. and Miller T.J.E., "Eddy Current Losses of Surface-Mounted Permanent Magnet Motors", *IEE Proceedings of Electrical Power Application*, 144(1) : pp61-64, 1997

[31]. Miller T. J. E. and Rabinovici R., "Back-Emf Waveforms and Core Losses of Brushless DC Motors", *IEE proceedings of Electrical Power Applications*, 141(3) : pp144-154, 1994

[32]. Rabinovici R., "Eddy Current Losses of Permanent Magnet Motors", *IEE Proceedings of Electrical Power Applications*, 141(1) : pp7-11, 1994

[33]. Miller T. J. E., *Brushless Permanent Magnet and Reluctance Motor Drives*, Clarendom Press, Oxford, pp70-75, 1989

[34]. Gerald G. G. and Walter J. M., "Efficiency Testing of Medium Induction Motors, A Comment on IEEE Std 112-1991", *IEEE Transactions on Energy Conversion*, 11(3) : pp495-499, 1996

[35]. *IEEE Guide: Test Procedure for Synchronous Machines*, IEEE Std. 115-1995, pp30

[36]. Anibal de A., Paolo B. and Werner L., *Energy Efficiency Improvements in Electrical Motors and Drives*, Springer, Verkag Berlin, 1997

[37]. Glew, C. N., "Efficiency Measurement Testing Standards Stray Loss, The Key to Efficiency Determination", *Energy Efficiency Improvements in Electrical Motors and Drives*, Springer, pp249-265, 1997

[38]. Farkas A.., *Permanent Magnet Motor Design for High Efficiency Industrial Drives*, Master's Thesis, University of Toronto, 1994

[39]. Hollitscher H. et al, "Steel Sample Tests #1 for University of Toronto", *Technical Report No. 75-HH-2*, Engineering Laboratory, General Electrical Canadian Inc., 1975

[40]. Sebastian T., *Permanent Magnet Motor Designed High Efficiency Industry Drives*, Ph.D Thesis, University of Toronto, 1992

[41]. Lavers J. D., Biringer P. P. and Hollitscher H., " A Simple Method Of Estimating The Minor Loop Hysteresis Loss In Thin Laminations", *IEEE Transactions on Magnetics*, 14(5) : pp386-388, 1978

[42]. *Classification and Evaluation of Electrical Motors And Pumps*, Washington DC, US

Department of Energy, November 1998

[43]. Jordan H. E., *Energy-Efficient Electrical Motors and Their Applications*, Plenum Press, New York and London, 1994

[44]. Andreas J. C., *Energy-Efficient Electrical Motors*, Marcel Dekker Inc., New York, 1992

[45]. Buschow K. H. J., "New Permanent Magnet Materials", *Material Science Report*, Vol.1 September 19886

[46]. Nadel S., et al, *Energy Efficient Motor Systems' Handbook*, America Council for a Energy Efficient Economy, 1991

[47]. Li T. Z. and Slemon G. R., "Reduction of Cogging Torque in Permanent Magnet Motors", *IEEE Transactions on Magnetics*, 24(6), pp2901-2903, 1988

[48]. Slemon G. R., "On The Design of Permanent Magnet Synchronous Motors," *IEEE Transactions on Industry Applications*, 30(1) : pp134-140, 1994

[49]. Chen S., *Electrical Machine Design*, Mechanical Press, Beijing, 1993